NTNU – Trondheim
Norwegian University of
Science and Technology

Structural Reliability Analysis and Robust Design of Offshore Wind Turbine Support Structures

Marc Garcia Llado

Wind Energy
Submission date: June 2015
Supervisor: Michael Muskulus, BAT
Co-supervisor: Lars Einar Stieng, BAT

Norwegian University of Science and Technology
Department of Civil and Transport Engineering

NORWEGIAN UNIVERSITY OF SCIENCE AND TECHNOLOGY
DEPARTMENT OF CIVIL AND TRANSPORT ENGINEERING

Report Title: Structural Reliability Analysis and Robust Design of Offshore Wind Turbine Support Structures	Date: 29/06/2015 Number of pages (incl. appendices): 184			
	Master Thesis	X	Project Work	
Name: Garcia Lladó, Marc				
Professor in charge/supervisor: Prof. Dr. Michael Muskulus Lars Einar Stieng				

Abstract:

The purpose of this master thesis is to develop and evaluate a novel approach for performing structural reliability analysis and robust design of offshore wind turbine support structures. Offshore wind turbines are structures especially prone to uncertainties due to its exposure to environmental conditions. Therefore, the models that take into account probabilistic descriptions of variability are more natural approaches. In this sense, a structural reliability analysis and a robust design are two complementary approaches that allow for incorporating uncertainty and randomness in the design process.

To achieve the objective of this study, it has been developed a simplified model of a monopile structure that allows for doing the necessary calculations efficiently. The simplified model is implemented as a time-domain simulation in MATLAB and allows to solve the transient dynamics of a beam. In parallel, the rotor loads are obtained from rotor simulations in FEDEM Windpower software. Uncertainty is studied in the following system parameters: aerodynamic damping, soil stiffness and cross section of the support structure. Simple probability distributions are used in order to describe the uncertainty on these parameters.

The basis of the research is a probability analysis based on several approaches. First, it is raised an individual analysis for each system parameter and wind speed. Secondly, the way used to add the aerodynamic damping in the simplified model has given rise to two different analyses. The effect of the soil stiffness and the structure cross section is investigated through a correlated and uncorrelated sampling of both variables. Finally, a combined probability analysis is performed in order to observe the effect of analysing the three system parameters at the same time. Additionally, the reference offshore wind turbine is also analysed in order to enable evaluate the effects of the other analyses. The probabilistic analysis is performed with a variable number of samples and the displacements at the tower top and the bending moments at the mud-line of the structure are obtained as a result. These outputs are used to evaluate the equivalent fatigue damage of the support structure.

The wind turbine considered is the 5-MW NREL, with the reference support structure defined in the OC3 project.

The results show that the response of the proposed simplified model is significantly different depending on the system parameter. The soil stiffness and the aerodynamic damping have shown a weak effect on the response of the structure. The reason could be an underestimation of the uncertainties associated to these parameters. Conversely, the structure cross section has shown a greater impact, probably due to dynamic amplifications linked to resonance'problems. The uncorrelated analysis of the soil stiffness and the structure cross section has shown the greater effects on the response of the structure, given that the sampling approach of this case leads to a greater scattering of the system parameters and, consequently, of the results.

Keywords:

1. Offshore Wind Turbine
2. Structural Reliability Analysis, Robust Design
3. Simplified Model, MATLAB
4. Probability Analysis, Uncertainty

En record de la Roser Parés Blasco.

Gràcies, Iaia. Descansa en Pau.

Preface

This thesis, Structural reliability analysis and robust design of offshore wind turbine support structures, has been written as a Master Thesis of Marc Garcia Lladó. The final work is the result of a 2-years studies of Master in Civil Engineering at the Universitat Politècnica de Catalunya (UPC). The thesis has been written in Trondheim, in the group of Marine Civil Engineering for the Department of Civil and Transport Engineering at the Norwegian University of Science and Technology (NTNU).

The main aim of the work is to develop and evaluate a novel approach for performing structural reliability analysis and robust design of offshore wind turbine support structures.

Acknowledgment

I would like to express my gratitude to those who helped me accomplish this study. I would like first to thank to my supervisors in charge: Michael Muskulus and Lars Einar Stieng, for their useful comments and remarks throughout all the meetings that we have had. I would like also to thank to my supervisor at the UPC: Albert de la Fuente Antequera, who has been always willing to help me, in spite of knowing that I was in Norway doing the thesis.

Secondly, I would like to express my sincerest gratitude and appreciation to my family for their unconditional love and support during this year. Special thanks to my grandmother, Roser Parés Blasco, and Manolo Rodríguez Pazos, to who would have loved to see this work finished.

Last but not least, I would like to thank to all my friends, especially to Patricia Hernández, Manon Pelzer and Judit Tomás for your support and advice.

Department of Civil and Transport Engineering, NTNU
June 2015, Trondheim

Marc Garcia Lladó

Abstract

The purpose of this master thesis is to develop and evaluate a novel approach for performing structural reliability analysis and robust design of offshore wind turbine support structures. Offshore wind turbines are structures especially prone to uncertainties due to its exposure to environmental conditions. Therefore, the models that take into account probabilistic descriptions of variability are more natural approaches. In this sense, a structural reliability analysis and a robust design are two complementary approaches that allow for incorporating uncertainty and randomness in the design process.

To achieve the objective of this study, it has been developed a simplified model of a monopile structure that allows for doing the necessary calculations efficiently. The simplified model is implemented as a time-domain simulation in MATLAB and allows to solve the transient dynamics of a beam. In parallel, the rotor loads are obtained from rotor simulations in FEDEM Windpower software. Uncertainty is studied in the following system parameters: aerodynamic damping, soil stiffness and cross section of the support structure. Simple probability distributions are used in order to describe the uncertainty on these parameters.

The basis of the research is a probability analysis based on several approaches. First, it is raised an individual analysis for each system parameter and wind speed. Secondly, the way used to add the aerodynamic damping in the simplified model has given rise to two different analyses. The effect of the soil stiffness and the structure cross section is investigated through a correlated and uncorrelated sampling of both variables. Finally, a combined probability analysis is performed in order to observe the effect of analysing the three system parameters at the same time. Additionally, the reference offshore wind turbine is also analysed in order to enable evaluate the effects of the other analyses. The probabilistic analysis is performed with a variable number of samples and the displacements at the tower top and the bending moments at the mud-line of the structure are obtained as a result. These outputs are used to evaluate the equivalent fatigue damage of the support structure.

The wind turbine considered is the 5-MW NREL, with the reference support structure defined in the OC3 project.

The results show that the response of the proposed simplified model is significantly different depending on the system parameter. The soil stiffness and the aerodynamic damping have shown a weak effect on the response of the structure. The reason could be an underestimation of the uncertainties associated to these parameters. Conversely, the structure cross section has shown a greater impact, probably due to dynamic amplifications linked to resonance problems. The uncorrelated analysis of the soil stiffness and the structure cross section has shown the greater effects on the response of the structure, given that the sampling approach of this case leads to a greater scattering of the system parameters and, consequently, of the results.

Resum

El propòsit d'aquesta tesi de màster és desenvolupar i avaluar una nova proposta per a la realització d'una anàlisi de fiabilitat estructural i disseny robust de les estructures de suport d'un aerogenerador en alta mar. Els aerogeneradors en alta mar són estructures especialment propenses a incerteses per la seva àmplia exposició a les condicions ambientals, de manera que els models que tenen en compte les descripcions probabilístiques de la variabilitat són plantejaments més naturals. En aquest sentit, una anàlisi de fiabilitat estructural i un disseny robust són dos models complementaris que permeten la incorporació de la incertesa i l'aleatorietat en el procés de disseny.

Per complir l'objectiu d'aquest estudi, s'ha desenvolupat un model simplificat d'una estructura mono-pilar que permet fer els càlculs necessaris de manera eficient. El model simplificat s'implementa com una simulació en el domini del temps utilitzant MATLAB i resolent la resposta dinàmica d'una biga. En paral·lel, les càrregues del rotor s'obtenen a partir de simulacions de rotor utilitzant el software FEDEM Windpower. La incertesa s'ha estudiat en els següents paràmetres del sistema: l'amortiment aerodinàmic, la rigidesa del sòl i la secció transversal de l'estructura de suport. S'han utilitzat distribucions de probabilitat simples per tal de descriure la incertesa en aquests paràmetres.

La base d'aquesta investigació és una anàlisi de probabilitat que s'ha dividit en diverses seccions. En primer lloc, es planteja una anàlisi individual de cada paràmetre del sistema i velocitat del vent. En segon lloc, la forma d'incorporar l'amortiment aerodinàmic al model simplificat dóna lloc a dues anàlisis diferents. L'efecte de la rigidesa del sòl i la secció transversal de l'estructura s'ha investigat a través d'un mostreig correlacionat i no correlacionat de les dues variables. Finalment, una anàlisi de probabilitat combinada es porta a terme per tal d'observar l'efecte d'analitzar els tres paràmetres del sistema al mateix temps. A més, també s'analitza l'aerogenerador de referència per tal de poder avaluar els efectes observats les altres anàlisis. L'anàlisi de probabilitat es realitza amb un nombre variable de mostres i s'obtenen com a resultat els desplaçaments a la part superior de la torre i els moments de flexió al punt on el pilar contacta amb el sòl. Aquests resultats es fan servir per avaluar el dany per fatiga equivalent de l'estructura de suport de l'aerogenerador.

L'aerogenerador que es fa servir com a referència és el 5-MW NREL, amb l'estructura de suport definida al projecte OC3.

Els resultats mostren que la resposta del model simplificat és significativament diferent en funció del paràmetre del sistema analitzat. La rigidesa del sòl i l'amortiment aerodinàmic han mostrat un efecte molt feble sobre la resposta de l'estructura. La raó podria ser una subestimació de les incerteses associades a aquests paràmetres. Per contra, la secció transversal de l'estructura ha mostrat un important impacte sobre els resultats, probablement a causa d'amplificacions dinàmiques lligades a problemes de ressonància. L'anàlisi no correlacionat de la rigidesa del sòl i la secció transversal de l'estructura ha mostrat els majors efectes sobre la resposta de l'estructura. En aquest cas, el motiu podria ser que el plantejament del mostreig condueix a una major dispersió dels paràmetres del sistema i, en conseqüència, dels resultats.

Table of Contents

List of Tables

List of Figures

Nomenclature

Abbreviations

CV	Variation coefficient
DOF	Degree of freedom
FEM	Finite Element Method
FORM	First Order Reliability Method
MSL	Mean-sea level
MPP	Most Probable Point
NREL	National Renewable Energy Laboratory
SORM	Second Order Reliability Method

Roman Symbols

$a^{(e)}$	Nodal displacements
b	Diameter of the pile
B	Constitutive matrix
c	Chord of turbine blade, viscous damping parameter, elemental damping matrix
C	Global damping matrix
C_1, C_2, C_3	Coefficients of the API *p-y* method
$c_{damping}$	Damping coefficient, aerodynamic damping
$C_{L\alpha}$	Lift coefficient
c_v	Coefficient of variation
D	Accumulated damage, Miner sum
dV_d	Change in wind speed perpendicular to rotor plane
f	Frequency
f_{1P}	Rotational frequency of the rotor
f_{3P}	Blade-passing frequency
F	Load projection into each DOF

F_V	Prescribed body forces
F_S	Prescribed surface tractions
F_X	Cumulative density function
f_X	Probability density function
k	Thickness exponent on fatigue strength, elemental stiffness matrix, modulus of subgrade reaction
k_t	Tangent stiffness
K	Global stiffness matrix
L_k	Scale parameter for (Kaimal) wind spectrum
$log\bar{a}$	Intercept of log N axis
m	Negative inverse slope of the S-N curve, elemental mass matrix
m_{1b}	First order (static) moment of the area of the chord along the blade
M	Global mass matrix
M_0	Modal mass
M_{eq}	Fatigue damage equivalent bending moment
M_i	Bending moment of intensity
N	Total number of measurements or time steps, shape function matrix
n	Indice of time steps
n	Number of amplitudes for calculation of logarithmic decrement
N_i	Number total of cycles to failure for stress range *i*
n_i	Number total of cycles for stress range *i*
n_b	Number of bins used for the cycle counting
p	Soil-pile resistance
p_i	Prescribed concentrated loads
p_f	Probability of structural failure
p_u	Ultimate lateral soil resistance
q	Generalized coordinates
r	Radius rotor
r^{int}	Internal forces

r^{ext}	External forces
$r_{y,z}$	Radius of gyration
S	Surface
$S(f)$	Response spectrum
$S_U(f)$	Spectral density of wind speed
T	Total length of time series
t	Thickness
Δt	Time step
T_p	Spectral peak period
T'	Change in thrust force with time
$\overline{U}$	Mean wind speed
$U(t)$	Wind speed at time instant t
U_{10}	10-minute mean wind speed
U_{hub}	Wind speed at hub height
$U_m(t)$	Mean wind speed component at time instant t
$U_t(t)$	Turbulence component of wind speed at time instant t
v	Fluctuating wind velocity
V	Volume, mean wind speed
V_0	Wind speed
V_{tot}	Total wind speed
W_{int}	Internal work
W_{ext}	External work
x_0	Amplitude of first oscillation for calculation of logarithmic decrement
x_n	Amplitude of last included oscillation in calculation of logarithmic decrement
x_k	Tributary length of the spring

Greek Symbols

α	Mass coefficient, Newmark's method parameter

β	Stiffness coefficient, Newmark's method parameter
γ'	Submerged unit weight of the soil
δ	Logarithmic decrement
$\delta\varepsilon$	Strain associated with the virtual displacement δu
δu	Virtual displacement
$\Delta\sigma$	Stress range
Ω	Angular velocity of rotor
ω	Angular frequency
ω_n	Natural frequency
ρ	Density of air, density of water
σ	Standard deviation
σ_U	Standard deviation of wind speed
ξ	Damping ratio
ξ_{aero}	Logarithmic decrement of aerodynamic damping
φ	Angle of internal friction, density function

CHAPTER 1

Introduction

During the past decades, wind power has been one of the fastest growing sources of energy. This expansion has also affected the offshore wind energy industry, where the need for a larger percentage of renewable energy sources has motivated the development of the sector. The general trend of this industry has been the increase of the number of wind turbines installed and their sizes. This trend can be translated into larger generators and rotors, and consequently higher hub heights and larger foundations for the support structure. The main reason behind this increase of size has been an economic incentive. A correlation between operation and maintenance costs and number of offshore wind turbines in a wind farm exists. Hence, by increasing the turbine sizes one aims to reduce the cost of the energy in the years to come. Looking forward, the EU targets for 2020 motivate a massive installation of offshore wind power and an increase of the sizes up to 20 MW if proven economically and technically feasible (Sieros *et al.*, 2012).

The design of offshore wind turbines is a complex issue that spans a wide range of disciplines. Although many challenges affect the design, it is possible to emphasize six main aspects that are dominant in this design stage. First, nonlinear effects and time-history dependence are characteristic in wind turbines. These nonlinearities are caused by unsteadiness in flow turbulent and structural nonlinearities. Secondly, offshore wind turbines are strongly influenced by the surrounding environment. Wind and waves induce complex, irregular and highly fluctuating environmental conditions. Thirdly, the dynamic complexity of offshore wind

turbines and their exposure to aerodynamic, hydrodynamic and mechanical loadings make the structures especially prone to fatigue damage. Fourthly, in order to obtain an optimal and cost-effective design it is required to perform an integrated system design of the offshore wind turbine, where all sub-components should be taken into account and simultaneously optimised as a whole. Fifthly, numerical models and load simulations are used in order to perform the analysis of wind turbines. It is needed to select the appropriate analysis software based on the particular conditions of the structure that is being studied. Finally, the number of variables and constrains could be an important issue, particularly in multi-member support structures, which are characterized by many parameters and design variables (Muskulus *et al.*, 2014).

Concurrently, structural optimization facilitates the formulation of a design problem in a mathematically rigorous way, which allows for finding optimal solutions using semi-automatic and algorithmic solutions. The concept of structural optimization is also linked with the cost reduction of the structure explained above. Support structure, tower and foundation represent around the 17 percent of the total capital costs. Hence, structural optimization offers the potential to reduce the costs associated to these parts of the structure (The Carbon Trust, 2008; The Crown Estate, 2012). At a more detailed level, for a long time structural optimization has been based primarily on deterministic models. Nevertheless, it has been recognized that these schemes involve a high degree of uncontrolled risk due to these models do not consider any kind of uncertainty in the variables that are part of the design. Conversely, uncertain and sources of errors are more natural approaches in models which take into account probabilistic descriptions of variability. A structural reliability analysis and a robust design are two complementary approaches that allow for incorporating uncertainty and randomness in the design process (Muskulus *et al.*, 2014). These methods are at least one order of magnitude more involved than standard structural optimization methods, which are usually established by deterministic procedures, since they involve nested analyses.

1.1. Motivation and Objectives

The motivation behind this thesis is based on the need to develop and evaluate a novel approach for performing structural reliability analysis and robust design in order to develop more cost effective designs for support structures for offshore wind turbines. As the support structure is one of the main contributors to the total cost of the installed offshore wind turbine, the potential of reducing cost by optimizing the design using probabilistic approaches is large and interesting.

The objective of this thesis is to look closer into the structural reliability analysis and robust design of support structures for offshore wind turbines. The effects related to the degree of damping and the soil stiffness on the response of the support structure will be investigated, focusing on the uncertainty associated with these parameters. Concurrently, the geometry of the support structure will be investigated in a probabilistic way in order to enable optimization or development of cost effective in future work. Furthermore, other specific objectives have to be achieved during the conduct of the research in order to achieve the main objective of this thesis, such as a literature review of the main aspects investigated or the development and test of a simplified analysis model.

Figure 1.1: Wind farm in the Baltic Sea, neat Zingst, Germany.

1.2. Approach

The investigation of developing and evaluating a novel approach for performing structural reliability analysis and robust design of offshore wind turbine support structures will be conducted by performing dynamic simulations using a simplified model of a monopile structure. The simplified model will be implemented by using the finite element method as a time-domain simulation in MATLAB, solving the transient dynamics for a beam. Furthermore, this simplified model will allow for doing the necessary calculations efficiently.

Environmental loads shall be represented by the wind acting on the wind turbine rotor which, in turn, produces rotor loads that are transferred to the support structure. These rotor loads will be obtained from rotor simulations in FEDEM Windpower software. On the other hand, uncertainty on the system and design parameters, such as degree of damping or soil stiffness, will be described by simple probability distributions. Finally, the fatigue damage of the structure shall be analysed in a probabilistic way.

Structural reliability analysis and a foundation for robust design will be investigated by performing probabilistic analyses with the simplified model mentioned above. Aerodynamic damping, soil stiffness and cross section of the support structure will be described by simple probabilistic distributions in order to investigate the effect of uncertainty in system parameters and enable to develop more cost effective designs in future work.

1.3. Structure of the Report

This research has been divided in 7 main chapters. The first chapter corresponds to this section, which represents the introduction of the thesis. The rest of the thesis is structured as follows.

- In Chapter 2 basic information about wind energy is presented, and the scope and limitations to the objectives of the thesis are given. Here, the dimensions and concepts used for the offshore wind turbine in the simulations, are described as well.
- Chapter 3 presents relevant background information needed for a complete understanding of the thesis. It including the finite element method, damping and its effects, environmental conditions and probabilistic analysis.
- In Chapter 4 the methods and models used to perform the structural reliability analysis and robust design are described, as well as how the relevant aspects such as damping effects or soil interaction have been treated.
- The results of the simulations are presented in Chapter 5
- Chapter 6 presents the discussion of the results obtained in the previous chapter in terms of the objectives of the thesis.
- In Chapter 7, conclusions regarding the obtained results and suggestions for further work are given.

CHAPTER 2

Scope and Limitations

2.1. System Definitions

2.1.1. Terminology

For a complete understanding of the rest of this thesis, the basic terminology that will be used is introduced. Such terminology refers to different topics for offshore wind turbines, with special emphasis on the components of the support structure (DNV, 2011).

- Blades: The flat panels on a wind turbine that are connected to a center shaft that coverts the push of the wind into a circular motion in a wind turbine. Most commercial turbines have three blades.
- Cut-in speed: The wind speed at which the turbine blades begin to rotate and produce electricity, typically around 4.47 m/s.
- Cut-out speed: The wind speed at which some wind turbines automatically stop the blades from turning and pitches out of the wind to avoid damage to the turbine, usually around 24.59 to 29.06 m/s.
- Foundation: The base structural and/or geotechnical component of the offshore wind turbine, from the transition piece down to the seabed.
- Gearbox: The gears connect the low-speed shaft to the high-speed shaft and increase the rotational speed of the shaft to the speed required by the generator.

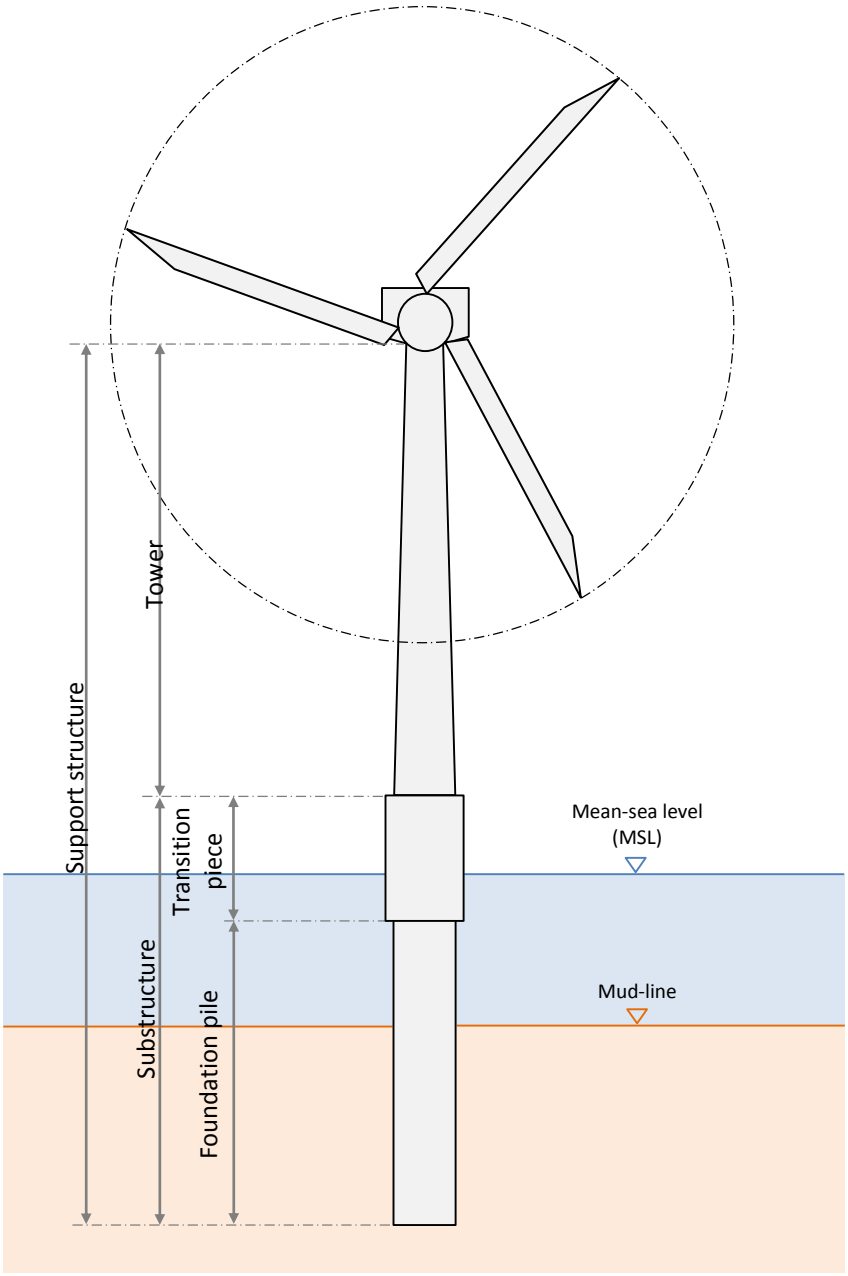

Figure 2.1: Representation of the different parts of an offshore wind turbine. Some of the terminology to be used in the rest of the thesis.

- Generator: Device that produces electricity from mechanical energy, in this case from the rotating turbine shaft.
- Nacelle: The structure at the top of the wind turbine tower just behind the wind blades. It houses the key components of the wind turbine, including the rotor, gearbox and generator.
- Pitch: The angle between the edge of the blade and the plane of the blades rotation. Blades are turned, or pitched, out of the wind to control the rotor speed.
- Rated wind speed: The wind speed at which the turbine is producing power at its rated capacity. The rated wind speed generally corresponds to the point at which the turbine can perform most efficiently.

- Rotor hub: The center of a turbine rotor, which holds the blades in place and attaches to the shaft. The rotor refers to both the turbine blades and the hub.
- Shaft: The rotating part in the center of a wind turbine that transfers power. A high-speed shaft drives the generator. A low-speed shaft is turned by a rotor at about 30 to 60 rpm.
- Substructure: Section of the support structure composed by the transition piece and the foundation, from the tower down to the seabed.
- Support structure: The base structure that supports and elevates the wind turbine rotor and nacelle.
- Tower: The top structural component of the support structure, from the transition nacelle down to the transition piece.
- Transition piece: The structural component of the support structure that connects the tower and the foundation. It is composed by a platform, ladder and boat landing.
- Yaw: The rotation of a horizontal-axis wind turbine around its tower or vertical axis.

The terms referring the different parts of the support structure in an offshore wind turbine are defined in Figure 2.1.

2.1.2. *Dimensions and Model Specifications*

The offshore wind turbine of this thesis with the U.S. Department of Energy's National Renewable Energy Laboratory (NREL) 5-MW turbine, as defined by Jonkman *et al.* (2009). This reference wind turbine will be used for the simulation because it provides standardized and accurate data for the properties of a realistically sized offshore wind turbine. The properties of this wind turbine model is shown in Table 2.1.

Table 2.1: Properties of the 5MW NREL wind turbine (Jonkman et al., 2009)

Wind Turbine Properties	
Rating	5 MW
Rotor Orientation, Configuration	Upwind, 3 blades
Control	Variable speed, Collective Pitch
Drivetrain	High speed, Multiple-stage Gearbox
Rotor, Hub Diameter	125.8 m, 3.0 m
Cut-in, Rated, Cut-out Wind Speed	3 m/s, 11.4, m/s, 25 m/s
Cut-in, Rated Rotor Speed	6.9 rpm, 12.1 rpm
Rated speed	80.0 m/s
Overhand, Shaft Tilt, Precone	5 m, 5°, 2.5°
Rotor Mass	110 000 kg
Nacelle Mass	240 000 kg

The support structure of the wind turbine is the offshore reference support structure defined by Jonkman *et al.* (2009) in the OC3 project, and it is constituted by a tower, substructure and foundation. The tower has different geometric properties along its height, with an outer base diameter of 6 m and a base thickness of 0.027 m, and an outer top diameter of 3.87 m and a top thickness of 0.019 m. Both diameter and thickness are assumed to be linearly tapered from base to top. The tower is connected to the substructure, which is constituted by a monopile with a constant diameter of 6 m and a constant thickness of 0.060 m.

The tower base begins at an elevation of 10 m above the mean-sea level until the tower top at an elevation of 87.60 m. The substructure extends from the tower base down to the base foundation, which is at 40 m below the mud-line, as can be shown in Figure 2.2.

Table 2.2: Geometrical dimensions of the support structure.

Support structure dimensions	
Total height of the support structure	147.6 m
Height of the submerged monopile	60 m
Height of the foundation	40
Height of the grouted part of monopile	70 m
Outer diameter of tower at bottom	6 m
Inner diameter of tower at bottom	5.946 m
Outer diameter of tower at top	3.87 m
Inner diameter of tower at top	3.832 m
Outer diameter of substructure	6 m
Inner diameter of substructure	5.88 m

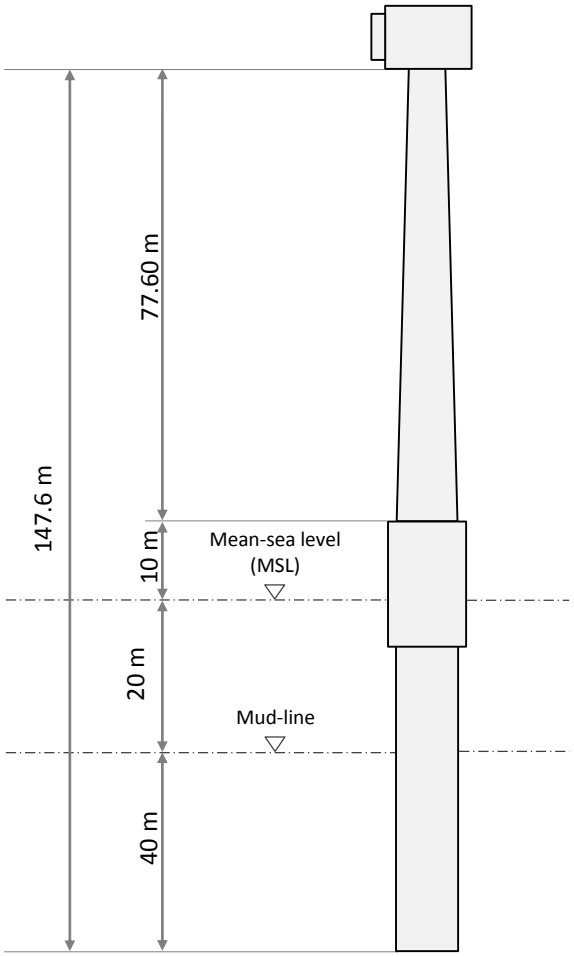

Figure 2.2: Dimensions of the offshore wind turbine.

The material used for the support structure is steel with a Young's modulus of 210 GPa and a shear modulus of 80.8 GPa. Taking into account the effect of paint, bolts, welds and flanges in the thickness, the mass density of steel is increased from 7850 kg/m^3 to 8500 kg/m^3.

The geographical location of the offshore wind turbine is a relevant factor to determine some environmental parameters, such as the soil properties. The North Sea is the location chosen due to the numerous investigations carried out in that location and used in the background of this thesis.

2.2. Limitations

The model used to develop and evaluate a novel approach for performing structural reliability analysis and robust design of offshore wind turbine support structures is based on a simplified model of a monopile structure. In other words, the complex behaviour of an offshore wind turbine is here simplified, making impossible to obtain the real response of the structure. Although that might be true, it should not be forgotten that the general methods used to simulate the response of a structure are, with more or less accuracy, approximations of this response. That said, the simplified model has been implemented by using the finite element method and the support structure has been simplified by using beam elements to represent the structure. Additionally, the analysis of the structure is not integrated, since the contribution of the rotor has been obtained from an external software. In conclusion, the different simplifications taken to define the simplified model have implied a limitation in this research due to the reduction in the real response of the structure that they suppose.

The time has been another limiting factor for several reasons. One of the objectives to implement a simplified model is to do the necessary calculations efficiently. Nevertheless, the finite element method requires choice between accuracy and computational cost, or in other words, time. In a practical sense this means that, by using the finite element method, it is necessary to select a determinate number of elements which provide enough accuracy in a reasonable time. Obviously, this is achieved with sufficient time, but the format of this research, a master's thesis, does not allow it, so it is required to reduce the accuracy of the model to save time.

On the other hand, the probability analysis raises a similar problem with regard to the time. This analysis is performed for a determinate number of samples, and this number of samples has to be large enough to ensure reliable results that give robustness to the probability analysis. The challenge, therefore, is similar to the one discussed in the previous paragraph, it is necessary to select a determinate number of samples which reduces the variance of the probability analysis, while maintaining a reasonable computational time. Furthermore, each sample implies a simulation of the simplified model, so the number of samples should also be taken into consideration when the time needed to perform each simulation is selected. To conclude, the number of samples required in the probability analysis is an important limitation in this thesis due to the significant amount time that will demand.

CHAPTER 3

Background and Literature Review

In this chapter, relevant background theory for the scope of this thesis will be presented. The information provided will give the necessary background for a good understanding of the objectives that will be investigated, the results obtained and the subsequent discussion.

3.1. Finite Element Method

The main objective of an engineer is always to analyse reality to extract the most relevant information and create a calculation model that allows study. All calculation models are based on a number of assumptions that simplify the object of the study without departing unduly from reality. Until recently, these calculation models were limited by the number of variables and elements that could be included because there were not the necessary tools for calculation. Now, with the advent of computers, the scope of these models is broadened.

The main drawback of models with discrete elements is the limitation in the representation of reality. The Finite Element Method (FEM) is a calculation tool that can represent an entire continuum, by grouping parts with similar properties and characteristics in elements of variable size. This increase of the number of elements and the variability of their size allow the use of differential equations associated to the problem studied. In this way, the loss of information when building the calculation model is reduced. For this reason it is possible to

say that the finite element method has been a breakthrough in the world of engineering, and particularly structural engineering.

The use of differential equations allows studying one-dimensional, two-dimensional and three-dimensional problems, as well their evolution in time. In particular, for the calculation of structures, different types of models can be used as, for instance, bar problems, 2D elasticity, plates and shells, solids of revolution, 3D models, fatigue or problems with heat fluxes. The only requirement is a precise knowledge of the constitutive equations and evolution over time.

3.1.1. Finite Element

In the FEM, the continuum is discretized in finite elements, which can be visualized as small portions of this continuum. The word finite distinguishes such a portion from the infinitesimal elements of differential calculus. The geometry of the continuum is considered to be formed by the assembly of a collection of non-overlapping domains with simple geometry termed finite elements. It is usually said that a mesh of finite elements "discretizes" the continuum (Figure 3.1). Since the exact analytical variation of such parameters is complex and generally unknown, the FEM only provides an approximation to the exact solution.

3.1.2. Deriving the General Equation of Motion

The principle of virtual work states that: "A structure is in equilibrium under a set of external loads if after imposing to the structure arbitrary (virtual) displacements compatible with the boundary conditions, the work performed by the external loads on the virtual displacements equals the work performed by the actual stresses on the strains induced by the virtual displacements" (Oñate, 2009).

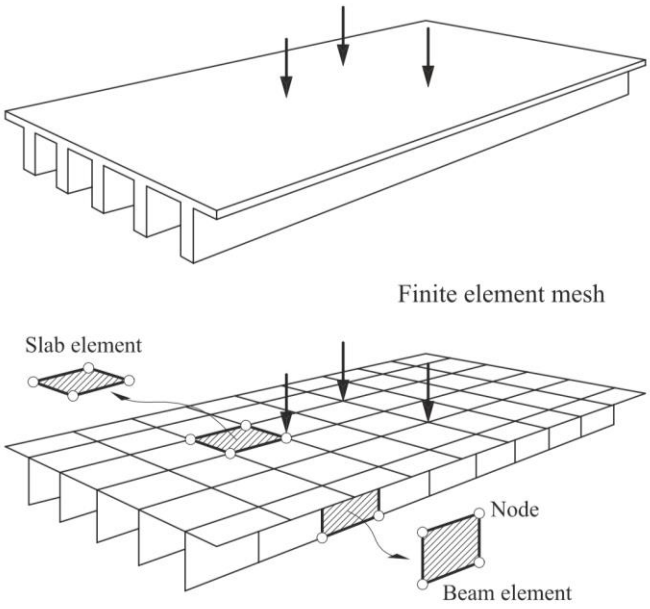

Figure 3.1: Discretization a bridge with finite elements (Oñate, 2009).

As shown by Cook *et al.* (2002), the principle of virtual work can be used to derive a general form of the equation of motion for a finite element discretized structural system. A virtual

displacement, δu, is called to any imagined small motion that satisfies essential boundary conditions and displacement continuity between elements. As shown in equation below, the equilibrium of work can be expressed for a single element of volume V and surface area S.

$$\int_V \{\delta u\}^T F_V dV + \int_S \{\delta u\}^T F_S dS + \sum_{i=1}^{n} \{\delta u\}_i^T p_i = \int_V [\{\delta u\}^T \rho \ddot{u} + \{\delta u\}^T c\dot{u} + \{\delta \varepsilon\}^T \sigma] dV \quad (3.1)$$

Where,

F_V: prescribed body forces
F_S: prescribed surface tractions
p_i: prescribed concentrated loads acting in the n corresponding virtual displacements $\{\delta u\}_i$
ρ: mass density
c: a viscous damping parameter.
$\{\delta \varepsilon\}$: strain associated with the virtual displacement $\{\delta u\}$

The finite element discretization of the continuous structure leads to the relationships below, where the generalized coordinates q are functions of time and the shape function matrix N depends on spatial position.

$$u = Nq \quad (3.2)$$

$$\dot{u} = N\dot{q} \quad (3.3)$$

$$\ddot{u} = N\ddot{q} \quad (3.4)$$

$$\epsilon = \frac{d}{dx} Nq = Bq \quad (3.5)$$

Substituting these relationships into the principle of virtual work, and assuming that the concentrated loads p_i act directly in nodes, would now provide,

$$\{\delta q\}^T \left(\int_V \rho N^T N dV \ddot{q} + \int_V c N^T N dV \dot{q} + \int_V B^T \sigma dV \right) - \{\delta q\}^T \left(\int_V N^T F_V dV + \int_S N^T F_S dS + \sum_{i=1}^{n} p_i \right) = 0 \quad (3.6)$$

From the last equation,

$$\int_V \rho N^T N dV = m \quad (3.7)$$

$$\int_V c N^T N dV = c \quad (3.8)$$

In these equations, the consistent element mass and damping matrices are m and c, respectively. Both matrices are called consistent because they are based on the same interpolation functions as the stiffness matrix, and because they result directly from finite element discretization. Therefore, it can be shown that both are symmetric and positive definite.

Equation 3.6 can be rearranged, to obtain two new vectors defined in Equations 3.9 and 3.10. r^{int} describes internal forces applied to the element by nodes to resist internal element stresses. r^{ext} describes external forces applied to nodes as a result of external loads acting on the element.

$$r^{int} = \int_V B^T \sigma dV \quad (3.9)$$

$$r^{ext} = \int_V N^T F_V dV + \int_S N^T F_S dS + \sum_{i=1}^{n} p_i \quad (3.10)$$

These relationships can be applied in general cases and can even be simplified in particular cases. For example, for a linearly elastic material, the internal force vector simplifies to $r^{int} = k \cdot q$, where k is the element stiffness matrix.

$$m\ddot{q} + c\dot{q} + kq = r^{ext} \quad (3.11)$$

By using the relationship between the element degrees of freedom and the global degrees of freedom, the global form of the equation of motion is found as:

$$M\ddot{Q} + C\dot{Q} + KQ = R^{ext} = F \quad (3.12)$$

Where M, C and K are the global mass, damping and stiffness matrices of the system, respectively. F represents the load projection into each degree of freedom and depends on time. The global generalized coordinates Q can be also expressed depending on time and describing the displacements of interest directly.

$$M\ddot{u}(t) + C\dot{u}(t) + Ku(t) = F(t) \quad (3.13)$$

The structural equation of motion can be expressed as matrices and vectors, where n is the total number of degrees of freedom used to discretize the system, and $u(t)$ represent the displacement along each degree of freedom.

$$\begin{bmatrix} M_{11} & M_{12} & \dots & M_{1n} \\ M_{21} & M_{22} & \dots & M_{2n} \\ \vdots & \vdots & \ddots & \vdots \\ M_{n1} & M_{n2} & \dots & M_{nn} \end{bmatrix} \begin{bmatrix} \ddot{u}_1(t) \\ \ddot{u}_2(t) \\ \vdots \\ \ddot{u}_n(t) \end{bmatrix} + \begin{bmatrix} C_{11} & C_{12} & \dots & C_{1n} \\ C_{21} & C_{22} & \dots & C_{2n} \\ \vdots & \vdots & \ddots & \vdots \\ C_{n1} & C_{n2} & \dots & C_{nn} \end{bmatrix} \begin{bmatrix} \dot{u}_1(t) \\ \dot{u}_2(t) \\ \vdots \\ \dot{u}_n(t) \end{bmatrix} + \begin{bmatrix} K_{11} & K_{12} & \dots & K_{1n} \\ K_{21} & K_{22} & \dots & K_{2n} \\ \vdots & \vdots & \ddots & \vdots \\ K_{n1} & K_{n2} & \dots & K_{nn} \end{bmatrix} \begin{bmatrix} u_1(t) \\ u_2(t) \\ \vdots \\ u_n(t) \end{bmatrix} = \begin{bmatrix} F_1(t) \\ F_2(t) \\ \vdots \\ F_n(t) \end{bmatrix} \quad (3.14)$$

The equation above is a system of coupled second-order ordinary differential equations in time because the equation is discretized in space, but the displacements and forcing are continuous in time. To solve this equation, one possible option is to discretize time and to use direct numerical time integration algorithms, such as the Newmark Method (Böker, 2009), to establish the structure response history.

3.2. Damping Effects

The lifetime of an offshore wind turbine is closely related to the damping ratio of the structure due to the importance of this parameter for the fatigue damage. The amplitude of vibrations is inversely proportional to the damping ratio. Consequently, an accurate value of the lifetime predictions of the structure will depend on a correct choice of the damping level of the structure (Devrient *et al.*, 2013). In the following subchapters, the damping contributions that are relevant for offshore wind purposes, namely, aerodynamic, soil and structural damping, will be described.

3.2.1. Aerodynamic Damping

Aerodynamic damping is an important parameter in the dynamics of offshore wind turbines since it constitutes a significant part of the total damping and, therefore, has a significant effect on the lifetime of the support structure. The reason why the aerodynamic damping has a large impact on the lifetime of the support structure is the reduction in fatigue that it produces. The effect of aerodynamic damping for an offshore wind turbine is essentially an aerodynamic force counteracting the motion of the tower top. In order to illustrate the effects of aerodynamic damping, ones can consider the motion of the tower top. Its forward motion will mean a small increase of wind speed experienced by the blade that will respond to it aerodynamically, giving a damping effect to the system. Consequently, an aerodynamic force will counteract the force motion of the tower top. In case of a backward motion of the tower top, the aerodynamic force will decrease, reducing the tower top motion. The counteracting

force is related to the velocity term of the system's equation of motion and is thus comparable to damping (Cerda and der Tempel, 2005).

The damping and, particularly, the aerodynamic damping will be dominating for the structural response when the turbine is in operation. So, the aerodynamic damping and the magnitude of the loading will have a prominent importance for the structural response to any excitation loads. The aerodynamic damping can be estimated analytically and numerically for constant speed turbines by a number of different methods. The following equations give an approximation of the damping term for a blade element and the aerodynamic damping ratio of the entire rotor, respectively.

$$c_{damping} = \frac{1}{2}\rho\Omega r c C_{L\alpha} \quad (3.15)$$

$$\xi_{aero} = \Omega(V_0)\frac{N_b \rho C_{L\alpha} m_{1b}}{4 M_0 \omega_n} \quad (3.16)$$

Where,

c_{aero}: damping constant for aerodynamic damping
ρ: density of air
Ω: rotational speed of the rotor
r: distance from the hub to the given point on the blade
c: = chord of the turbine blade
$C_{L\alpha}$: lift coefficient
ξ_{aero}: damping ratio for aerodynamic damping
N_b: number of blades on the turbine
$\Omega\ (V_0)$: rotational speed as a function of wind speed
m_{1b}: first order (static) moment of the area of the chord along the blade
M_0: modal mass
ω_n: natural frequency

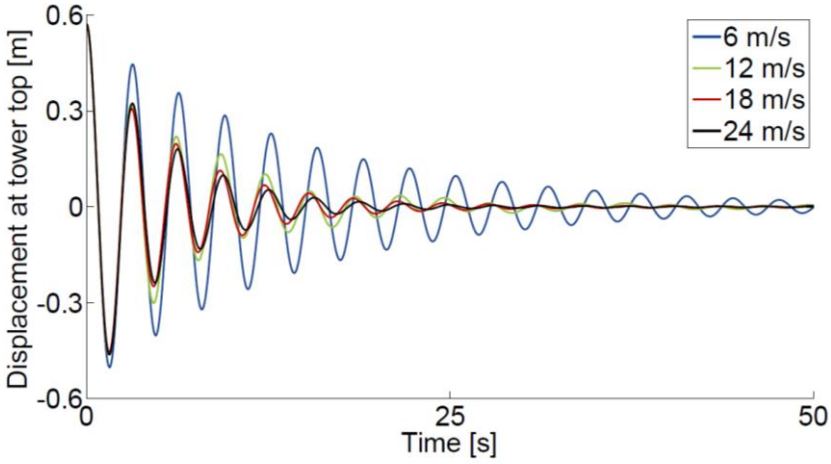

Figure 3.2: Examples of free vibration decays for four different wind speed (Schafhirt, 2014).

The Van der Tempel's method (Van der Tempel, 2006) can be used to obtain a theoretical estimation for the aerodynamic damping from time domain simulation results. In this case, the aerodynamic damping is obtained from the ratio between the change in thrust force and the change in wind speed normal to the rotor plane.

$$c_{damping} = \frac{T'}{dV_d} \quad (3.17)$$

$$\xi_{aero} = \frac{T'}{dV_d}\frac{1}{2M_0\omega_n} \quad (3.18)$$

Another option to obtain the aerodynamic damping more accurately could be by performing nonlinear time domain simulations in an aero-servo-hydro-elastic software. The transient decay of the free vibrations of the tower can give an estimation of the aerodynamic damping (Kühn, 2001). The response of a combined loading in terms of deflection of the tower is obtained by subjecting the wind turbine to loading from a turbulent wind field and a step pulse loading in a simulation. However, the results of this simulation are influenced by the stochastic nature of the turbulent wind field, therefore it is necessary to remove the stochastic part of the response to derive the damping. For this propose, it is assumed that linear superposition is valid. By performing a simulation with the same wind field but without the step pulse loading, the response of this simulation is subtracted from the simulation with the step pulse loading. As a result, the remaining part of the original response is regarded at the deterministic part of the response and the combined aerodynamic damping is determined by calculating the logarithmic decrement, δ, of *n* successive cycles of the deterministic response. Finally, the damping ratio is obtained as a function depending on the logarithmic decrement, δ.

$$\delta = \frac{1}{n} ln \frac{x_0}{x_n} \quad (3.19)$$

$$\xi = \frac{1}{\sqrt{1 + \left(\frac{2\pi}{\delta}\right)^2}} \quad (3.20)$$

As earlier pointed out, there are different damping contributions. If these contributions are known, the aerodynamic damping ratio can be determined by subtracting these ratios from the total damping ratio.

3.2.2. Structural Damping

The damping of the structure is the damping in the structural material and is related with the mechanic properties of the structure. This damping is usually studied as Rayleigh Damping in the form of:

$$[C] = \alpha[M] + \beta[K] \quad (3.21)$$

The above equation says that the global damping matrix is a linear combination of the mass and stiffness matrices (Langen and Sigbjörnsson, 1979). This linear combination depends on two parameters called mass coefficient (α) and stiffness coefficient (β).

The modal damping coefficient $\bar{c}_i$ can be expressed assuming that the mass matrix and the stiffness matrix have the orthogonality properties needed for expressing the mass and stiffness in terms of modal mass $\bar{m}_i$ and modal stiffness $\bar{k}_i$.

$$\bar{c}_i = \alpha \bar{m}_i + \beta \bar{k}_i \qquad (3.22)$$

Therefore, the damping ratio ξ_i can be expressed in terms of the natural frequencies of the modes of the structure ω_i.

$$\xi_i = \frac{\bar{c}_i}{2\bar{m}_i \omega_i} = \frac{1}{2}\left(\frac{\alpha}{\omega_i} + \beta \omega_i\right) \qquad (3.23)$$

Where,

$$\xi = \frac{1}{2}\frac{\alpha}{\omega} \quad \longrightarrow \quad Stiffness\ proportional$$
$$\xi = \frac{1}{2}\beta\omega \quad \longrightarrow \quad Mass\ proportional$$

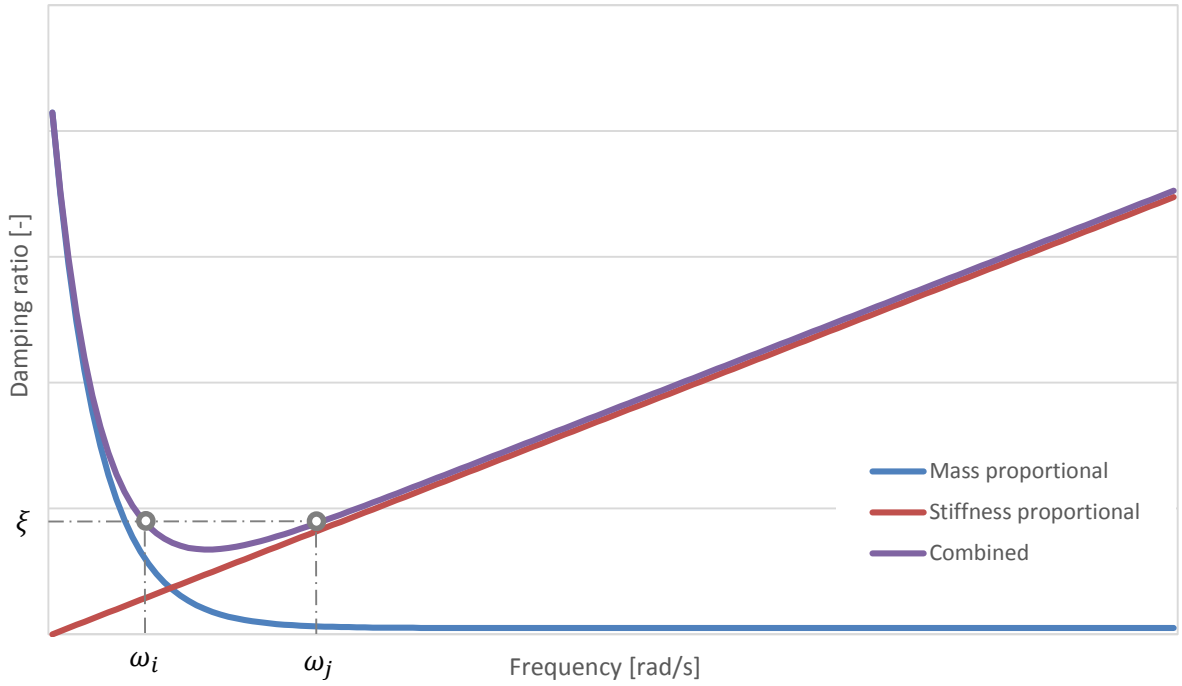

Figure 3.3: Proportional damping scheme.

As can be seen, the Rayleigh Damping is dependent on the natural frequency of the nodes and there is a relationship of proportionality between the level of the mode shapes and the mass/stiffness of the structure. The mass proportional damping will lead to damping of the lower mode shapes, whereas the stiffness proportional damping will be effective in damping the higher mode shapes.

3.2.3. Soil Damping

The soil is another source of damping due to the dissipation of energy from vibrations into the soil. As in the case of the structural damping, a portion of the soil damping comes from the material properties of the soil, the inner material damping. A second source of soil damping, the geometric damping, is related with the propagation of wave energy away from the foundation (Langen and Sigbjörnsson, 1979). The soil damping has an equivalent damping ratio of 2-5% for structures in the North Sea.

Due to dependence existing between the displacements of the foundation in the surrounding soil and the effect of the soil damping on the entire structure, it should be underlined that the damping effect of the soil and foundation depends on the dynamic response in the foundation (Tarp-Johansen *et al.*, 2009). Consequently, a low dynamic response of the foundation results in a low damping effect of the soil on the total dynamics of the structure.

3.3. Foundation

The foundation of an offshore wind turbine depends on the typology of substructure that has been used to support the wind turbine. There are different types of substructures, such as monopiles, gravity based structures, space frame structures or floating structures (Kallehave *et al.*, 2014). The substructure used in this study is a monopile, as mentioned earlier in Chapter 2. This type of substructure consists of a steel pile that is inserted into the sea bed and is the most common foundation used in waters under 20-25 meters. As a disadvantage, it cannot be used in waters more than 25 meters deep as it becomes unstable.

3.3.1. Soil Properties

The design of an offshore wind turbine requires a detailed knowledge of the properties of the seabed where the structure will be build. The seabed of the North Sea is composed, to a large extent, by layers of clay and sand. These types of soil are characterized in capacities of loose, medium, dense to very dense for sand, and soft, stiff to hard for clay. This characterization gives a first indication of the ability of the soil to carry loads (Zaaijer, 2000).

In-situ sampling and analysis of drilled samples in the laboratory can give a more detailed information about the state of the seabed. An important parameter of the soil conditions is the angle of internal friction, defined as the angle on the graph (Mohr's circle) of the shear stress and normal effective stresses at which failure occurs and determined in the laboratory by the Direct Shear Test or the Triaxial Stress Test.

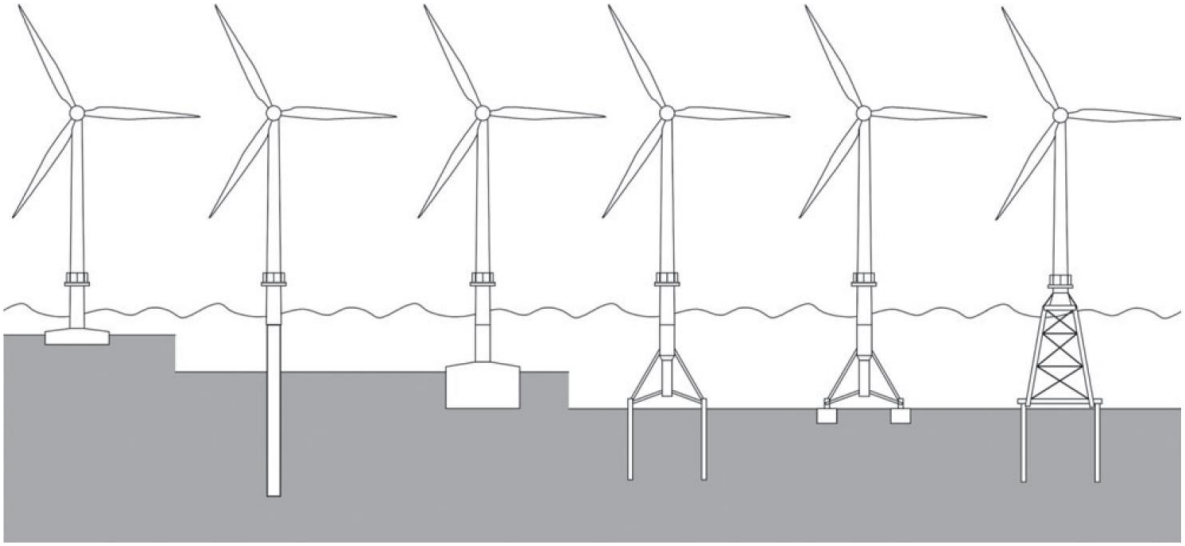

Figure 3.4: Some typical foundation concepts: Gravity-based foundation, monopile foundation, caisson foundation, multiple foundation, multi-caisson foundation and jacket foundation, from left to right respectively (Kallehave et al., 2014)

3.3.2. API p-y Method

The American Petroleum Institute (API) *p-y* method models soil-pile resistance using a series of non-linear springs along the length of the pile, where the deflection of a certain soil spring at position *x* below the mud-line is denoted by *y*. The soil-pile resistance *p* for sands based upon Winkler Foundation theory are defined below.

$$p = Ap_u \tanh\left(\frac{kx}{Ap_u}y\right) \quad (3.24)$$

Where,

$$A = \begin{cases} \left(3 - 0.8\frac{x}{b}\right) \geq 0.9 & for\ static\ loading \\ 0.9 & for\ cyclic\ loading \end{cases} \quad (3.25)$$

$$p_u = min\begin{cases} (C_1 x + C_2 b)\gamma' x \\ C_3 b\gamma' x \end{cases} \quad (3.26)$$

C_1, C_2, and C_3 are coefficients, k is the modulus of subgrade reaction determined as a function of φ' using correlations provided by API, b is the diameter of the pile and γ' is the submerged unit weight of the soil (API, 2005).

For large diameters there is a combination of soil stiffness overestimation at large depths and a very large bending stiffness typical of large diameters. As a result, there may lead to overestimation of pile-soil stiffness using the API *p-y* method for large-diameter piles. Although other models exists, this method is proven to be one of the most suitable for offshore wind design.

3.3.3. Foundation Modelling

Vertical loads, horizontal loads and moments must be transferred directly to horizontal soil reactions. The pile is free to rotate and translate because it is not fixed at the top. In the type of substructure selected, the pile must be long enough to mobilize enough soil over its length to transfer all loads and prevent displacements of the tip of the pile.

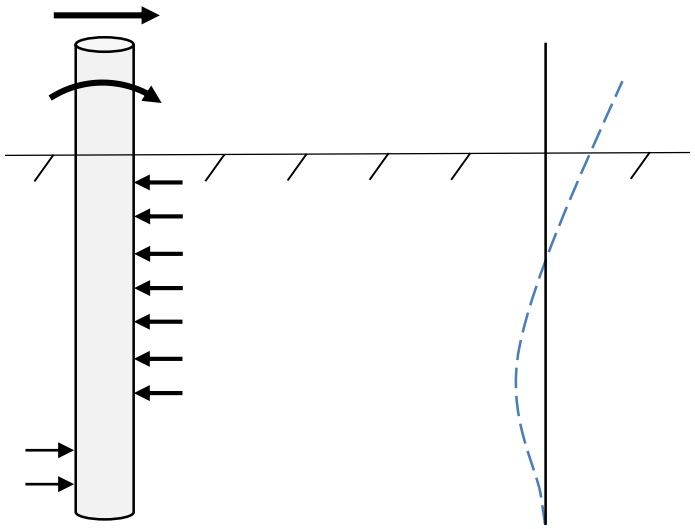

Figure 3.5: Transfer of horizontal loads and moments in monopile structures and a schematic representation of the pile deformation.

The soil reaction loads can be modelled using a set of soil springs with non-linear properties described in standards. This non-linear spring model can be created using the finite element method by coupling the non-linear spring model to the stiffness matrix of the structure. Although other models exists, this model is proven to be one of the most suitable for offshore wind design.

3.4. Environmental Conditions

3.4.1. Stochastic Processes

Offshore wind turbines are subjected to irregular external loads as they are excited by wind and waves. The generation of these loads is due to stochastic processes, so it varies with time and cannot easily be reproduced or predicted in advance. In order to analyse the data from these two variables, it is necessary to assume that both parameters can be modelled as stationary processes over a certain time period.

The wind process is assumed stationary for a period of 10 minutes, even if it is a quite fluctuating process. Wave requires a longer time period to assume it is stationary, three hours. This difference between both processes could be a problem when performing analysis, but in this study only the wind is used as an external load, so this problem will not be treated.

3.4.2. Time Domain

The response of offshore wind turbines varies in time because load also vary with time, so it is possible to analyse this response in the time domain. The analysis time series in the time domain contains information regarding mean, maximum and minimum values, standard deviation, strange peaks or slow variations of the process.

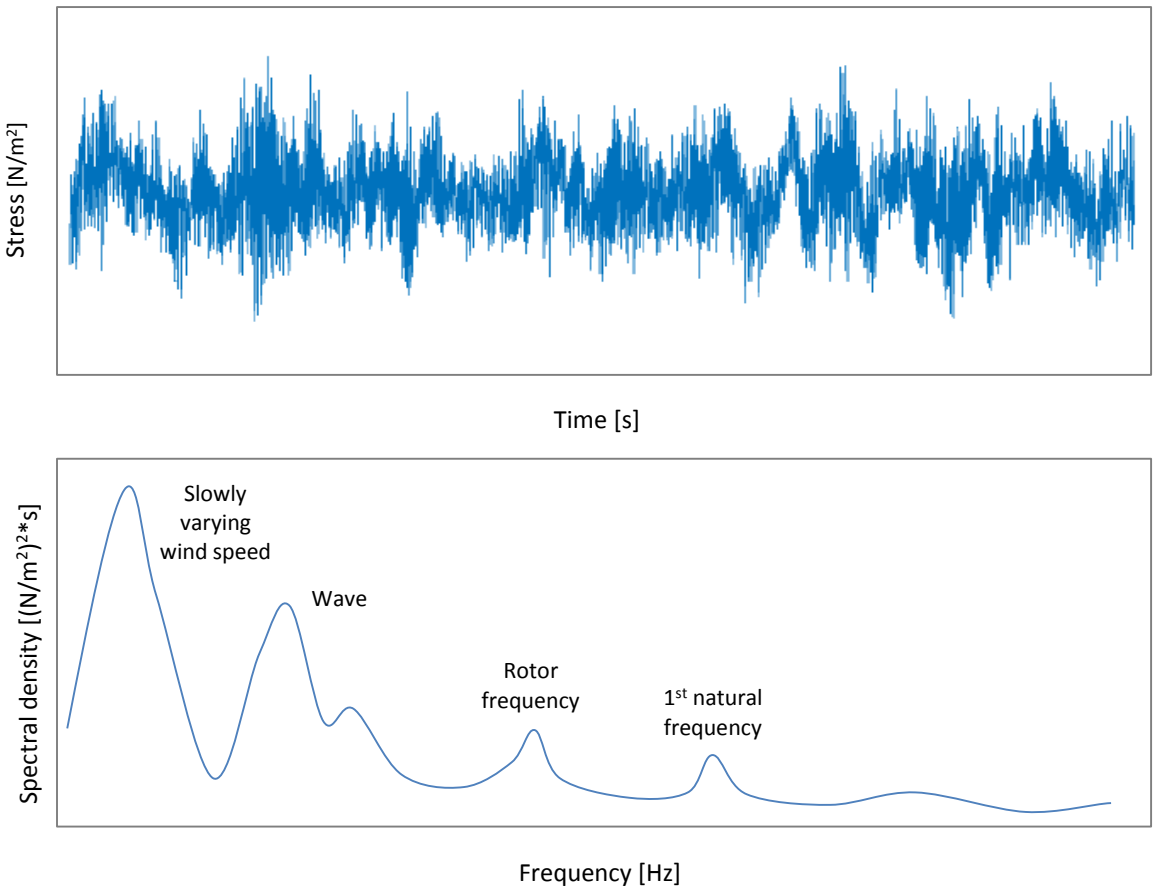

Figure 3.6: Representation of the time domain record of measured mud-line bending stress variation (top) and the frequency domain spectrum of the same time trace (bottom).

This information shall be sufficient to perform properly the different parts of this study, but it is interesting to explain that the time series can be transformed into the frequency domain to make the data more accessible, as can be seen in the Figure 3.6.

3.4.3. Wind

The wind conditions acting on a structure in the main wind direction are characterized by the mean wind speed and the fluctuating wind velocity. The total wind speed as a function of height and time is commonly described as the sum of a mean wind velocity as a function of height, and a turbulent component dependent on height and time.

$$V_{tot}(z,t) = V(z) + v(z,t) \qquad (3.27)$$

The mean velocity could be described by the Normal Wind Profile (NWP).

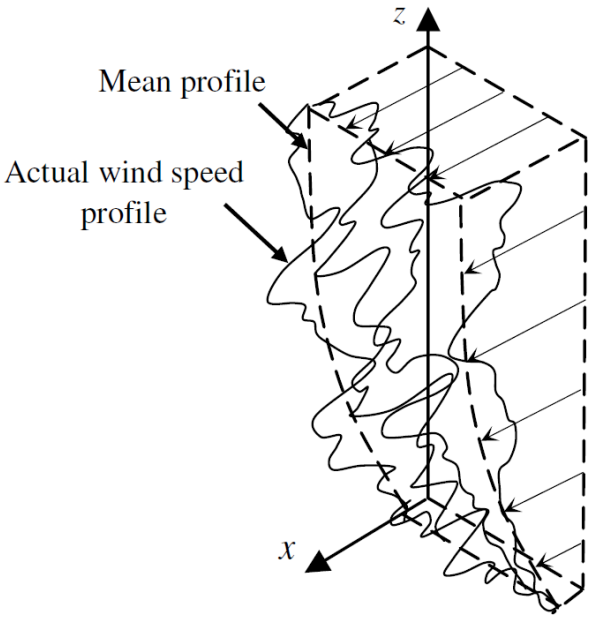

Figure 3.7: Superposition of the time dependent and mean wind velocities (Van der Tempel, 2006).

$$V(z) = V(z_{hub}) \cdot \left(\frac{z}{z_{hub}}\right)^{\alpha} \quad (3.28)$$

The exponent α is dependent on the surface roughness and has a recommended value of 0.12 for sites located offshore, a low value compared to onshore sites, where α has typically a value of 0.2 due to higher surface roughness (Böker, 2009).

Just as was started earlier, over a period of ten minutes the wind conditions are assumed to be stationary. Hence, the mean wind speed and standard deviation due to turbulence are defined over this period of time and there are different statistical options to describe these parameters. DNV (2010a) recommends the Kaimal turbulence spectrum for representation of the wind speed spectral density.

$$S_u(f) = \sigma_U^2 \frac{4\frac{L_k}{U_{10}}}{\left(1 + 6\frac{f \cdot L_k}{U_{10}}\right)} \quad (3.29)$$

3.5. Natural Frequencies and Dynamic Response

The resonance of a structure is an important factor to keep in mind due to the negative effect of this phenomena on the fatigue life. The response depends closely on the natural frequency of the first mode and the dynamic interaction with the external loads. On the other hand, the natural frequency of offshore wind turbines cannot be within the range of frequencies corresponding to the rotational frequency of the rotor, f_{1P}, and the blade-passing frequency,

f_{3P}. These frequencies are produced by rotor imbalances and aerodynamic impulse loads when the blades pass the tower. The natural frequency of the first mode needs to be between the f_{1P} and f_{3P} frequency ranges because the peak frequency of linear wave excitation is usually situated below the rotational frequency of the rotor (Kallehave, 2014), as can be seen in the following Figure 3.8.

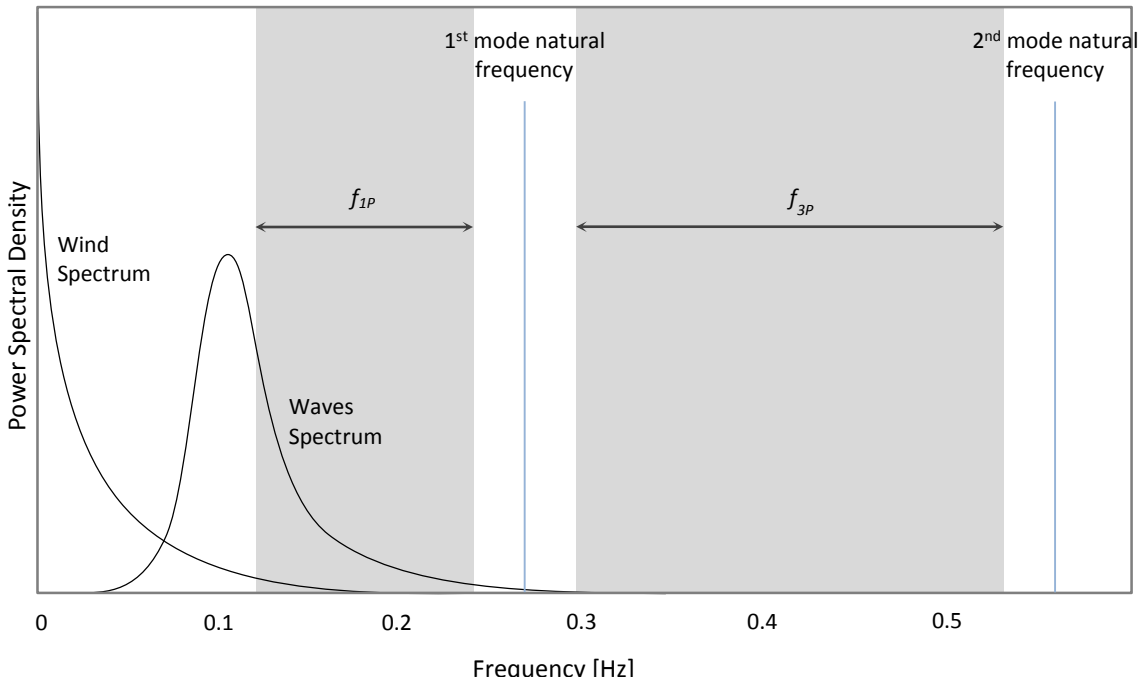

Figure 3.8: Illustration of the typical excitation ranges of a modern offshore wind turbine and the location of the 1st and 2nd mode natural frequencies.

The dynamic response of the structure, therefore, can be described as the dynamic amplification due to loads with a frequency close to the natural frequency of the structure. The natural frequency of the first mode would resonate with the waves at low wind speeds and be exposed to high spectral energy of waves during higher wind speeds. During operation of the turbine, the response of the first natural frequency due to loading acting orthogonal to the rotor plane will be low due to a rotor in operation provides a high degree of aerodynamic damping. Consequently, if the aerodynamic damping does not contribute during stand-still periods, the fatigue loading can become very severe. However, this consideration will not be taken into account in the study.

3.6. Fatigue Loading

Fatigue is a phenomenon associated with variable loading or more precisely to cyclic stressing or straining of a material. Thus fatigue loading is primarily the type of loading which causes variations in the applied stress or strain on a component, so any variable loading is basically a fatigue loading.

In structural perspective, fatigue loading produces fatigue damage, which is an important parameter to consider for the design of offshore wind turbines. Environmental loading, that is to say, loads form wind and waves are responsible for the main contributions to fatigue

loading. The mean value of these loads and the deviation of these loads from their mean value are of significance in a fatigue perspective.

3.6.1. Evaluation of Fatigue Damage

Fatigue damage may be calculated under the assumption of linear cumulative damage, which is done by the Palmgren-Miner rule. This method consists of the sum of the damage from each stress range in the stress history.

$$D = \sum_{i=1}^{k} \frac{n_i}{N_i} \qquad (3.30)$$

Where,

n_i: Number of cycles for each stress range *i*.
N_i: Constant amplitude endurance for the given stress range.

Failure due to fatigue will occur if the Palmgren-Miner sum is above 1 for the given stress history (Berge, 2006). In order to obtain the total number of stress cycles before failure, an S-N curve is used for this propose.

$$\log(N) = \log(\bar{a}) - m \cdot \log\left(\Delta\sigma\left(\frac{t}{t_{ref}}\right)^{k}\right) \qquad (3.31)$$

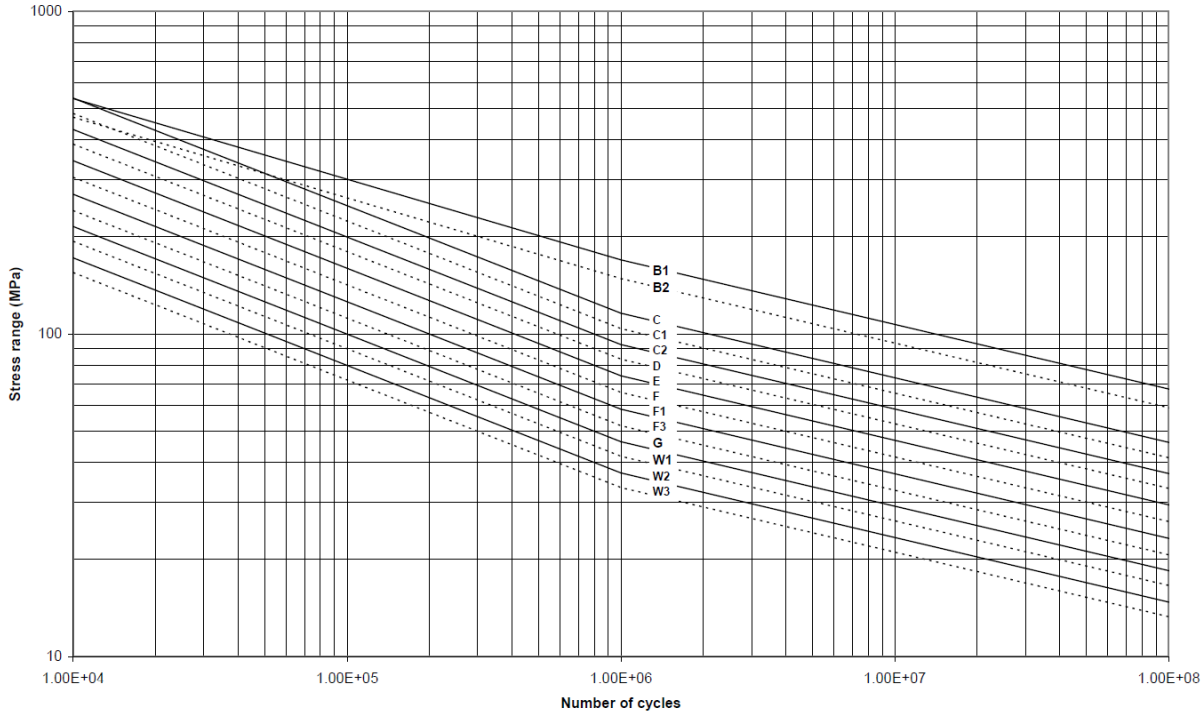

Figure 3.9: SN-curves for steel in seawater with catholic protection (DNV, 2012).

The mathematical formulation of the S-N curve is expressed by the equation above, where $\log(\bar{a})$ is the intercept of the $\log(N)$ axis, m is the negative inverse slope of the S-N curve, $\Delta\sigma$ is the stress range, t and t_{ref} are the ratio between the thickness in the expected direction of crack propagation and the reference thickness, and finally k is the thickness exponent on fatigue strength.

The number of cycles to be counted from the stress time history can be obtained using several methods such as crossing counting, peak counting, simple counting or rainflow counting. However, rainflow counting is generally considered as the most suitable of these method due to the fact that this counting procedure, for wide-banded loading, produces the same stress-strain loops as a material undergoing the same loading history (Almar-Næss, 1985).

3.7. Probabilistic Analysis

3.7.1. Models of Uncertainty

The modeling of uncertainty is an important point in the formulation of structural problems of offshore wind turbines. There are several mathematical models of uncertainty when dealing with structural design problems, such as the probabilistic model. Stochastic randomness is the most common model for uncertainties in structural engineering (Doltsinis, 1999). In this analysis, there is uncertainty associated with the value of some parameters. On the one hand, uncertainty on the load side is based on the stochastic variation of the environmental forces; and, on the other hand, there is uncertainty on some system parameters as the degree of damping or the soil stiffness.

A probability distribution of a random variable is a mathematical function that assigns the probability of occurrence to each measurable subset of the possible outcomes of a random experiment. The probability distribution is defined over the set of events and each event is the range of values of the random variable. The probability distributions are related to the frequency distribution. In fact, the probability distribution can be imagined as a theoretical frequency distribution. Theoretical frequency distribution is a probability distribution which describes how the results should change. Since these distributions deal with the expectation that something happens, these models are useful to make inferences and decisions regarding uncertainty (Badii *et al.*, 2007).

The probability density function and cumulative distribution function are used to define the occurrence properties of uncertain quantities which are random in nature. The statistical description of a random variable X can be completely described by a cumulative density function $F_X(x)$ or probability density function $f_X(x)$, as given by,

$$F_X(x) = P(X \leq x) = \int_{-\infty}^{x} f_X(x)dx \qquad (3.32)$$

Associated with the probability distribution are some parameters used to describe how the variables are distributed, the statistical moments. The most common statistical moments are the first and second moment, known as mean value $\mu(X)$, also referred to as expected value

and denoted by $E(X)$, and variance denoted by $Var(X)$ or $\sigma^2(X)$, respectively. These two statistical parameters are defined below.

$$Mean: \quad \mu(X) = E(X) = \int_{-\infty}^{\infty} x dF_X(x) = \int_{-\infty}^{\infty} x f_X(x)\, dx \tag{3.33}$$

$$\begin{aligned} Variance: \quad \sigma^2(X) &= \int_{-\infty}^{\infty} \big(x - \mu(X)\big)^2 \, dF_X(x) \\ &= \int_{-\infty}^{\infty} \big(x - \mu(X)\big)^2 f_X(x) dx \end{aligned} \tag{3.34}$$

Log-normal, Weibull and uniform are the probability distributions most commonly used in structural engineering. Additionally, the coefficient of variation (CV) will be defined since it a standardized measure of the dispersion of a probability distribution and it will be useful in the data analysis of the results.

$$c_v = \frac{\sigma}{\mu} \tag{3.35}$$

3.7.1.1. Normal and Log-Normal Distributions

The normal or Gaussian distribution is a very common continuous probability distribution because many natural phenomena are often approximated by this distribution. The density function of this probability distribution is defined below.

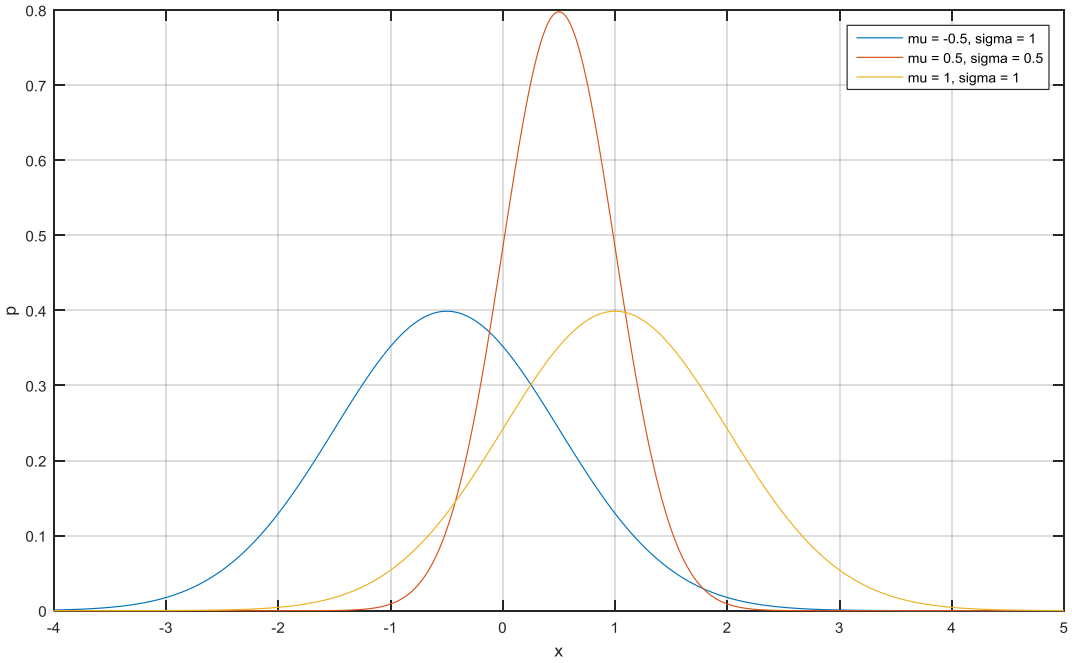

Figure 3.10: Some normal density functions with different mean and standard deviation.

$$f(x;\mu,\sigma) = \frac{1}{\sigma\sqrt{2\pi}} e^{-\frac{(x-\mu)^2}{2\sigma^2}} = \frac{1}{\sigma}\varphi\left(\frac{x-\mu}{\sigma}\right) \quad (3.36)$$

Where,

$$\varphi(x) = \frac{1}{\sqrt{2\pi}} e^{-\frac{1}{2}x^2} \quad (3.37)$$

The density function is defined by $\varphi(x)$, and the graph of this density function has a bell shape and is symmetric about its mean. The term Gaussian bell curve is used to refer to the curve observed in the graph, as it can be seen in the Figure 3.10.

The log-normal distribution is another continuous probability distribution of a random variable whose logarithm is normally distributed. In order to model a variable as log-normal, it is required that the variable is the multiplicative product of many independent random variables, each of which is positive. The central limit theorem in the log domain justifies this criteria. The density function of this probability distribution is defined below.

$$f(x;\mu,\sigma) = \frac{1}{x\sigma\sqrt{2\pi}} e^{-\frac{(In(x)-\mu)^2}{2\sigma^2}} \quad (3.38)$$

In the Figure 3.11 it can be seen the shape of the curve obtained with the log-normal distribution function defined above.

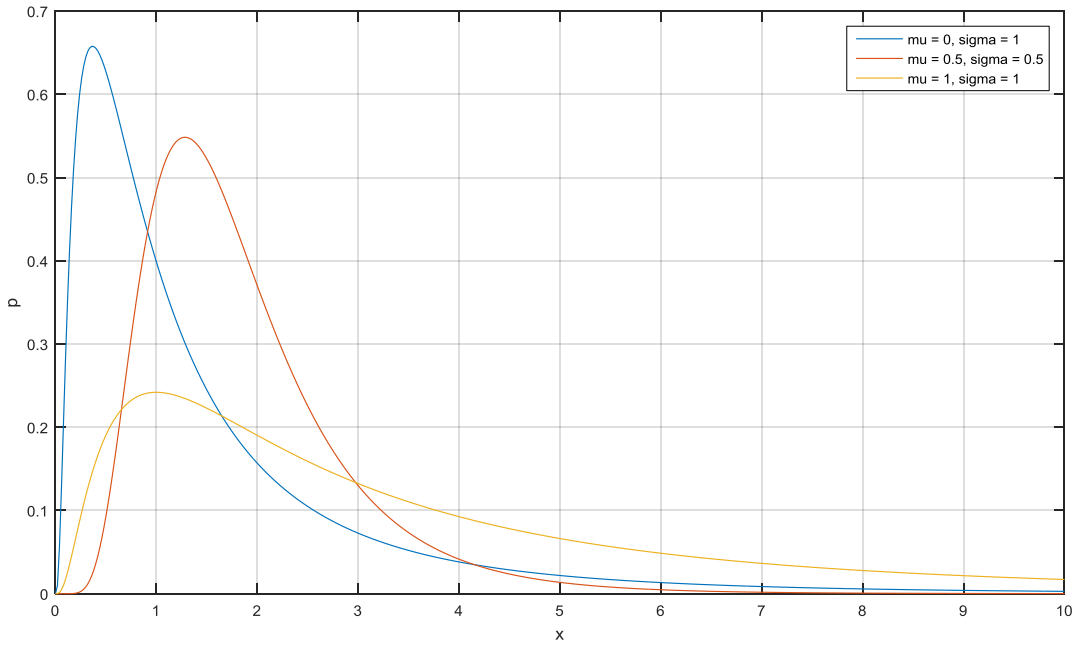

Figure 3.11: Some log-normal density functions with different mean and standard deviation.

3.7.2. Reliability Analysis

In structural reliability theory, uncertainties in, for instance, system parameters and in environmental loads are treated in a rational way. Structural engineering with a deterministic approach design is based on specified minimum material properties and specified load intensities. Furthermore, stresses and deflections follow a certain procedure of calculation that is often prescribed in deterministic based codes. However, it has been recognized that this deterministic thinking involves a high degree of uncertainty. The uncertainties mentioned combined with several similar forms of uncertainty result in an uncontrolled risk. Moreover, deterministic design leads to very expensive and conservative designs because it is required a too high safety level due to not handling uncertainties properly. Therefore, the deterministic approach poses a serious issue because a real measure of the safety or reliability of the structure is not obtained.

In modern structural reliability theory it is manifestly recognized that some risk of structural failure must be accepted. A probabilistic model is a suitable approach to obtain some measure of this risk, that is to say, the probability of failure. This approach allows to design a structure with an acceptable level of failure probability during the lifetime of the structure.

The basic structural reliability problem is going to be considered to illustrate this theory. Consider now only one load effect S resisted by one resistance R. Each parameter is described by a known probability density function, f_S and f_R respectively, and both R and S are expressed in the same units.

The safety of a structural element will be the unique consideration taken. The structural element will be considered to reach failure if the resistance *R* is less than the stress resultant *S* acting on the structural element. The probability of failure of the structural element p_f can be stated with the following equation (Melchers, 1999):

$$p_f = P(g(R,S) \leq 0) \qquad (3.39)$$

Where g is termed the limit state or performance function and the probability of failure is identical with the probability of limit state violation. The Equation 3.39 can be adapted to a probabilistic model to obtain the probability of failure for the number of samples considered in the analysis. The statistical description of the failure of the performance functions $g_i\ (i = 1,2,\dots,n)$ requires a reliability analysis. Prior to the reliability analysis, the statistical characteristics of the random quantities are first defined using the tools explained in the previous section, that is, by suitable probability distributions. Then the probability of failure is evaluated by numerically stable and affordable procedures. Numerically stable and affordable procedures are then used to evaluate the probability of failure.

There are several methods developed with the aim of obtaining the probability integration in the structural reliability analysis (Rackwitz, 2001). In the direct Monte Carlo simulation or Importance Sampling method, the probability of failure is derived from the test data of a large amount of samples. Conversely, in the First Order Reliability Method (FORM), the Second Order Reliability Method (SORM) or the Advanced Mean Value method, an additional nonlinear constrained optimization procedure is required for locating the Design Point or Most Probable Point of failure (MPP) and thus the reliability based design optimization

becomes a two-level optimization process with lengthy calculations of sensitivity analysis in the inner loop for locating the MPP.

3.7.3. Robust Design

Robust design is an engineering methodology for optimal design of products and process conditions that are less sensitive to system variations. The structural performance is required to be less sensitive to the random variation induced in the different stages of the structural service life cycle. Robust design has been recognized as an effective design method to improve the quality of the product/process (Taguchi, 1993).

Structural performance, for design optimization problems, defined by design objectives or constraints may be subject to large scattering at different stages of the service life-cycle. In structures with nonlinearities, it is expected that this fact might be more critical. The scattering mentioned may significantly worsen the structural quality and cause deviations from the desired performance. Additionally, the structural life-cycle costs, including inspection, repair and other maintenance costs, can be increased due to such scattering. Excessive variations in the structural performance indicate a poor quality of the product, which raises the necessity of structural robust design. A first option to decrease the scattering of the structural performance is to reduce or even eliminate the scattering of the input parameters. This may be impossible in a practical sense or it may result in an excessive increase of the total costs of the structure. On the other hand, another way is to find a design in which the structural performance is less sensitive to the variation of parameters, but without eliminating the cause of parameter variations, that is to say, by performing a robust design.

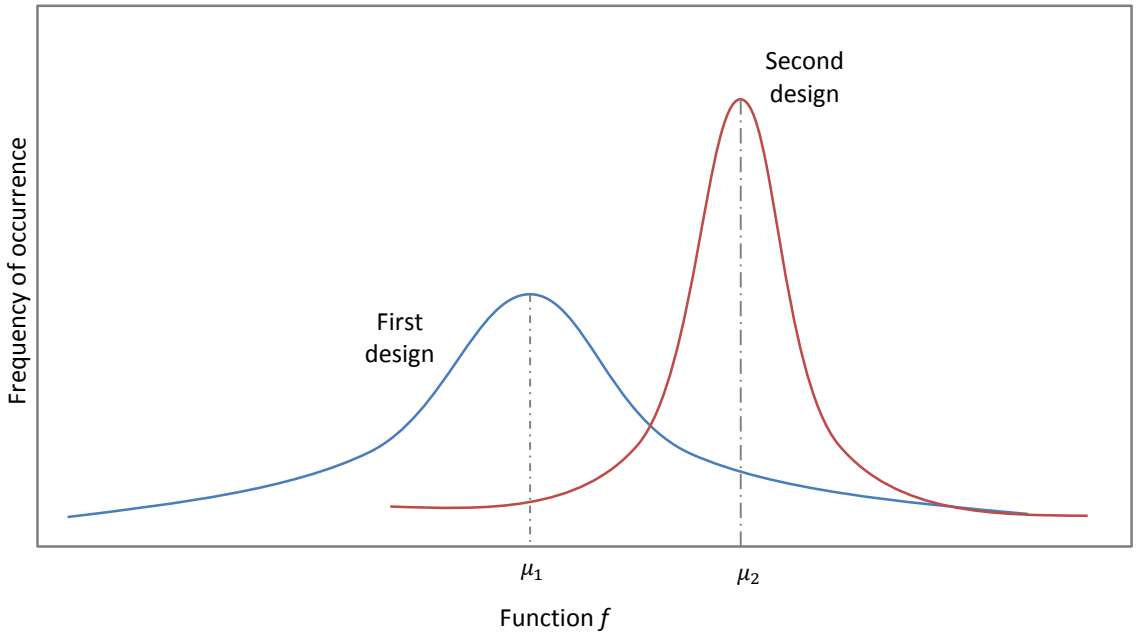

Figure 3.12: Concept of robust design.

To illustrate the concept of robustness, the Figure 3.12 is presented, where the value of a structural performance function f is represented in the horizontal axis, and the occurrence frequency of the value of f is represented in the vertical axis. As objective function, the function f is required to be minimized. The two curves correspond to two individual designs

with the system parameters randomly perturbed from the nominal values. The values of μ_1 and μ_2 represent, respectively, the mean values of the performance function f for the two designs. Based on the objective function explained before, the first design is more appropriate because it presents a smaller mean value of the performance function. From the robustness perspective, however, the second design is preferable because it is much less sensitive to variations in the uncertain system parameters.

The structural robust design, therefore, raises that the merit or quality of a design is justified not only by the mean value but also by the variability of the structural performance. One way to optimize the design of structures with stochastic parameters is to define the optimality conditions of the problems on the basis of expected function values. The task of robustness of the design stems from the fact that the design which minimizes the expected value of the objective function as a measure of structural performance may be still sensitive to the fluctuation of the stochastic parameters.

CHAPTER 4

Methodology

The methods and models used to reach the main objectives of this thesis are described in the following subchapters. First, the finite element model used to solve the transient dynamics of a beam is described in detail. The following is an explanation of the methods used to obtain the damping effects, soil stiffness and environmental loads. Finally, the probabilistic analysis and the fatigue approach on the offshore wind turbine are described. The offshore wind turbine defined in Chapter 2, Scope and Limitations, is used for all the analyses.

4.1. Finite Element Modelling

One of the first challenges of this thesis is to implement a simplified model as a time-domain simulation in MATLAB, which is able to solve the transient dynamics of a beam, and that will allow for doing the calculations efficiently.

4.1.1. Three-Dimensional Beam

The point of implementing a simplified model is to reduce the computational cost of a complex system. The probabilistic analysis requires the simulation of an important number of samples, so it is necessary to create a simplified model that is able to perform the probabilistic analysis in a reasonable amount of time.

Given these considerations, the simplified model used is composed by three-dimensional beams, where the proposed element for this study is comprised of 2 nodes and 6 degrees of freedom (dof) per node, with constant cross-section, shear deformation effects and rotatory inertia. This type of element allows displacements and rotations in three directions, so its behaviour is appropriate for the study of a support structure of an offshore wind turbine.

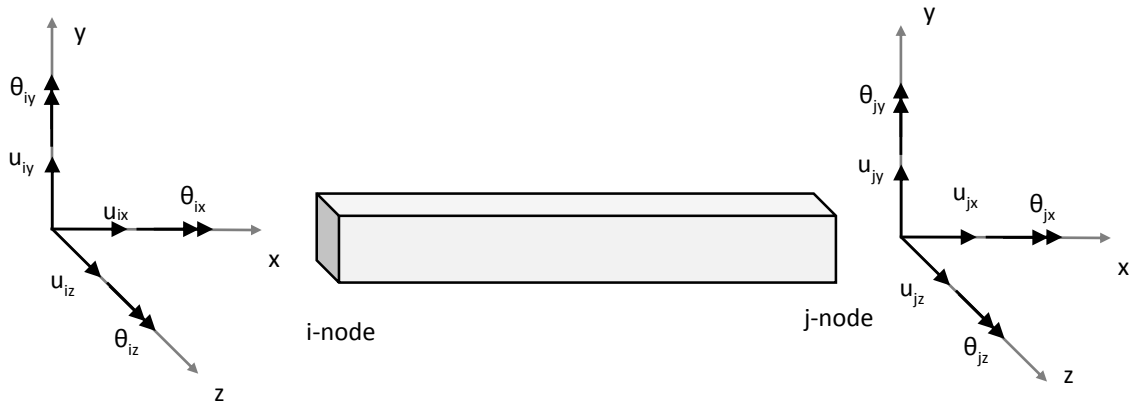

Figure 4.1: Beam segment of a space frame showing displacements and rotations at the nodal coordinates.

Detailed below are the main characteristics of the described model that allows to perform properly the finite element model.

4.1.1.1. Element Stiffness Matrix

Given the theory about the finite element method previously referred to in the Chapter 3, for linear isotropic materials the constitutive relation can be written as function of the material properties and the strains. In this case, this relation will be analysed for an element with the properties described in the previous section.

$$\sigma = DBa^{(e)} \tag{4.1}$$

Where,

D: Matrix of mechanical properties or constitutive matrix
B: Deformation matrix
$a^{(e)}$: Vector of nodal displacements

From the principle of virtual work for an isolated element, the internal work can be obtained and written in matrix form as follows:

$$W_{int} = \int_{l^{(e)}} \delta\varepsilon^T \sigma \, dx \tag{4.2}$$

Where,

$$\delta\varepsilon^T = \left[\delta a^{(e)}\right]^T B^T \quad (4.3)$$

Substituting the previous relationship and the constitutive relation into the internal work would now provide:

$$\int_{l^{(e)}} \left[\delta a^{(e)}\right]^T B^T DB a^{(e)}\, dx = \left[\delta a^{(e)}\right]^T \left(\int_{l^{(e)}} B^T DB\, dx\right) a^{(e)} \quad (4.4)$$

The local element stiffness matrix and the vector of nodal displacements for the element studied are then obtained as:

$$K^{(e)} = \int_{l^{(e)}} B^T DB\, dx \quad (4.5)$$

$$a^{(e)} = \left\{u_{1x}\ u_{1y}\ u_{1z}\ \theta_{1x}\ \theta_{1y}\ \theta_{1z}\ u_{2x}\ u_{2y}\ u_{2z}\ \theta_{2x}\ \theta_{2y}\ \theta_{2z}\right\} \quad (4.6)$$

The shear deformation effects are taken into account through the transverse deformation of the beam with shear and bending strains, which may be separated into a portion related to shear deformation and a portion related to bending deformation. This contribution has been introduced in the model with the following parameter, which gives the relative importance of the shear deformations to the bending deformations.

$$\Phi_y = \frac{12EI_y}{G\left(\frac{A}{\alpha}\right)L^2} \quad (4.7)$$

$$\Phi_z = \frac{12EI_z}{G\left(\frac{A}{\alpha}\right)L^2} \quad (4.8)$$

Finally, after some calculations the local stiffness matrix for the element shown in Figure 4.1 is obtained.

$$K^{(e)} = \begin{bmatrix} \frac{EA}{L} & & & & & & & & & & & \\ 0 & \frac{12EI_z}{L^3\beta_y} & & & & & & & & & & \\ 0 & 0 & \frac{12EI_y}{L^3\beta_z} & & & & & & SYM & & & \\ 0 & 0 & 0 & \frac{GJ}{L} & & & & & & & & \\ 0 & 0 & -\frac{6EI_y}{L^2\beta_z} & 0 & \gamma_z\frac{EI_y}{L} & & & & & & & \\ 0 & \frac{6EI_z}{L^2\beta_y} & 0 & 0 & 0 & \gamma_y\frac{EI_z}{L} & & & & & & \\ -\frac{EA}{L} & 0 & 0 & 0 & 0 & 0 & \frac{EA}{L} & & & & & \\ 0 & \frac{12EI_z}{L^3\beta_y} & 0 & 0 & 0 & \frac{-6EI_z}{L^2\beta_y} & 0 & \frac{12EI_z}{L^3\beta_y} & & & & \\ 0 & 0 & -\frac{12EI_y}{L^3\beta_z} & 0 & \frac{6EI_y}{L^2\beta_z} & 0 & 0 & 0 & \frac{12EI_y}{L^3\beta_z} & & & \\ 0 & 0 & 0 & -\frac{GJ}{L} & 0 & 0 & 0 & 0 & 0 & \frac{GJ}{L} & & \\ 0 & 0 & -\frac{6EI_y}{L^2\beta_z} & 0 & \eta_z\frac{EI_y}{L} & 0 & 0 & 0 & \frac{6EI_y}{L^2\beta_z} & 0 & \gamma_z\frac{EI_y}{L} & \\ 0 & \frac{6EI_z}{L^2\beta_y} & 0 & 0 & 0 & \eta_y\frac{EI_z}{L} & 0 & -\frac{6EI_z}{L^2\beta_y} & 0 & 0 & 0 & \gamma_y\frac{EI_z}{L} \end{bmatrix} \quad (4.9)$$

The different parameters that compose the local stiffness matrix of the Equation 4.9 are detailed in the Appendix A.1.

4.1.1.2. Element Mass Matrix

The way to obtain the element mass matrix is analogous to the procedure followed in order to obtain the element stiffness matrix. In this case, however, the analysis is based on the external work of the inertial forces and, after modifications, the following relationship is obtained:

$$\begin{aligned} W_{ext} &= -\int_{l^{(e)}} \left[\delta a^{(e)}\right]^T B^T \rho B \ddot{a}^{(e)}\, dx \\ &= -\left[\delta a^{(e)}\right]^T \left(\int_{l^{(e)}} B^T \rho B\, dx\right) \ddot{a}^{(e)} \end{aligned} \quad (4.10)$$

The local element mass matrix is then expressed as:

$$M^{(e)} = \int_{l^{(e)}} B^T \rho B\, dx \quad (4.11)$$

The shear deformation effects are introduced in the element mass matrix using the parameters Φ_y and Φ_z defined above. Additionally, the rotatory inertia has been taken into account introducing the radius of gyration.

$$r_y = \sqrt{\frac{I_y}{A}} \quad (4.12)$$

$$r_z = \sqrt{\frac{I_z}{A}} \quad (4.13)$$

Finally, after some calculations the local mass matrix for the element is obtained as can be seen bellow.

$$M_{el} = \begin{bmatrix} 1/3 & & & & & & & & & & & \\ 0 & a_z & & & & & & & & & & \\ 0 & 0 & a_y & & & & & & & SYM & & \\ 0 & 0 & 0 & \frac{J}{3A} & & & & & & & & \\ 0 & 0 & -c_y & 0 & e_y & & & & & & & \\ 0 & c_z & 0 & 0 & 0 & e_z & & & & & & \\ 1/6 & 0 & 0 & 0 & 0 & 0 & 1/3 & & & & & \\ 0 & b_z & 0 & 0 & 0 & d_z & 0 & a_z & & & & \\ 0 & 0 & b_y & 0 & -d_y & 0 & 0 & 0 & a_y & & & \\ 0 & 0 & 0 & \frac{J}{6A} & 0 & 0 & 0 & 0 & 0 & \frac{J}{3A} & & \\ 0 & 0 & d_y & 0 & f_y & 0 & 0 & 0 & c_y & 0 & e_y & \\ 0 & -d_z & 0 & 0 & 0 & f_z & 0 & -c_z & 0 & 0 & 0 & e_z \end{bmatrix} \quad (4.14)$$

As with the local stiffness matrix, the different parameters that compose the local mass matrix of the Equation 4.14 are detailed in the Appendix A.2.

4.1.1.3. Element Damping Matrix

The damping matrix have been calculated using the Rayleigh proportional damping as a linear combination of the mass and stiffness matrices. This method to get the damping can be applied to a singular element of the finite element model, obtaining the element damping matrix as a linear combination of the element mass and element stiffness matrices.

$$C^{(e)} = \alpha M^{(e)} + \beta K^{(e)} \quad (4.15)$$

As can be seen in the equation above, the element damping matrix depends on the mass coefficient (α) and stiffness coefficient (β). This two parameters depends on the different damping contributions taken into account in this study, and their values will be described on the following chapters.

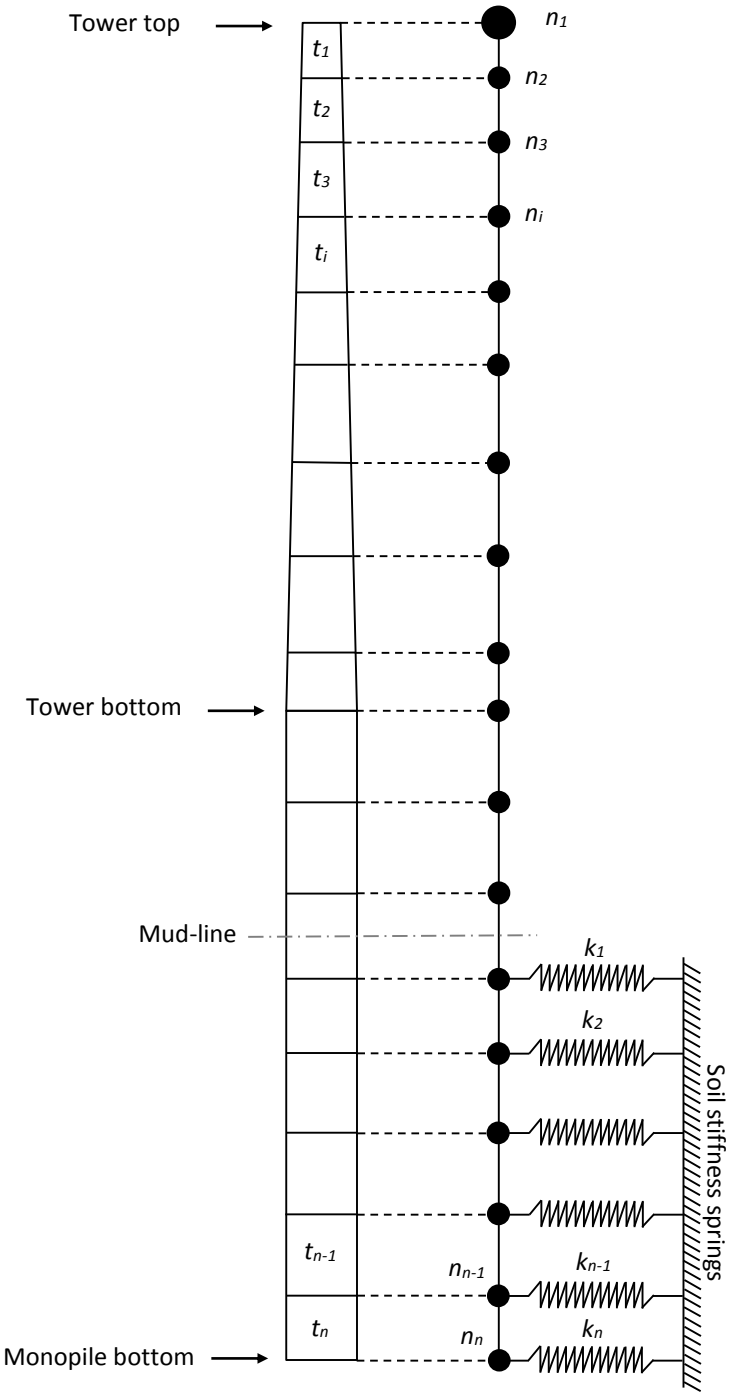

Figure 4.2: Schematic representation of the support structure and the finite element model, with lateral springs under the mud-line where they represent the soil stiffness.

4.1.2. Discretization

The discretization of the support structure is the modelling process of the body of the structure consisting in the equivalent division of itself in a system conformed by smaller bodies, which are called finite elements. These are interconnected through common points or nodes, which form surfaces that behave as independent control volumes. The finite element analysis does not attempt to solve the problem as if it were a single piece, but rather the body

is subdivided into a finite number of elements which in turn give individual results that finally merge to create a single solution.

The support structure defined in Chapter 2 has been discretized taking into account the main objectives of this study. The accuracy of the FEM depends on the number of elements used on the analysis, where a large number of elements implies a large accuracy, but at the same time a large computational cost. For this reason, the structure have been treated differently depending on the importance of each part of the structure.

4.1.2.1. Number of Elements

The tower has different geometric properties along its height, so it is necessary a minimum number of elements to observe the contribution of this variance on the results of the finite element model. Furthermore, a segment of the foundation, from the mud-line to the bottom of the monopile, has an important function since it introduces the contribution of the soil stiffness in the model. The soil is modeled as a series of linear lateral springs, which represents the stiffness of the soil at different sections. In order to form a unified stiffness matrix of both soil and structure, these sectional soil stiffness matrices are added to the structural stiffness matrix of the support structure.

The distribution of selected elements for each section of the support structure can be seen below.

Table 4.1: Number of elements for each part of the support structure discretized.

Structural section	Number of elements
Tower	11
Bottom tower to mud-line	3
Below mud-line	40

4.1.2.2. Rotor Mass

The mass matrix defined above is based on the properties of the support structure of the offshore wind turbine. Nevertheless, rotor and nacelle have a significant mass that must be taken into account. To achieve that, the rotor and nacelle mass has been added to the FE model in the same way as the soil stiffness, that is to say, adding the sectional mass matrix of the turbine to the structural mass matrix in the tower top element of the structure.

4.1.3. Boundary and Load Conditions

The boundary conditions of the structure can be divided into two different groups, the ones regarding to the lower part of the foundation pile and the linear lateral springs added to the foundation to simulate the contribution of the stiffness of the soil.

The lowest part of the foundation pile has been designed as a three-dimensional mobile articulate support, so at this point the movements are allowed in the two directions y and z, and the rotations are allowed in the three directions x, y and z. The sole restriction has been imposed to the movements in the x directions, where the displacements are not allowed. On the other hand, the contribution of the soil stiffness in the model has been introduced to the

model adding linear lateral springs from the mud-line to the bottom of the monopile. The sectional soil stiffness matrices introduced by these springs have been added to the structural stiffness matrix of the support structure in the directions y and z, and on alternate nodes, so these contributions ase added to two nodes each.

The load conditions of the structure are marked by the influence of the wind on the wind turbine, situated on the top of the tower. The loads, therefore, are introduced in the top of the structure in the three directions x, y and z. The kind of loads and the way used to obtain them will be explained in the following chapters.

4.1.4. Newmark Method

In Chapter 3, it has seen that it is required to solve a system of coupled second-order ordinary differential equations in time in order to find the response of the structure when it is subject to a dynamic load. There are different methods capable of solving this problems, they are primarily the implicit and explicit schemes of step-by-step integration.

The implicit methods present the major advantage that the solution is not artificially amplified whatever the time increment selected for the integration. For this reason and for its widespread use, the Newmark method is chosen to solve the system of coupled second-order ordinary differential equations (Canet, 2013).

Let consider the variation of the acceleration $\ddot{u}(t)$ between the different times t_i and $t_{i+1} = t_i + \Delta t$. The variable change $\tau = t - t_i$ is introduced in order to obtain that τ is null when $t = t_i$, and τ is equal to Δt when $t = t_{i+1}$. The acceleration vector at the time $\tau \leq \Delta t$ will be expressed as follows,

$$\ddot{u}(\tau) = \ddot{u}_i + f(\tau)(\ddot{u}_{i+1} - \ddot{u}_i) \qquad (4.16)$$

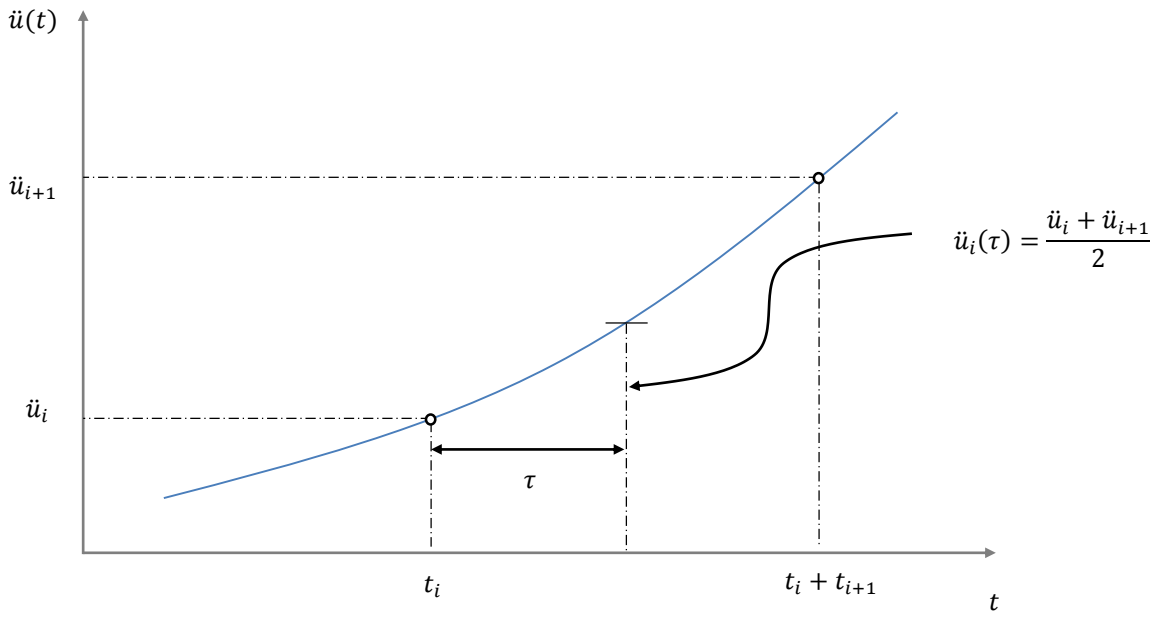

Figure 4.3: Illustration of time-varying acceleration.

Where the function $f(\tau)$ is equal to zero when $\tau = 0$ and is equal to one when $\tau = \Delta t$. The previous equation implies that the variation's law of accelerations at the times $[t_i, t_{i+1}]$ is the same for all the degrees of freedom.

Therefore, the velocity $\dot{u}(\tau)$ can be obtained integrating the acceleration expressed before.

$$\begin{aligned} \dot{u}(\tau) &= \dot{u}_i + \int_0^\tau \ddot{u}(\tau)\, d\tau \\ &= \dot{u}_i + \int_0^\tau \ddot{u}_i\, d\tau + \int_0^\tau f(\tau)(\ddot{u}_{i+1} - \ddot{u}_i)\, d\tau \end{aligned} \quad (4.17)$$

$$\dot{u}(\tau) = \dot{u}_i + \ddot{u}_i\tau + (\ddot{u}_{i+1} - \ddot{u}_i)\int_0^\tau f(\tau)\, d\tau \quad (4.18)$$

This expression can be rewritten by substituting the following relations in the equation.

$$g(\tau) = \int_0^\tau f(\tau)\, d\tau \quad (4.19)$$

$$\Delta t\gamma = \int_0^{\Delta t} f(\tau)\, d\tau \quad (4.20)$$

Obtaining,

$$\dot{u}(\tau) = \dot{u}_i + \ddot{u}_i\tau + (\ddot{u}_{i+1} - \ddot{u}_i)g(\tau) \quad (4.21)$$

And for the case of $\tau = \Delta t$,

$$\begin{aligned} \dot{u}_{i+1} &= \dot{u}_i + \ddot{u}_i\Delta t + (\ddot{u}_{i+1} - \ddot{u}_i)\gamma\Delta t \\ &= \dot{u}_i + [(1-\gamma)\ddot{u}_i + \gamma\ddot{u}_{i+1}]\Delta t \end{aligned} \quad (4.22)$$

Using the same idea to obtain the equation of velocity, the displacements can be calculated from the integration of the velocity.

$$u(\tau) = u_i + \dot{u}_i\tau + \ddot{u}_i\frac{\tau^2}{2} + (\ddot{u}_{i+1} - \ddot{u}_i)\int_0^{\Delta t} g(\tau)d\tau \quad (4.23)$$

Introducing the following relation,

$$\Delta t^2\beta = \int_0^{\Delta t} g(\tau)\, d\tau \quad (4.24)$$

And for the case of $\tau = \Delta t$, it is finally obtained,

$$u_{i+1} = u_i + \dot{u}_i \Delta t + \left[\left(\frac{1}{2} - \beta\right)\ddot{u}_i + \beta \ddot{u}_{i+1}\right]\Delta t^2 \qquad (4.25)$$

The Equations 4.22 and 4.23 are the difference equations of Newmark. These equations, together with the differential equation of the motion, allow to obtain the displacements, velocities and accelerations at the time t_{i+1} depending on the values of t_i. As can be observed, the Newmark's method depends on the value of the parameters α and β, and they require an accurate choice because the stability of the method depends on the values selected.

In this case, the set of choices correspond to the Average Acceleration Method, where the values of both parameters are as follows,

$$\gamma = \frac{1}{2} \quad ; \quad \beta = \frac{1}{4}$$

As earlier pointed out, the equation of motion of a structure with several degrees of freedom for the time $t = t_{i+1}$ can be expressed as,

$$M\ddot{u}_{i+1} + C\dot{u}_{i+1} + Ku_{i+1} = F_{i+1} \qquad (4.26)$$

With *M*, *C* and *K* as the mass, damping and stiffness matrices, respectively; and *F* as the vector of externally applied loads. The Equations 4.22 and 4.25 are directly introduced into equation of motion, which leads to a set of algebraic equations which can be linear or non-linear depending on the type of problem. With u_{i+1} as the resulting unknowns, the equations can be written as,

$$\ddot{u}_{i+1} = \frac{1}{\beta \Delta t^2}[u_{i+1} - u_i - \dot{u}_i \Delta t] + \left(\frac{1}{2\beta} - 1\right)\ddot{u}_i \qquad (4.27)$$

$$\dot{u}_{i+1} = \frac{\gamma}{\beta \Delta t^2}(u_{i+1} - u_i) + \left(1 - \frac{\gamma}{\beta}\right)\dot{u}_i + \left(1 - \frac{\gamma}{2\beta}\right)\Delta t \ddot{u}_i \qquad (4.28)$$

Finally, substituting these equations into the equation of motion is obtained a system of equations as follows,

$$\widehat{K} u_{i+1} = P_{i+1} \qquad (4.29)$$

Where,

$$\widehat{K} = K + \frac{1}{\beta \Delta t^2} M + \frac{\gamma}{\beta \Delta t} C \qquad (4.30)$$

$$P_{i+1} = F_{i+1} + M\left[\frac{1}{\beta\Delta t^2}u_i + \frac{1}{\beta\Delta t}\dot{u}_i + \left(\frac{1}{2\beta} - 1\right)\ddot{u}_i\right] + C\left[\frac{\gamma}{\beta\Delta t}u_i + \left(\frac{\gamma}{\beta} - 1\right)\dot{u}_i + \left(\frac{\gamma}{2\beta} - 1\right)\Delta t\ddot{u}_i\right] \quad (4.31)$$

The displacements are obtained at the time t_{i+1} solving the system of equations in Equation 4.29. Substituting this value in the Equations 4.27 and 4.22, the accelerations and velocities are finally obtained.

4.1.4.1. Algorithm

Newmark's method can be synthesized with the following scheme. The algorithm is divided into two parts. First, basics parameters are obtained, which will allow to perform the second part of the algorithm. Secondly, the intended outputs, in this case displacements, velocities and accelerations, are obtained at each time step.

Initialization:

- Initial conditions u_0, $\dot{u}_0$ and $\ddot{u}_0$.
- Choice of Δt, γ and β.
- Assembly of K, M, and C.
- Computation of the effective stiffness matrix, $\widehat{K}$.
- Cholesky factorization of $\widehat{K}$.

At each time step:

- Computation of the effective loading P_{i+1}.
- Solution of the system $\widehat{K}u_{i+1} = P_{i+1}$, obtaining the value of u_{i+1}.
- Calculation of the velocities and accelerations, $\dot{u}_{i+1}$ and $\ddot{u}_{i+1}$, at time t_{i+1}.

4.2. Rotor Loading

The wind acting on the wind turbine rotor produces loads which are transferred to the support structure of the offshore wind turbine. The wind speeds, therefore, are an important parameter since they determine the magnitude of the loads acting on the support structure. The histogram in Figure 4.4 below gives to probability of occurrence for each wind speed for a wind turbine generator situated at a height of 100 meters.

As can be seen from the histogram presented in Figure 4.4, the wind speeds between 3 m/s and 15 m/s have the largest probability of occurrence. The time needed to perform the probability analysis requires a limited number of wind speeds to perform the analysis, so it has been decided to analyse three wind speeds: 8 m/s, 14 m/s and 18 m/s. The design standards of offshore wind turbines specify a higher number of wind speeds to perform the structural analysis of these structures. Nevertheless, the aim of this thesis is to study a specific problem of the support structure of offshore wind turbines, so a simplified model has been considered to perform the analysis and, consequently, the number of wind speeds analysed has been reduced.

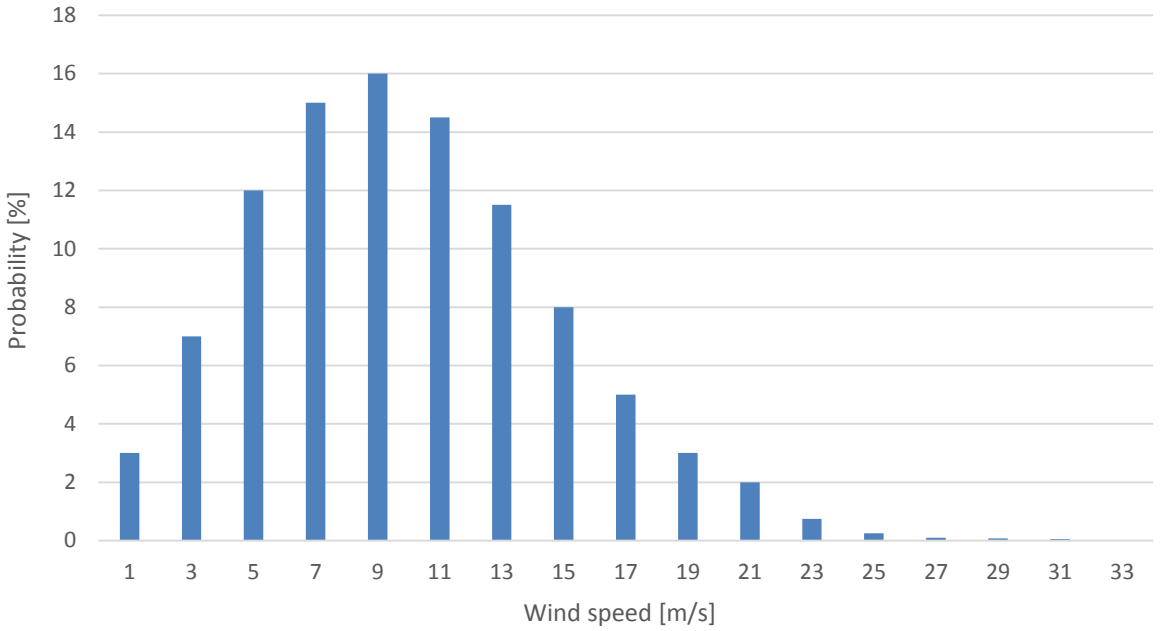

Figure 4.4: Histogram of the probability of occurrence of different wind speeds.

As has been mentioned, the wind acting on the wind turbine generator produces rotor loads which are transferred to the support structure, so it is not possible to introduce the wind speeds in the finite element model as a load. Consequently, in order to obtain the rotor loads, it has performed rotor simulation in FEDEM Windpower software.

Table 4.2: Wind speeds selected to perform the simulation of this research.

Case	Wind Speed [m/s]
1	8
2	14
3	18

The rotor of the wind turbine described in Chapter 2 has been modelled using this software and subsequently the rotor simulations for the three wind speeds have been performed. Additionally, the simulations have been done taking into account that FEDEM Windpower allows to perform the simulation with turbulent wind, which allows to perform a more realistic analysis.

In the Figure 4.5 below it can be seen the loads in the top of the support structure from the rotor simulations performed in FEDEM Windpower for a wind speed of 8 m/s. The fluctuation of the results are caused by the turbulent component of the wind. Furthermore, the loads in the X-axis, so the axis aligned with the support structure shaft, have a mean value corresponding to the total weight of the rotor, approximately equivalent to 350 000 kg.

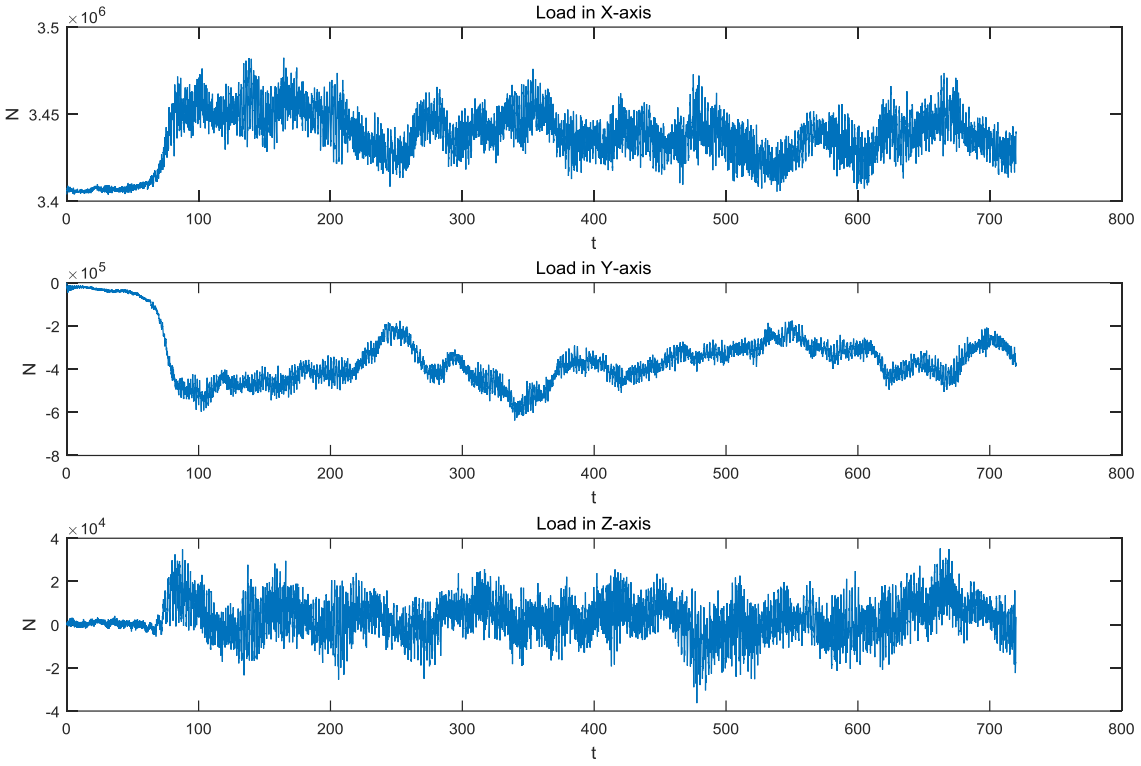

Figure 4.5: Rotor loads from rotor simulations in FEDEM Windpower software. The time-series loads correspond to the X, Y and Z axis, from top to bottom respectively.

4.3. Damping Estimation

The damping contributions that are relevant for offshore wind purposes are caused by aerodynamic, soil and structural effects. In this study, however, only aerodynamic and structural damping are going to be considered to determine the global damping of the structure.

The structural damping, as noted before, is the damping produced by the mechanical properties of the structure. The structural damping had been taken from the OC3 project, where a structural damping ratio of 1% is specified for the monopile support structure (Jonkman *et al*,. 2007).

The aerodynamic damping of the offshore wind turbine is obtained from the study of aerodynamic damping under constant and turbulent wind realized in Schafhirt (2014). The aerodynamic damping is predicted by performing logarithmic decay tests in FEDEM Windpower. The simulations are performed for the entire offshore wind turbine under turbulent wind with a turbulence intensity of 10% and for different wind speeds between 3 m/s and 24 m/s.

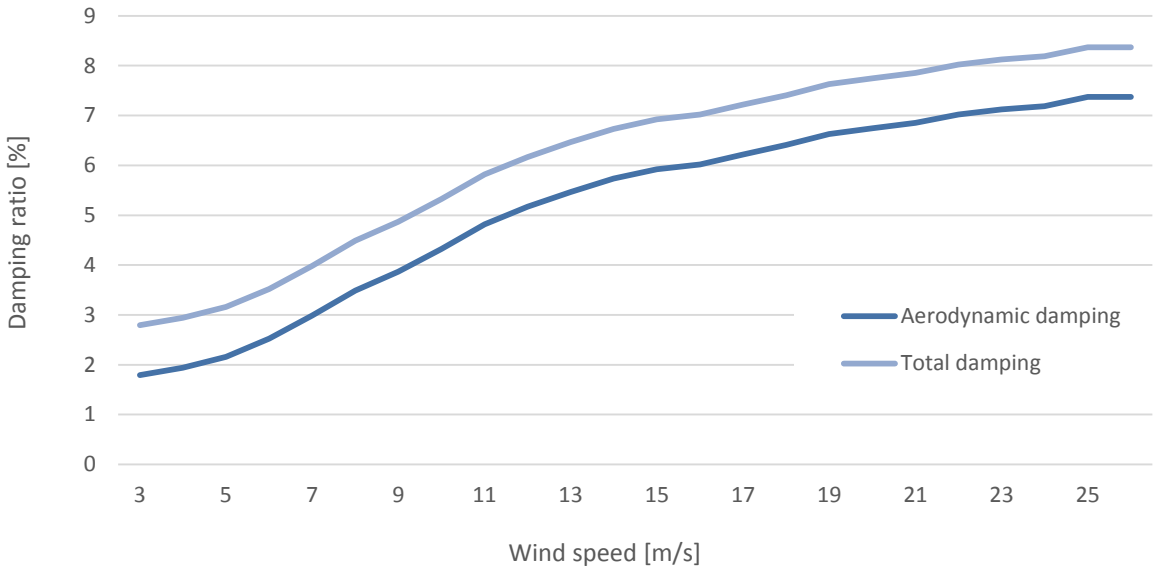

Figure 4.6: Variation of the total damping with wind speed.

As stated above, the analysis done in this thesis is performed for three different wind speeds, so it is necessary to determine the aerodynamic damping associated to each wind speed selected. The following Table 4.3 shows the mean and the standard deviation of the aerodynamic damping for the three wind speeds studied.

Table 4.3: Mean and standard deviation of the aerodynamic damping for each wind speed.

Wind speed [m/s]	Aerodynamic damping	
	Mean [%]	Standard deviation
8	3.49	0.0025
14	5.73	0.0015
18	6.41	0.0031

Finally, as pointed out above, the element damping matrix depends on two parameters, the mass coefficient (α) and stiffness coefficient (β). In order to add the damping contributions defined in this section, in this research it has been considered that the damping matrix only depends on the stiffness component. Consequently, the two coefficients that defines the element damping matrix are given by,

$$\alpha = 0$$

$$\beta = Structual\ damping + Aerodynamic\ damping$$

4.4. Soil Stiffness Approach

The interaction between soil and foundation has been studied using the API *p-y* method explained previously. The soil-pile resistance *p* is modelled by using a series of non-linear springs along the length of the pile, where the deflection of a certain soil spring at position *x* below the mud-line is denoted by *y*.

$$p = Ap_u \tanh\left(\frac{kx}{Ap_u} y\right) \quad (4.32)$$

As described in Carswell *et al.* (2014), the tangent stiffness k_t is taken from the derivative of the *p-y* curve (Equation 4.23) with respect to *y* and multiplied by the tributary length of the spring (x_k).

$$k_t = x_k \frac{dp}{dy} = x_k \left(-kx\left(tanh^2 \frac{kxy}{Ap_u} - 1\right)\right) \quad (4.33)$$

A deterministic relationship can be assumed between the soil properties, relative density D_R and friction angles φ due to the dependence of the parameters *k* and p_u from the equation above on φ and D_R. By assuming a relationship between φ and D_R, all soil property parameters of the non-linear soil-pipe stiffness can be expressed as functions of the single parameter φ. API implies the relationship between φ and D_R by defining *k* as a function of either φ or D_R. By adopting this implied relationship and assuming γ' to be constant, the non-linear soil-pile stiffness can be determined as a function of only one soil parameter, φ. Finally, the equivalent soil stiffness used in this study is defined below.

$$k_{eq} = D \cdot H \cdot k\big(\varphi(x)\big) \quad (4.34)$$

Where *D* is the diameter of the pile, *H* is the position of the spring with respect to the mud-line and $k(\varphi(x))$ is the soil stiffness as function of the friction angle.

Table 4.4: Angle of internal friction for each range of depth (Fischer, 2010).

Depths [m]	Angle of internal friction [°]
0-3	38
3-5	35
5-7	38
7-10	38
10-15	42
15-50	42.5

The UpWind project (Fischer, 2010) has been used to obtain the values of the friction angle, which depend on the depth where the spring is situated. The above Table 4.4 shows the angles of internal friction used in the analysis. These values correspond to soil conditions for hard profile.

4.5. Fatigue Approach

The Palmgren-Miner method is used as the basis for calculation of the fatigue damage. As already explained in previous chapters, this method consists of the sum of the damage from

each stress range in the stress history. Nevertheless, the results of this research are obtained as displacements and bending moments instead of stress, so it has been required to adapt this method to the outputs obtained in the analysis.

For that purpose, the damage equivalent moment as presented in, e.g., Blasques *et al.* (2013) has been used, where the evaluation of the damage is based on the mud-line bending moment that comes from the wind, wave and current forces. The fatigue analysis procedure is here based on the bending moment.

The fatigue damage in the monopile foundation is analysed in terms of the fatigue damage equivalent bending moment. The fatigue damage is given by,

$$D_i = \frac{1}{N_i} \tag{4.35}$$

Where D_i is the fatigue damage and N_i is the number of cycles to failure for a bending moment of intensity M_i. The accumulated damage from a varying number of cycles with different stress intensities is given in the equation below.

$$D = \sum_{i=1}^{n_c} D_i = \sum_{i=1}^{n_c} \frac{n_i}{N_i} \tag{4.36}$$

Here n_c is the total number of cycles, and n_i is the number of cycles for which N_i is the limit value at the corresponding bending moment level. Finally, the fatigue damage equivalent bending moment is given by,

$$M_{eq} = \left(\frac{\sum_{i=1}^{n_b} n_i M_i^m}{N} \right)^{\frac{1}{m}} \tag{4.37}$$

Where n_b is the number of bins used for the cycle counting, n_i is the number of cycles at bin *i*, M_i is the moment intensity at bin *i*, m is the S-N curve slope and depends on the material, and N is a number of cycles previously defined. The fatigue damage based on the displacements of the structure can be defined analogously to the fatigue damage equivalent bending moment.

To determine the amplitudes and means of the underlying loads cycles on irregular load signals, a cycle counting technique is used. In this study is used an implementation of the rainflow cycle counting technique due to the fact that this algorithm matches experimental results better.

4.6. Probabilistic Analysis Approach

The probability analysis performed in this thesis arises from the wish to perform a structural reliability analysis and robust design of the support structure of an offshore wind turbine.

Nevertheless, the method used to obtain the fatigue damage, as explained above, by calculating the equivalent displacements and bending moments, it is not really the basis of a conventional reliability analysis and can therefore not be assessed the probability of failure of the structure. Instead, it will be obtained general or qualitative statements about which parameters could give a higher or lower probability of failure based on the distribution of the results of the parameter analysed. In a practical sense, this means that if a variable has a wide distribution, then it results in an expected higher probability of failure since high damage is achieved by a significant number of samples, but it is not possible to calculate the actual probability of failure.

In robust design, the intention is to reduce the variability of the structural performance while improving its mean level. However, in the literature there is not a unified numerical representation of the structural robustness. The scattering of the structural response is usually the most important parameter when the robustness of the design is considered in structural optimization problems. The best way to represent the variability of the structural response is with its standard deviation. Therefore, the standard deviation of the structural performance is used in this research as a measure of the structural robustness.

4.6.1. Variables of the Probabilistic Analysis

One fundamental issue in the analysis raised here is to determine which parameters have associated a certain degree of uncertainty. In this case, uncertainty is associated with some system parameters and the goal of study the geometry of the support structure of an offshore wind turbines in a probabilistic way. The system parameters taken into account in the analysis have been the degree of damping of the structure and the soil stiffness. On the other hand, for the geometry of the support structure, it has been decided to also analyse the cross section of the structure as a probabilistic variable.

Furthermore, the probabilistic distributions of the geometry of the structure and the soil stiffness may be performed in two different ways. Both variables have different values along the height of the support structure, so it may be performed a first analysis where the variables has a probabilistic distributions along the height of the structure as a function of a reference value. Secondly, another analysis may be performed where the values of the variables have no correlation along the height of the structure.

Finally, the probabilistic analysis offers a different approach. The variables can be analysed individually, so that one variable is analysed probabilistically while the others variables remain constant; or another option is to analyse all the variables probabilistically at the same time.

4.6.1.1. Degree of Damping

The degree of damping has been obtained for different wind speeds and is divided in two contributions, structural and aerodynamic damping. The aerodynamic damping provides a larger proportion of degree of damping and uncertainty associated to this type of damping is larger. For both reasons, the probability analysis linked to the degree of damping has been performed by analysing the aerodynamic damping with simple probabilistic distributions.

On the other hand, two options are often considered to analyse the contribution of the aerodynamic damping. The first option, based on the finite element model presented above, is to consider that the aerodynamic damping is distributed in the entire structure, so this

damping is added at each element damping matrix of the model. The second option consists of considering that the aerodynamic damping can only be added to one finite element, which represents the wind turbine in the model and is located in the top of the support structure. This second approach is used more frequently in the modelling of offshore wind turbines because it is more realistic and conservative. Anyway, both options are taken into account in this research.

To that end, the mean and standard deviation of the aerodynamic damping obtained in Schafhirt (2014) have been used to perform the analysis (Table 4.3). The standard deviation is different for each wind speed, but on average has a variation coefficient of 5%. A log-normal function has been chosen to represent the probability distribution.

4.6.1.2. Soil Stiffness

The soil stiffness has been approximated with the model presented in Carswell *et al.* (2014), where an equivalent soil stiffness is defined as function of the diameter of the pile, the position of the spring with respect to the mud-line and the soil stiffness at this position as function of the friction angle. In this case, the probability analysis has been performed by analysing the angle of internal friction with simple probabilistic distributions.

For this propose, the angles of internal friction in the Table 4.4 have been used as the mean values of the probabilistic distributions. The standard deviation is obtained for each mean value using a coefficient of variation (CV) of 5%, as it is described in Carswell *et al.* (2014). Finally, a log-normal function has been chosen to represent the probability distribution.

4.6.1.3. Support Structure Geometry

The probability analysis has been performed by analysing the area of the cross section with simple probabilistic distributions. However, the cross section of the support structure depends on two different variables, the outer and inner diameter, so it is necessary to fix one of these variables to perform the analysis. The outer diameter is susceptible to higher variation due to their large exposure to environmental effects and the effect of paint, bolts, welds and flanges. For this reason, it has been decided to keep constant the inner diameter of the cross section with the values defined in Chapter 2.

To that end, the different areas of the cross section of the reference support structure have been used as the mean values of the probabilistic distributions. In all cases, the standard deviation is obtained using a variation coefficient of 5%. This value is in concordance with the variation coefficients selected in the other variables. Therefore, this ensures that the analyses of the system parameters are equivalent. Finally, a log-normal function has been chosen to represent the probability distribution.

4.6.2. Correlated and Uncorrelated Case

The geometry of the structure and the soil stiffness are variables with different values along the height of the support structure. The area of the cross section of the structure varies along the height of the tower, and the soil stiffness has different values along the height of the foundation due to the dependence of this parameter in the angle of internal friction of the soil, which varies along the depth. Anyway, an offshore wind turbine can be designed with

variable values of both parameters along the height of the support structure, although evidently there is a correlation between the values selected for the design.

In practice, this fact means that it may be performed a correlation analysis, where the variables have probability distributions along the height of the structure as a function of a reference value, for instance, the area of the cross section of the top of the support structure. On the other hand, an uncorrelated analysis may be performed, where the values of the variables have no correlation along the height of the structure.

4.6.3. Combined Analysis

Putting the probability analysis into perspective, the different variables presented can be analysed using different approaches. First, the variables can be analysed individually, so that a variable is analysed probabilistically while the others variables remain constant. Secondly, it may be done a second analysis where all the variables are analysed probabilistically at the same time.

As a result, each variable has been analysed individually and then a combined case has been performed. Therefore, this consideration involves performing four different analysis, one for each variable and a combined one.

4.6.4. Summary

The probabilistic analysis presented involves an elevated number of cases taking into account the two ways explained to add the degree of damping in the structure, the three variables considered, the correlation or no correlation between these variables and their probability distributions, and the three different wind speeds considered. In order to summarize and provide further clarity, in Table 4.5, Table 4.6, Table 4.7 and Table 4.8 are presented all the cases considered in this research.

As can be seen in the two tables below, the combined case is divided in four sections. This is due to the fact that the geometry of the structure and the soil stiffness are variables that may or may not be analysed in a correlated manner. The alternative analysis of these two variables results in four possible alternatives.

To reference the different cases a special nomenclature has been used. The first acronym refers to the form used to add the damping to the model (*D* for “distributed” and *T* for “top” aerodynamic damping), the second acronym refers to the variable analysed probabilistically (*AD* for aerodynamic damping, *S* for soil, *A* for area, *C* for combined and *R* for the reference case), the third acronym to the wind speed selected (8 m/s, 14 m/s and 18 m/s wind speeds), and the fourth acronym to the correlated/non-correlated analysis of the variables (*C* for correlated and *N* for non-correlated case).

Table 4.5: Analysis cases when the aerodynamic damping is distributed aerodynamic in the entire structure.

Case	Damping	Variable	Correlation	Wind speed [m/s]
DAD8	Distributed damping (DD)	Aerodynamic damping	-	8
DAD14				14
DAD18				18
DS8C		Soil	Correlated	8
DS14C				14
DS18C				18
DS8N			No correlated	8
DS14N				14
DS18N				18
DA8C		Area	Correlated	8
DA14C				14
DA18C				18
DA8N			No correlated	8
DA14N				14
DA18N				18
DC8CC		Combined	Correlated - Correlated	8
DC14CC				14
DC18CC				18
DC8C			Correlated – No correlated	8
DC14C				14
DC18C				18
DC8NC			No correlated - Correlated	8
DC14NC				14
DC18NC				18
DC8N			No correlated- No correlated	8
DC14N				14
DC18N				18

The different cases presented above have been analysed probabilistically performing 200 simulations. This number of samples is enough to ensure reliable results that give robustness to the probabilistic analysis. Furthermore, the computation cost, measured in time, to perform 200 simulations is approximately of 20 minutes, so this number of simulations is appropriate to the total number of cases of the probabilistic analysis of this study. As has been seen in relation to the wind speeds, the design standards of offshore wind turbines specify a higher number of simulations to perform the structural analysis of these structures. Nevertheless, the aim of this thesis is to study a specific problematic, without needing to perform a complete analysis of the support structure of an offshore wind turbine. Furthermore, the computational effort required to carry out the number of simulations specified in these standards cannot be assumed in this research.

Table 4.6: Analysis cases when the aerodynamic damping is added to the finite element located in the top of the structure.

Case	Damping	Variable	Correlation	Wind speed [m/s]
TAD8	Top tower damping (TD)	Aerodynamic damping	-	8
TAD14				14
TAD18				18
TS8C		Soil	Correlated	8
TS14C				14
TS18C				18
TS8N			No correlated	8
TS14N				14
TS18N				18
TA8C		Area	Correlated	8
TA14C				14
TA18C				18
TA8N			No correlated	8
TA14N				14
TA18N				18
TC8CC		Combined	Correlated - Correlated	8
TC14CC				14
TC18CC				18
TC8CN			Correlated – No correlated	8
TC14CN				14
TC18CN				18
TC8NC			No correlated - Correlated	8
TC14NC				14
TC18NC				18
TC8NN			No correlated- No correlated	8
TC14NN				14
TC18NN				18

Additionally, when the degree of damping and the cross section of the structure are analysed probabilistically, the results obtained for the fatigue damage seem to show that the number of samples is not enough, as will be seen later. Therefore, the analyses of these cases have been repeated by performing 1000 simulations instead of 200. With this consideration is not intended to explain the results obtained in the following chapter, but rather that the total number of cases is clear due to their importance in the methodology of this thesis.

Table 4.7: Additional analysis for the study cases of the degree of damping and the geometry of the structure.

Case	Damping	Variable	Correlation	Wind speed [m/s]
TAD8_2	Top tower damping (TD)	Aerodynamic damping	-	8
TAD14_2				14
TAD18_2				18
TA8C_2		Area	Correlated	8
TA14C_2				14
TA18C_2				18
TA8N_2			No correlated	8
TA14N_2				14
TA18N_2				18

All simulations have been performed with a simulation time of 720 seconds and a time step of 0.025 seconds. The two first minutes of each simulation have been deleted from the results order to avoid errors in the outputs caused by distortions in the first instants of simulation. By this way, the results presented in the following chapter correspond to the 10 last minutes (600 seconds) of simulation.

Table 4.8: Analysis cases for the reference support structure of the offshore wind turbine.

Case	Damping	Wind speed [m/s]
DRef8	Distributed damping (DD)	8
DRef14		14
DRef18		18
TRef8	Top tower damping (TD)	8
TRef14		14
TRef18		18

Finally, a similar probabilistic analysis has been made for the reference support structure of the offshore wind turbine. The results of this analysis have enabled to validate the structure modelled in the finite element model and, at the same time, have been used to understand the response of the structure from the different analysis explained above by comparing the outcomes of both analysis.

CHAPTER 5

Results

This section presents representative results obtained in this study. Simulations have been performed to investigate the effect of damping, soil stiffness and geometry of the structure on the response of an offshore wind turbine analysed probabilistically. The MATLAB scripts used to perform the calculations in this section can be found in Appendix B.

The outputs analysed are the displacements on the top of the support structure and the bending moments in the mud-line. The displacements are analysed in the direction of the *y* and *x* axes, corresponding to the axes where the main load of the wind is applied and the axis of the support structure, respectively; and the bending moments are analysed in the *y* and *z* axes. The displacements in the direction of the *y* axis and the bending moments in the direction of the *z* axis are prioritized with respect to the following analysis due to their higher influence on the response of the structure. On the other hand, the fatigue damage from the displacements and the bending moments of the support structure represents the most relevant output of this thesis and for this reason a detailed analysis of the obtained results have been performed. Additionally, the dynamic response of the support structure is linked to the variables analysed probabilistically and, in turn, the variation of these variables is reflected in the global mass and stiffness matrix of the FEM. Therefore, the natural frequencies of the first mode have been analysed in order to have a better understanding of the results.

With the intention of getting a more flexible analysis of the data, the name of certain parameters are simplified and the terminology introduced in the Table 4.5, Table 4.6, Table 4.7 and Table 4.8 is used to refer to the different cases of the analysis. Consequently, it will be used terminology such as *DD* (or *DStr*) to refer to the case with the aerodynamic damping is distributed in the entire structure, *DT* (or *DTop*) to refer to the case with the aerodynamic damping located in the top of the support structure, or the numbers *8*, *14* and *18* to refer to the different wind speeds.

Finally, the probabilistic analysis performed requires special tools to analyse the data obtained. With that purpose in mind, histograms and boxplots are a convenient way of graphically depicting groups of numerical data. As will be seen later, the boxplots are represented with a box, where the central mark is the median, the edges of the box are the 25^{th} and 75^{th} percentiles and the whiskers extend to the most extreme data points not considered outliers.

5.1. Reference Case

The reference structure has been used to validate the FE model and to analyse the damping approach. The validation of the model will be performed by comparing the natural frequency obtained in the proposed model with the one obtained in a model built in FEDEM Windpower software. The analysis of the damping approach will allow the study of the main differences between the alternatives proposed and thereby simplify the others analysis of the thesis.

5.1.1. Validation of the Model

The structure has been completely defined in terms of geometry, materials and boundary conditions using MATLAB software. The validation of the structure modelled is required to ensure that the results obtained are correct.

For that propose, the reference structure has been modelled in FEDEM Windpower software in order to compare the results of this model with the results obtained in the finite element model presented in this study. The validation has been based on the natural frequency of the structure. Although others outputs could be used to validate the model, the natural frequency has been selected since it gives relevant information about the response of the structure. This is due to the fact that the natural frequency of the structure is obtained by solving a problem of eigenfrequencies where the main inputs are the mass and stiffness matrix of the structure. These two parameters contain a great deal of information about the structure so, in conclusion, it is appropriate to study the natural frequency of the structure in order to validate the FE model. Furthermore, some time series of displacements have been analysed in FEDEM and it has been verified that they were mostly similar with the ones of the simplified FE model. Nevertheless, these results are not shown here.

Table 5.1: Natural frequency of the first mode obtained in FEDEM Windpower software and the FEM in MATLAB.

Model	Natural frequency
FEDEM Windpower	0.2771
FEM in MATLAB	0.2871

The natural frequency of the first mode in FEDEM Windpower is slightly lower than the same frequency obtained in the simplified finite element model, with a percentage variance of 3.6%. This difference could be caused by the fact that the proposed approach assumes some simplifications/assumptions respect to the model used in FEDEM Windpower. For instance, the way used to model the rotor is different in each model. The model in FEDEM Windpower proposes a complete modelling of the rotor, where each blade is modelled using beams. Nevertheless, in the proposed approach the rotor is not modelled, instead the loads engendered by the rotor are obtained from rotor simulations in FEDEM Windpower and the mass of the rotor is added to the global mass matrix of the structure. Moreover, the number of elements is lower in the case of the simplified FE model, resulting in a reduced accuracy in the results. Anyway, this difference in the value of the natural frequency of the first node is small enough to claim that the proposed model is valid for the analysis to be carried out in the research.

5.1.2. Damping Approach

In the model, the aerodynamic damping may be distributed in the entire structure, i.e. the damping is added in each element damping matrix, or may be added to one finite element only, which in this case is the element that represents the wind turbine and is located in the top of the support structure.

A summary of the results is presented below. This analysis is based on the response of the reference structure to the two alternatives presented in order to consider the aerodynamic damping. The results consist of are displacements, bending moments and fatigue damage of the structure.

5.1.2.1. Displacements

The displacements in the *y* and *x* axes for each case of the reference support structure are listed in Table 5.2 and Figure 5.1. The displacements for the case with the aerodynamic damping distributed in the entire structure have mean values lower than those obtained for the case with the aerodynamic damping located in the top of the structure. In both cases, the mean value and the standard deviation of the displacements increase when the wind speed is higher.

Table 5.2: Mean, standard deviation and variation coefficient value of the displacements in the y and x axes on the top of the structure for the reference case.

Case	Top displacements Y			Top displacements X		
	μ [m]	σ [m]	CV [%]	μ [m]	σ [m]	CV [%]
DRef8	3,98E-02	3,75E-02	94,26	1,29E-05	1,50E-05	116,72
DRef14	7,29E-02	8,52E-02	117,00	4,02E-05	3,79E-05	94,27
DRef18	9,55E-02	8,22E-02	86,12	5,73E-05	5,05E-05	88,29
TRef8	7,11E-02	4,76E-02	66,88	1,42E-05	1,53E-05	108,14
TRef14	1,38E-01	1,12E-01	81,69	3,58E-05	3,96E-05	110,61
TRef18	3,10E-01	1,53E-01	49,30	4,66E-05	5,38E-05	115,46

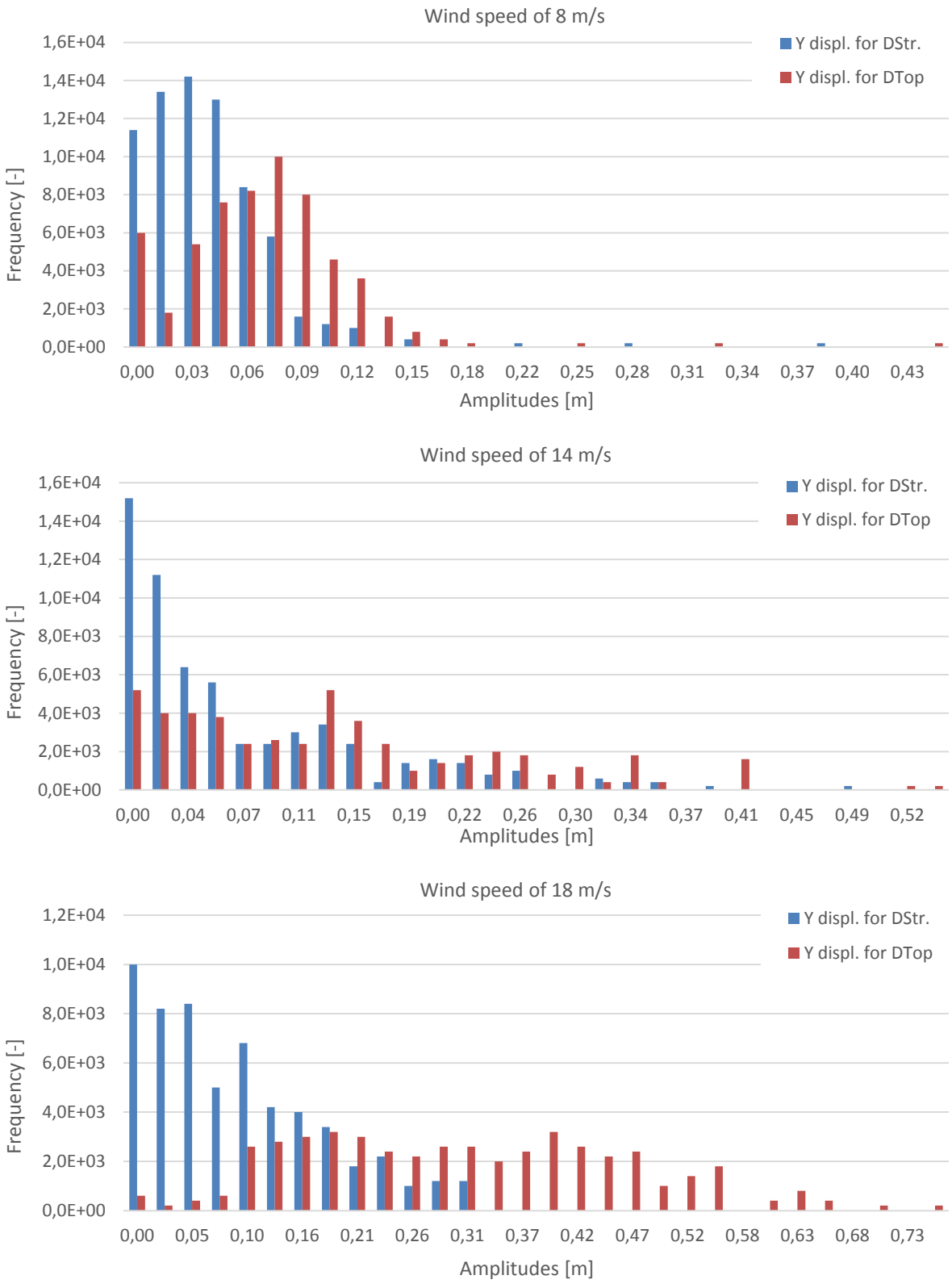

Figure 5.1: Distribution of amplitudes of the displacements in the y axis for the reference case. Each histogram correspond to a wind speed: 8 m/s (top), 14 m/s (centre) and 18 m/s (bottom).

5.1.2.2. Bending Moments

Values obtained for bending moments in the *y* and *z* axes for each case of the reference support structure are given in Table 5.3 and Figure 5.2. For the case of the aerodynamic damping distributed in the entire structure, the bending moments have mean values lower than the ones obtained for the case with the aerodynamic damping located in the top of the structure. Nevertheless, the distribution of amplitudes observed in the histograms show that the scattering of the bending moments is different since the most part of the amplitudes are in a reduced range of values.

Table 5.3: Mean, standard deviation and variation coefficient value of the bending moments in the y and z axes on the mud-line of the structure for the reference case.

Case	Mud-line bending moment Y			Mud-line bending moment Z		
	μ [Nm]	σ [Nm]	CV [%]	μ [Nm]	σ [Nm]	CV [%]
DRef8	8,50E+05	8,31E+05	97,77	3,94E+06	4,70E+06	119,25
DRef14	1,38E+06	1,44E+06	104,33	6,77E+06	9,92E+06	146,44
DRef18	2,19E+06	2,43E+06	110,97	1,01E+07	1,07E+07	105,90
TRef8	9,65E+05	1,18E+06	122,41	4,74E+06	6,23E+06	131,49
TRef14	2,31E+06	2,87E+06	124,55	7,64E+06	1,22E+07	159,29
TRef18	4,56E+06	5,32E+06	116,57	2,60E+07	2,53E+07	97,47

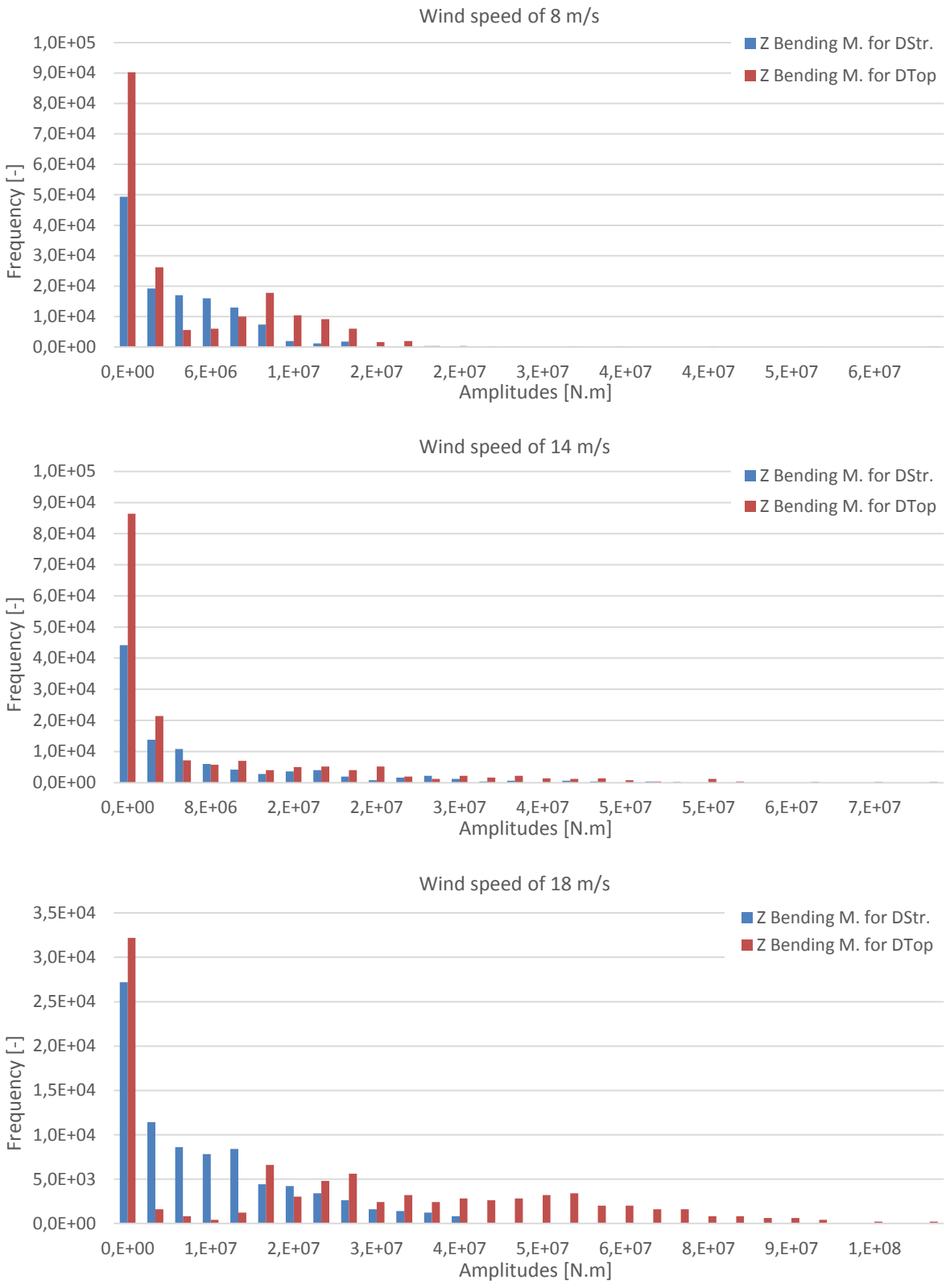

Figure 5.2: Distribution of amplitudes of the bending moments in the z axis for the reference case. Each histogram correspond to a wind speed: 8 m/s (top), 14 m/s (centre) and 18 m/s (bottom).

5.1.2.3. Fatigue Damage

As seen from Table 5.4 the equivalent fatigue damage of the reference structure for the different outputs generally increases when the wind speed is higher. Here also, the fatigue damage is higher for the case with the aerodynamic damping located in the top of the structure. This behaviour is reasonable because it has been observed that with this damping approach the displacements and the bending moments are higher, which in turn results in higher damage in the structure.

Table 5.4: Mean value of the equivalent fatigue damage of displacements and bending moments for the reference case.

Case	Top displacement Y [m]	Top displacement X [m]	Mud-line bending moment Y [Nm]	Mud-line bending moment Z [Nm]
DRef8	2,73E-03	1,31E-06	5,30E+04	3,68E+05
DRef14	4,49E-03	3,03E-06	1,01E+05	5,99E+05
DRef18	4,33E-03	4,00E-06	1,58E+05	5,86E+05
TRef8	3,29E-03	1,53E-06	7,36E+04	4,60E+05
TRef14	5,89E-03	3,63E-06	1,80E+05	8,12E+05
TRef18	9,86E-03	4,85E-06	3,14E+05	1,38E+06

5.1.2.4. Summary

The mean values of the results obtained for the case with the aerodynamic damping distributed in the entire structure are lower than those obtained for the case with the aerodynamic damping located in the top of the structure. This means that the fact of locating the aerodynamic damping in the top of the structure results in considerable increases of the displacements, bending moments of and, in turn, fatigue damage in the support structure.

As already mentioned in the previous chapter, the fact of locating the aerodynamic damping in the top of the structure is an approach more realistic and conservative of the dynamic response of the structure and it correspond to the approach more frequently in the modelling of offshore wind turbines. For this reason, the results presented in the following subchapters are focused in the case with the aerodynamic damping located in the top of the structure.

The results presented in this subchapter are used in the following sections to compare the results obtained in the different cases with the dynamic response of the reference support structure of this research.

5.2. Case of Study: Damping

5.2.1. Displacements and Bending Moments

As can be seen in the results presented below, the mean value of the displacements in the *y* and *x* axes increases when the wind speed is higher. The standard deviation also increases when the wind speed is higher but has different behaviour for each axis and for each damping approach. On the one hand, the variation coefficient of the displacements of the *y* axis has an irregular trend and it is not possible to make assumptions about it. The maximum and minimum values are obtained for a wind speed of 14 m/s and 18 m/s, respectively. On the other hand, the variation coefficient of the displacements of the *x* axis for the DD case is reduced when the wind speed is higher, whereas for the TD case it is increased.

The behaviour of the bending moments is analogous to which has been observed in the displacements. The mean value and the standard deviation in both axes increase when the wind speed is higher; and, however, the variation coefficient reaches the maximum and minimum values for a wind speed of 14 m/s and 18 m/s, respectively.

Comparing the results obtained in these cases with the results of the reference case, it can be observed that both displacements and bending moments are similar to those obtained in the simulations of the reference case, including the mean value and the scattering of the results. It is interesting to note that the main differences with the reference case are observed in the DD case, while the TD case shows minimum variations of less than 1%.

Figure 5.3 and Figure 5.4, and Table 5.5 and Table 5.6 present the results obtained in the study case of the damping effects. These figures show with boxplots the displacements and bending moments. Additionally, both tables present the mean values, variation coefficients and the percentage variances between the mean values of the different cases analysed in this section and the reference cases.

Table 5.5: Mean, variation coefficient and variation with respect to the reference case of the displacements in the y and x axes for the study case of the damping.

Case	Displacements Y			Displacements X		
	μ [m]	CV [%]	Diff. with ref. case [%]	μ [m]	CV [%]	Diff. with ref. case [%]
DAD8	4,54E-02	89,36	13,977	1,32E-05	114,53	2,077
DAD14	7,67E-02	114,77	5,209	3,92E-05	97,04	-2,574
DAD18	1,08E-01	86,49	13,612	5,41E-05	94,68	-5,434
TAD8	7,11E-02	66,90	-0,008	1,43E-05	107,59	0,605
TAD14	1,38E-01	81,62	0,068	3,59E-05	110,51	0,209
TAD18	3,10E-01	49,30	0,008	4,67E-05	115,36	0,240

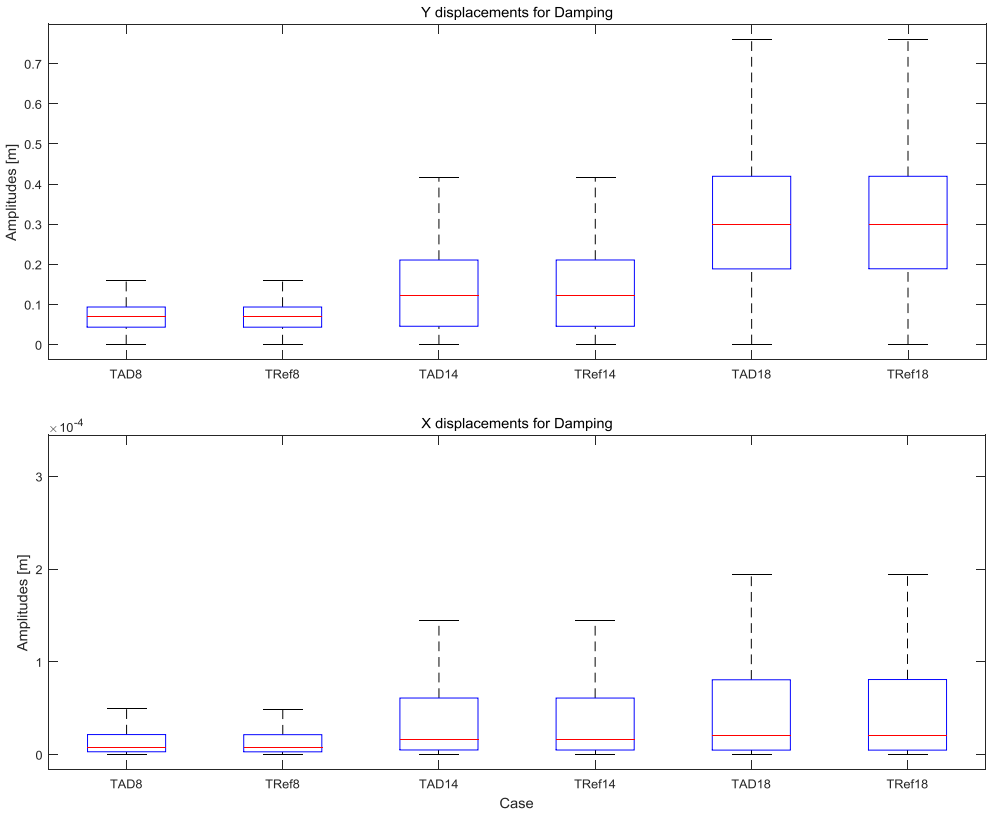

Figure 5.3: Boxplot of the amplitudes of the displacements obtained in the rainflow counting for the study case of the damping. Each graph correspond to the displacements in the y axis (top) and in the x axis (bottom).

Table 5.6: Mean, variation coefficient and variation with respect to the reference case of the bending moments in the y and z axes for the study case of the damping.

Case	Mud-line bending moment Y			Mud-line bending moment Z		
	μ [Nm]	CV [%]	Diff. with ref. case [%]	μ [Nm]	CV [%]	Diff. with ref. case [%]
DAD8	8,66E+05	107,10	1,790	4,04E+06	125,76	2,401
DAD14	1,43E+06	108,31	3,192	6,79E+06	148,28	0,302
DAD18	2,35E+06	117,03	7,375	1,11E+07	109,88	10,417
TAD8	9,61E+05	122,81	-0,394	4,75E+06	131,28	0,187
TAD14	2,31E+06	124,62	-0,062	7,67E+06	159,01	0,362
TAD18	4,56E+06	116,62	-0,030	2,59E+07	97,74	-0,268

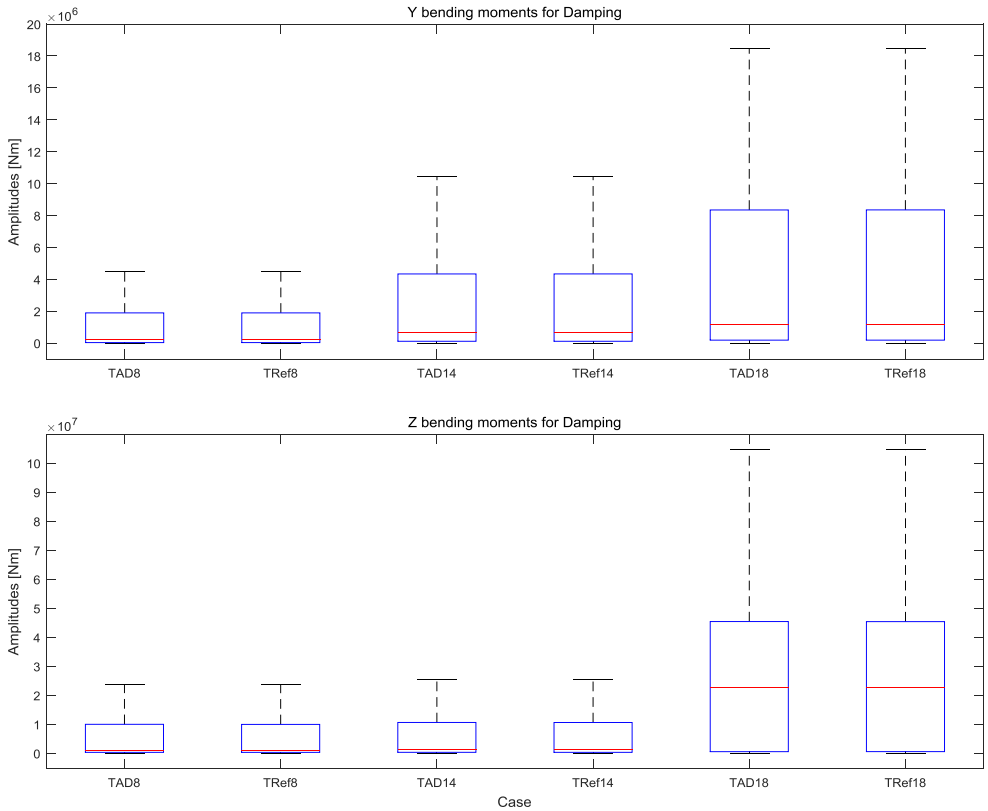

Figure 5.4: Boxplot of the amplitudes of the bending moments obtained in the rainflow counting for the study case of the damping. Each graph correspond to the displacements in the y axis (top) and in the z axis (bottom).

5.2.2. Fatigue Damage

5.2.2.1. Displacements

From the fatigue damage results presented in Table 5.7 and Figure 5.5, one can see that the fatigue damage equivalent displacement increases when the wind speed is higher, as well as its standard deviation. The variation coefficient reaches the maximum and minimum values for a wind speed of 18 m/s and 14 m/s, respectively.

Looking at the differences with the reference case, the mean values of the fatigue damage obtained here are comparable to those obtained in the reference case. Once again, the lower differences with the reference case are observed in the TD case. From the histograms presented in Figure 5.5, it can be observed that the peak frequency of equivalent fatigue damage is obtained for a higher value than the mean value of the reference case for the three wind speeds. In the histograms can also be noted that the distribution of the amplitudes is not uniform and there are some amplitudes without values. This could be due to an inadequate number of samples, perhaps insufficient for the analysis performed here.

Table 5.7: Mean, variation coefficient and variation with respect to the reference case of the fatigue damage equivalent displacement in the y and x axes for the study case of the damping.

Case	Damage - Top displacements Y			Damage - Top displacements X		
	μ [m]	CV [%]	Diff. with ref. case [%]	μ [m]	CV [%]	Diff. with ref. case [%]
DAD8	2,84E-03	7,52	4,190	1,34E-06	12,28	12,277
DAD14	4,57E-03	5,32	1,686	3,03E-06	10,10	10,100
DAD18	4,71E-03	16,47	8,794	4,01E-06	13,76	13,764
TAD8	3,29E-03	1,76E-02	-3,66E-04	1,54E-06	1,37	4,60E-01
TAD14	5,89E-03	4,78E-03	6,26E-04	3,63E-06	1,13	1,39E-01
TAD18	9,86E-03	6,81E-02	1,82E-02	4,87E-06	1,63	3,28E-01

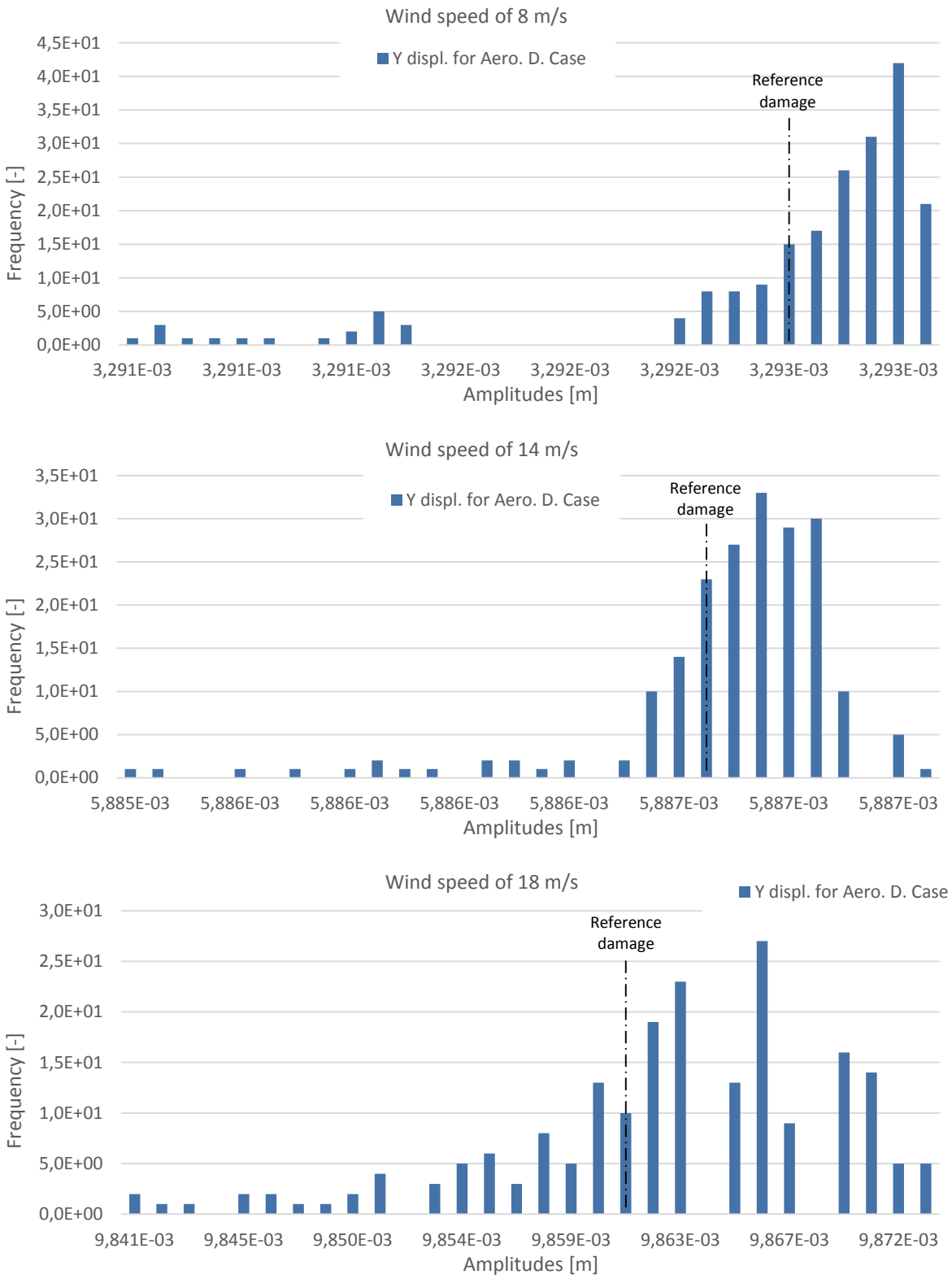

Figure 5.5: Distribution of amplitudes of the equivalent fatigue damage displacement in the y axis for the study case of the damping. Each histogram correspond to a wind speed: 8 m/s (top), 14 m/s (centre) and 18 m/s (bottom).

5.2.2.2. Bending Moments

As seen from Table 5.8 and Figure 5.6, the mean value and the standard deviation of the fatigue damage equivalent bending moment increases when the wind speed is higher. The variation coefficient for the DD case reaches the maximum and minimum value for a wind speed of 18 m/s and 14 m/s, respectively. For the TD case, however, it is observed an irregular behaviour and it is difficult to make assumptions about it.

Regarding the differences with the reference case, the results of the mean values of the equivalent fatigue damage have a behaviour equivalent to that observed in the reference case. The lower differences are again observed in the TD case, with values of less than 0.5%. From the histograms presented in Figure 5.6, here too, it can be observed that the peak frequency of equivalent fatigue damage is obtained for a higher value than the mean value of the reference case for the three wind speeds. It can also be seen that the distribution of the amplitudes is not uniform and there are many amplitudes without values. An insufficient number of samples could be the reason and, therefore, the simulation of these cases have been repeated by performing 1000 simulations instead of 200.

Table 5.8: Mean, variation coefficient and variation with respect to the reference case of the fatigue damage equivalent bending moment in the y and z axes for the study case of the damping.

Case	Damage -Mud-line bending moment Y			Damage -Mud-line bending moment Z		
	μ [Nm]	CV [%]	Variation coefficient [%]	μ [Nm]	CV [%]	Diff. with ref. case [%]
DAD8	5,66E+04	14,25	6,918	3,86E+05	9,01	4,873
DAD14	1,05E+05	10,93	3,705	6,11E+05	5,96	2,008
DAD18	1,71E+05	17,28	8,454	6,40E+05	18,10	9,345
TAD8	7,36E+04	3,80E-02	1,73E-03	4,60E+05	4,20E-02	6,14E-03
TAD14	1,80E+05	4,17E-02	8,22E-03	8,13E+05	1,32E-01	9,22E-02
TAD18	3,14E+05	8,61E-02	9,44E-03	1,38E+06	1,00E-01	4,24E-03

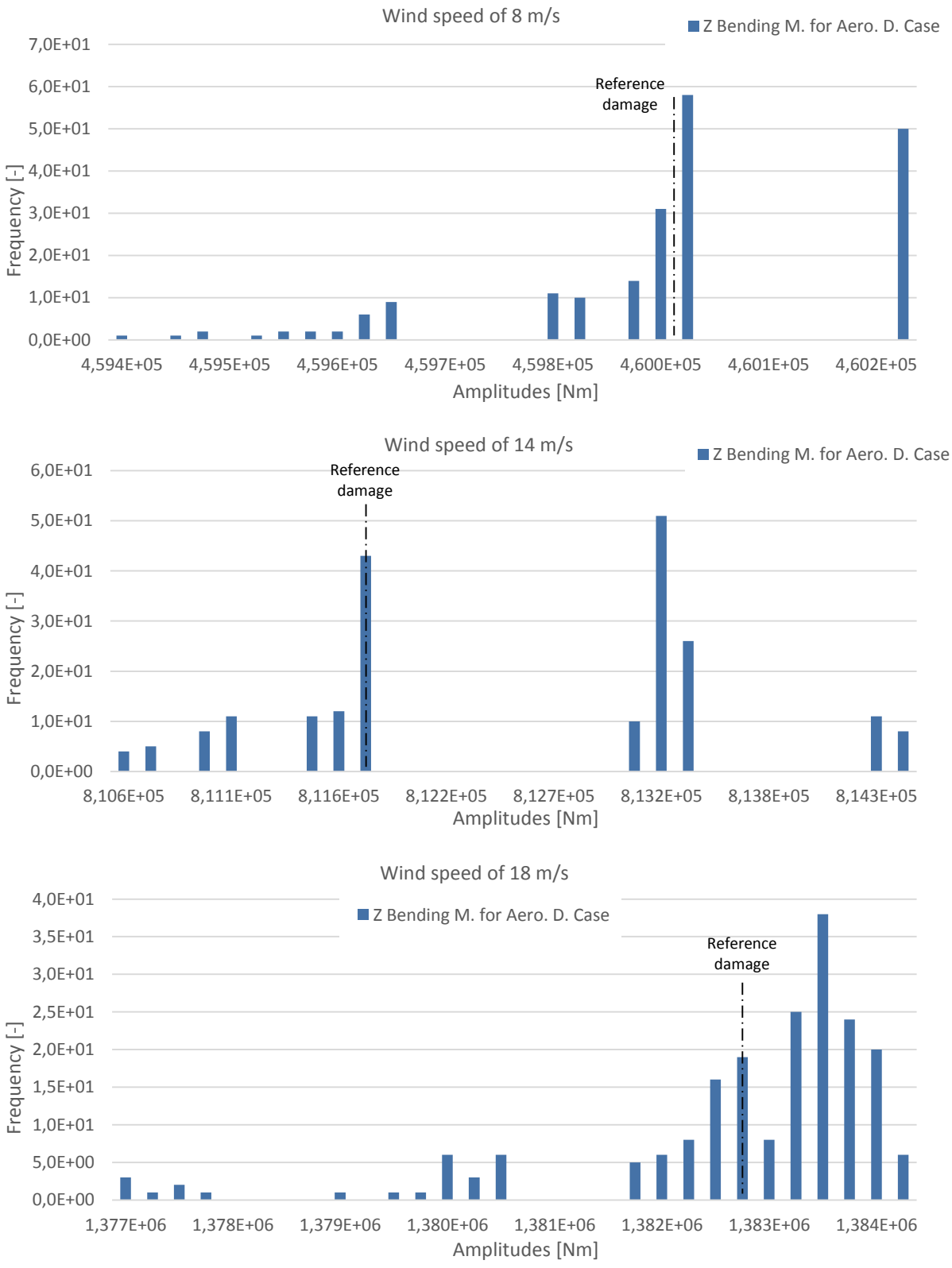

Figure 5.6: Distribution of amplitudes of the equivalent fatigue damage bending moment in the z axis for the study case of the damping. Each histogram correspond to a wind speed: 8 m/s (top), 14 m/s (centre) and 18 m/s (bottom).

5.2.3. Additional Fatigue Damage Analysis

From the fatigue damage results presented in Table 5.9 and Table 5.10, and Figure 5.7 and Figure 5.8, one can see that the results obtained are comparable to those obtained for 200 simulations. By increasing the number of simulation until 1000 samples, the histograms show a non-uniformed distribution of the amplitudes, equivalent to the one obtained in the previous cases.

Focusing on other considerations, the mean values, standard deviations and variation coefficients are analogous to which has been observed previously, as well as the differences with the reference case.

Table 5.9: Mean, variation coefficient and variation with respect to the reference case of the fatigue damage equivalent displacement in the y and x axes for the additional study case of the damping.

Case	Damage - Top displacements Y			Damage - Top displacements X		
	μ [m]	CV [%]	Diff. with ref. case [%]	μ [m]	CV [%]	Diff. with ref. case [%]
TAD8_2	3,29E-03	1,80E-02	-7,81E-05	1,54E-06	1,37E+00	4,72E-01
TAD14_2	5,89E-03	6,64E-03	2,28E-04	3,63E-06	1,80E-02	8,89E-02
TAD18_2	9,86E-03	6,90E-02	2,08E-02	4,87E-06	5,00E-02	3,72E-01

Table 5.10: Mean, variation coefficient and variation with respect to the reference case of the fatigue damage equivalent bending moment in the y and z axes for the additional study case of the damping.

Case	Damage -Mud-line bending moment Y			Damage -Mud-line bending moment Z		
	μ [Nm]	CV [%]	Diff. with ref. case [%]	μ [Nm]	CV [%]	Diff. with ref. case [%]
TAD8_2	7,36E+04	4,43E-02	1,13E-03	4,60E+05	4,02E-02	6,99E-03
TAD14_2	1,80E+05	4,55E-02	6,29E-03	8,13E+05	1,33E-01	9,09E-02
TAD18_2	3,14E+05	1,14E-01	9,89E-03	1,38E+06	9,88E-02	7,39E-03

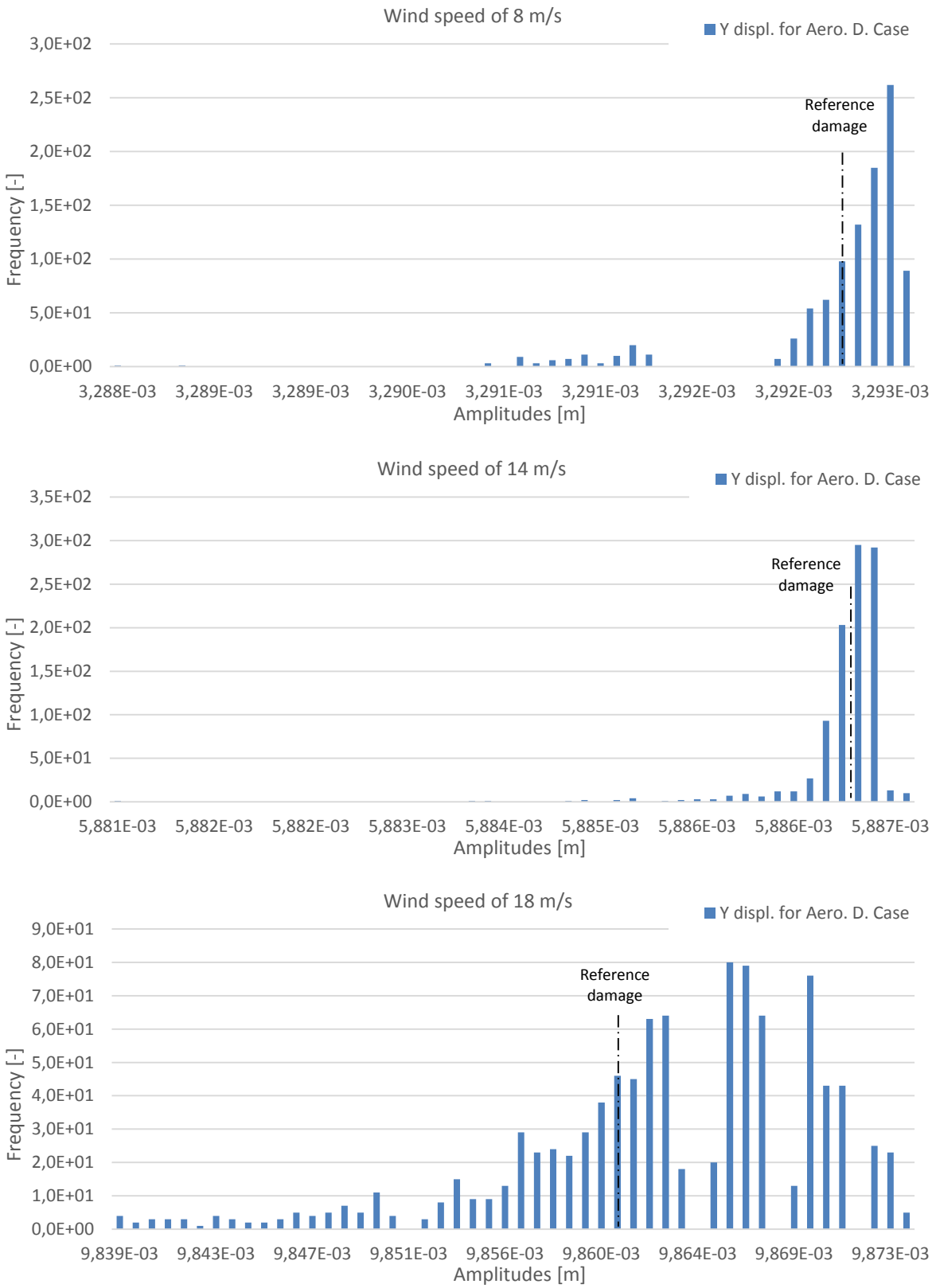

Figure 5.7: Distribution of amplitudes of the equivalent fatigue damage displacement in the y axis for the additional study case of the damping. Each histogram correspond to a wind speed: 8 m/s (top), 14 m/s (centre) and 18 m/s (bottom).

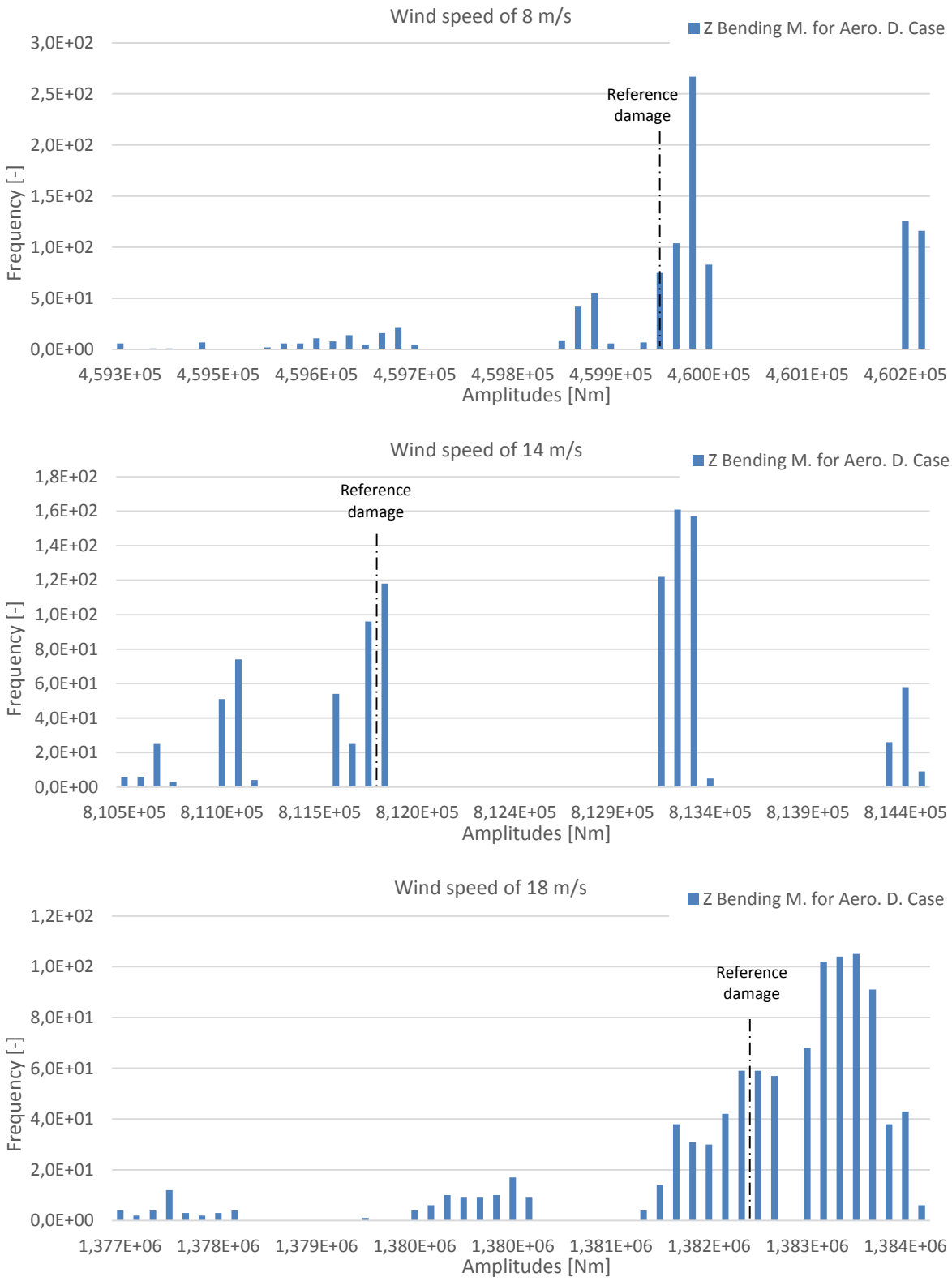

Figure 5.8: Distribution of amplitudes of the equivalent fatigue damage bending moment in the z axis for the additional study case of the damping. Each histogram correspond to a wind speed: 8 m/s (top), 14 m/s (centre) and 18 m/s (bottom).

5.2.4. Summary

It can clearly be observed from the results presented that the displacements and the bending moments are comparable to which has been observed in the reference case, particularly in the TD case. In this sense, the fact of analysing the aerodynamic damping in a probabilistic manner does not translate into significant results of these two variables.

As regards fatigue damage, here too the mean values of the equivalent fatigue damage are equivalent to which has been observed in the reference case. Nevertheless, the distribution of the amplitudes shows that the peak frequencies of fatigue damage are obtained for higher values than the average values of the reference case, which implies greater damage in the structure. Furthermore, it has been seen some histograms with irregular distributions that suggested an inadequate number of samples. For this reason, some simulations have been repeated by increasing the number of samples to 1000. However, the results obtained have been equivalents and it has not been possible to extract additional conclusions.

5.3. Case of Study: Soil Stiffness

5.3.1. Displacements and Bending Moments

The displacements in the *y* and *x* axes and the bending moments in the *y* and *z* axes obtained in this section are presented below. In all cases, the mean value and standard deviation of the displacements increase when the wind speed is higher. The standard deviation has different behaviour for each axis and for each damping approach, as has been observed in the results of the previous section. On the one hand, the variation coefficient of the displacements of the *y* axis has an irregular behaviour and it is observed that the maximum and minimum values are obtained for a wind speed of 14 m/s and 18 m/s, respectively. The variation coefficient of the displacements of the *x* axis for the DD case is reduced when the wind speed is higher, whereas for the TD case it is increased.

The behaviour of the bending moments is analogous to which has been observed in the displacements. The mean value and standard deviation of the bending moments in both axes increase when the wind speed is higher. The standard deviation also has an irregular behaviour as well as the variation coefficient, making difficult to achieve a clear conclusion.

Looking at the differences between the correlated and non-correlated case, it can be seen that there is almost not variations in the results obtained. There are small differences between the two cases but it is not possible to observe any general trend.

On the other hand, by comparing the results obtained in these cases with the ones of the reference case, one can see that the differences are small and the mean values are located around the mean values of the reference case. It is worth stressing that the mean values of the displacements in *x* axis are the same as for the reference case, observing, therefore, a null variation percentage between both cases. Conversely, the widest variations are to be found in the bending moments of the TD case, with variations around 1.5%.

Figure 5.9 and Figure 5.10 present the results obtained in the study case of the soil stiffness. These figures show the displacements and bending moments with boxplots. Additionally, the Table 5.11 and Table 5.12 present the mean values, variation coefficients and the percentage variances between the mean values of the different cases analysed in this section and the reference cases.

Table 5.11: Mean, variation coefficient and variation with respect to the reference case of the displacements in the y and x axes for the study case of the soil stiffness.

Case	Top displacements Y			Top displacements X		
	μ [m]	CV [%]	Diff. with ref. case [%]	μ [m]	CV [%]	Diff. with ref. case [%]
DS8C	3,99E-02	94,01	0,112	1,29E-05	116,72	0
DS14C	7,23E-02	117,64	-0,764	4,02E-05	94,27	0
DS18C	9,56E-02	86,01	0,145	5,73E-05	88,29	0
DS8N	3,99E-02	93,99	0,119	1,29E-05	116,72	0
DS14N	7,25E-02	117,45	-0,466	4,02E-05	94,27	0
DS18N	9,54E-02	86,11	-0,035	5,73E-05	88,29	0
TS8C	7,20E-02	66,15	1,253	1,42E-05	108,14	0
TS14C	1,38E-01	82,04	0,460	3,58E-05	110,61	0
TS18C	3,09E-01	49,89	-0,363	4,66E-05	115,46	0
TS8N	7,20E-02	66,20	1,192	1,42E-05	108,14	0
TS14N	1,37E-01	82,20	-0,100	3,58E-05	110,61	0
TS18N	3,09E-01	49,92	-0,416	4,66E-05	115,46	0

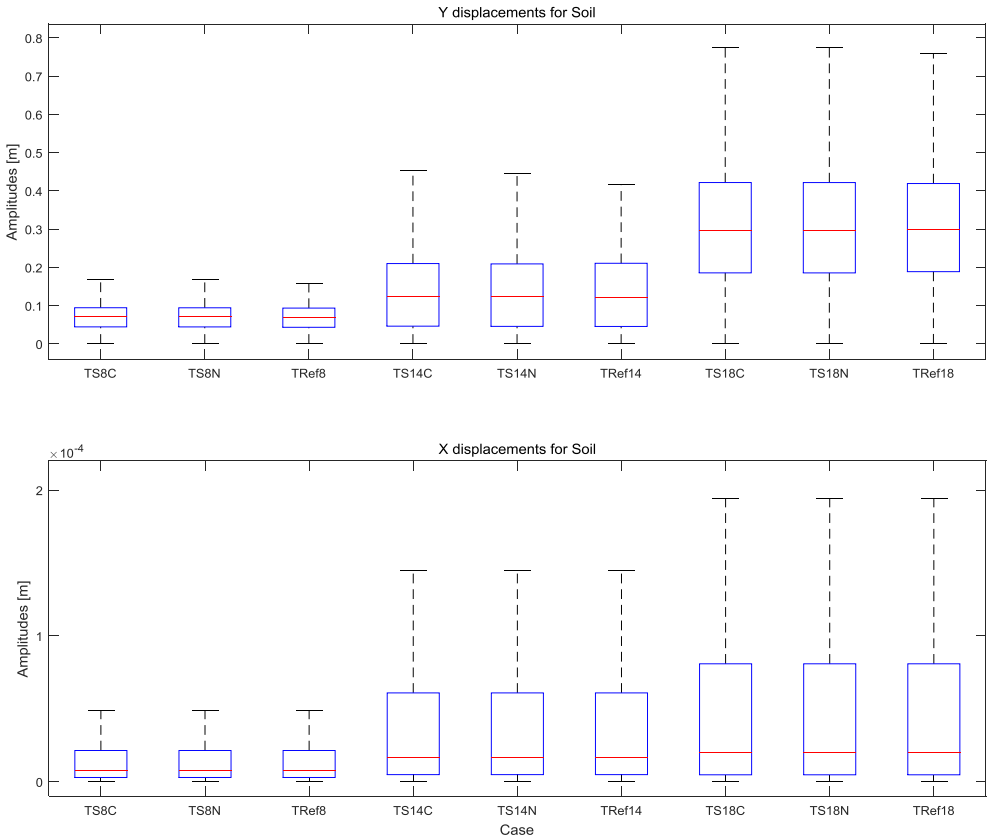

Figure 5.9: Boxplot of the amplitudes of the displacements obtained in the rainflow counting for the study case of the soil stiffness. Each graph correspond to the displacements in the y axis (top) and in the x axis (bottom).

Table 5.12: Mean, variation coefficient and variation with respect to the reference case of the bending moments in the y and z axes for the study case of the damping.

Case	Mud-line bending moment Y			Mud-line bending moment Z		
	μ [Nm]	CV [%]	Diff. with ref. case [%]	μ [Nm]	CV [%]	Diff. with ref. case [%]
DS8C	8,49E+05	97,89	-0,187	3,94E+06	119,18	0,058
DS14C	1,38E+06	104,71	-0,378	6,73E+06	146,90	-0,604
DS18C	2,18E+06	111,10	-0,180	1,01E+07	105,58	0,509
DS8N	8,49E+05	97,89	-0,144	3,94E+06	119,18	0,073
DS14N	1,38E+06	104,58	-0,278	6,74E+06	146,83	-0,464
DS18N	2,18E+06	111,18	-0,280	1,01E+07	105,64	0,410
TS8C	9,72E+05	122,92	0,683	4,80E+06	130,37	1,279
TS14C	2,37E+06	123,37	2,688	7,79E+06	158,38	1,960
TS18C	4,47E+06	117,29	-1,991	2,55E+07	99,24	-2,064
TS8N	9,68E+05	122,86	0,294	4,80E+06	130,54	1,212
TS14N	2,36E+06	123,73	2,348	7,73E+06	158,66	1,232
TS18N	4,49E+06	117,10	-1,617	2,55E+07	99,08	-1,985

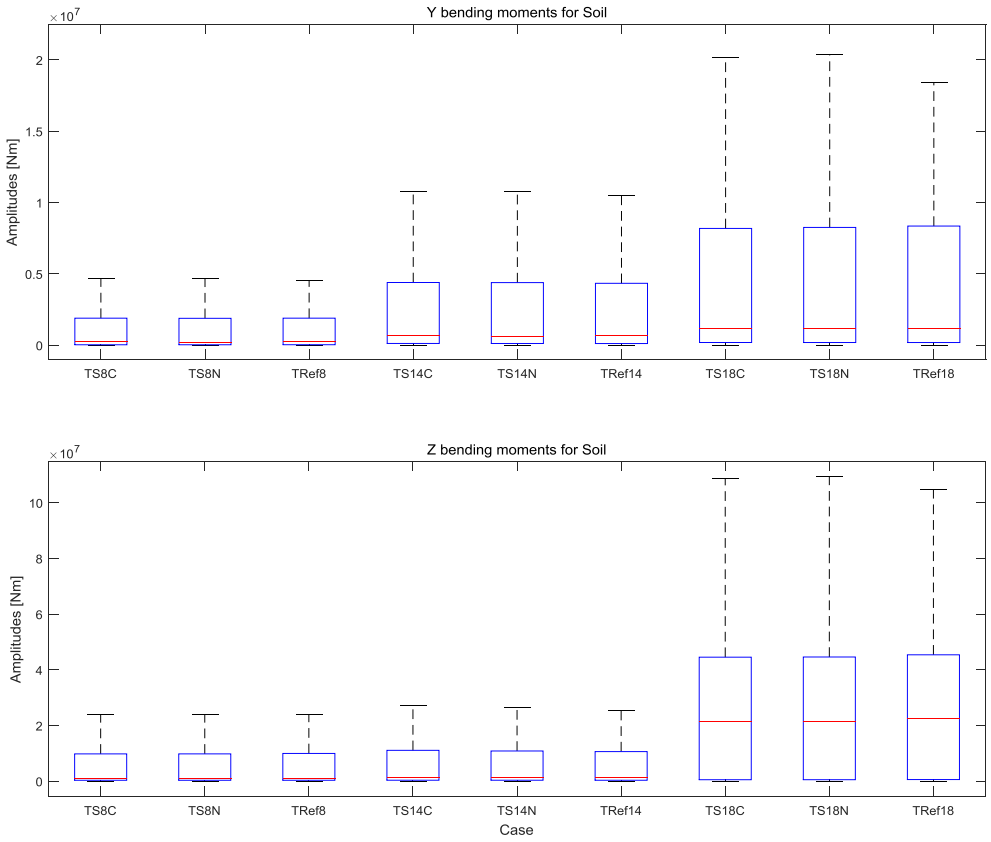

Figure 5.10: Boxplot of the amplitudes of the bending moments obtained in the rainflow counting for the study case of the soil stiffness. Each graph correspond to the displacements in the y axis (top) and in the z axis (bottom).

5.3.2. Fatigue Damage

5.3.2.1. Displacements

From the fatigue damage results presented in Table 5.13 and Figure 5.11, one can see that, in general, the fatigue damage equivalent displacement increases when the wind speed is higher, as well as its standard deviation. It is interesting to observe that the standard deviation of the displacements of the *y* axis for the TD and uncorrelated cases has a different behaviour, with a maximum value for a wind speed of 14 m/s. Although the variation coefficient has different values for each case and it is hard to achieve an overall conclusion, the variation coefficient is an order of magnitude higher in the TD case, which results in a higher scattering of the results and, in turn, in a higher fatigue damage of the structure. Additionally, the displacements of the *x* axis has really small values of the variation coefficient.

The correlated and uncorrelated cases show analogous results. The differences between these two alternative are very small, making difficult to know which case the greatest fatigue damage occurs.

Looking at the differences with the reference case, the mean values of the fatigue damage obtained here are approximately the same as the ones obtained in the reference case, with a deviation of less than 1% with respect to the mean values of the reference case. From the histograms presented in Figure 5.11, one can see that the peak frequency of the equivalent fatigue damage is close to the mean value of the reference case for the three wind speeds. The distribution of the amplitudes has a certain degree of symmetry around an average value corresponding, approximately, to the mean value of the reference case.

Table 5.13: Mean, variation coefficient and variation with respect to the reference case of the fatigue damage equivalent displacement in the y and x axes for the study case of the soil stiffness.

Case	Damage - Top displacements Y			Damage - Top displacements X		
	μ [m]	CV [%]	Diff. with ref. case [%]	μ [m]	CV [%]	Diff. with ref. case [%]
DS8C	2,73E-03	1,79E-01	6,43E-02	1,31E-06	1,13E-13	7,75E-13
DS14C	4,49E-03	4,81E-01	-1,23E-01	3,03E-06	8,40E-14	0
DS18C	4,33E-03	5,24E-01	-1,96E-02	4,00E-06	2,76E-13	-2,33E-13
DS8N	2,73E-03	1,57E-01	4,81E-02	1,31E-06	1,13E-13	7,75E-13
DS14N	4,49E-03	3,48E-01	-7,44E-02	3,03E-06	8,40E-14	0
DS18N	4,33E-03	4,53E-01	-1,22E-02	4,00E-06	2,76E-13	-2,33E-13
TS8C	3,28E-03	1,38	-2,97E-01	1,53E-06	3,46E-13	0
TS14C	5,93E-03	3,56	6,62E-01	3,63E-06	3,51E-13	-2,69E-13
TS18C	9,86E-03	1,28	-2,63E-02	4,85E-06	3,67E-13	2,09E-13
TS8N	3,29E-03	1,25	-1,85E-01	1,53E-06	3,46E-13	0
TS14N	5,91E-03	2,50	3,56E-01	3,63E-06	3,51E-13	-2,69E-13
TS18N	9,86E-03	1,32	-1,54E-02	4,85E-06	3,67E-13	2,09E-13

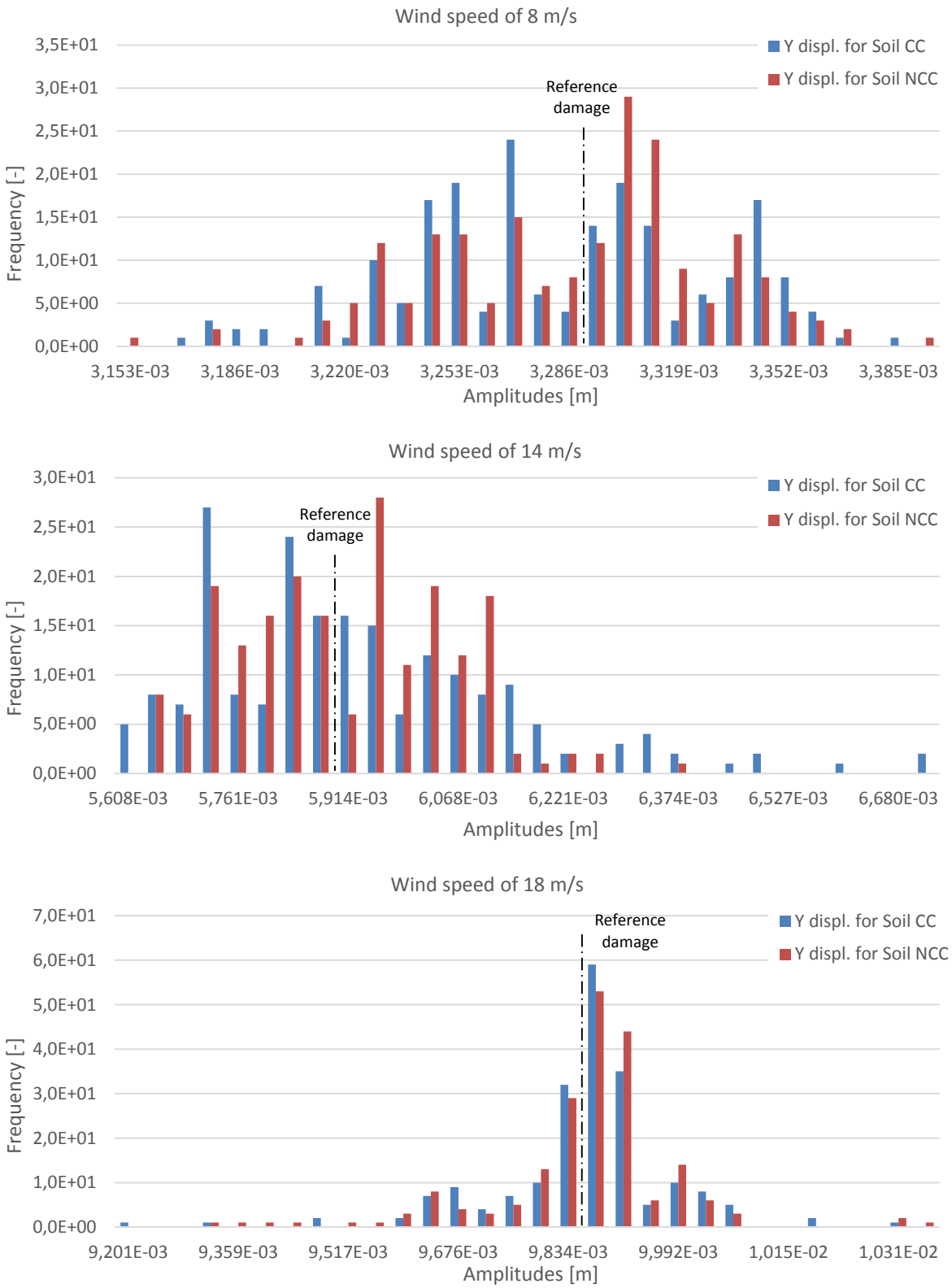

Figure 5.11: Distribution of amplitudes of the equivalent fatigue damage displacement in the y axis for the study case of the soil stiffness. Each histogram correspond to a wind speed: 8 m/s (top), 14 m/s (centre) and 18 m/s (bottom).

5.3.2.2. Bending Moments

As seen from Table 5.14 and Figure 5.12, the fatigue damage equivalent bending moments generally increase when the wind speed is higher. The scattering of these results is difficult to analyse because there is not a clear trend that explains the distribution of the values of the standard deviation and the variation coefficient. Here too, the variation coefficient is an order of magnitude higher in the TD case, with the resulting consequences that involves.

As in the case of the displacements, the correlated and uncorrelated cases show analogous results. The differences between this two cases are very small, making difficult to observe if there is more fatigue damage in the correlated or uncorrelated case.

Regarding the differences with the reference case, the mean values of the equivalent fatigue damage obtained here are similar to those obtained in the reference case, with a maximum deviation of 1.5% with respect to the mean values of the reference case. The other considerations made in the analysis of the fatigue damage equivalent displacement regarding the distribution of the results are analogous in this case.

Table 5.14: Mean, variation coefficient and variation with respect to the reference case of the fatigue damage equivalent bending moment in the y and z axes for the study case of the soil stiffness.

Case	Damage - Mud-line bending moment Y			Damage - Mud-line bending moment Z		
	μ [Nm]	CV [%]	Diff. with ref. case [%]	μ [Nm]	CV [%]	Diff. with ref. case [%]
DS8C	5,30E+04	2,93E-01	2,03E-02	3,68E+05	3,36E-01	1,24E-02
DS14C	1,01E+05	1,08E-01	1,33E-01	5,99E+05	2,25E-01	-1,46E-03
DS18C	1,58E+05	2,12E-01	-8,13E-02	5,86E+05	1,03E-01	-1,33E-02
DS8N	5,30E+04	2,56E-01	4,64E-02	3,68E+05	3,04E-01	4,19E-03
DS14N	1,01E+05	1,03E-01	1,20E-01	5,99E+05	2,03E-01	1,50E-03
DS18N	1,57E+05	1,61E-01	-9,56E-02	5,86E+05	7,69E-02	-3,19E-02
TS8C	7,41E+04	2,93	6,93E-01	4,60E+05	1,68	-6,63E-04
TS14C	1,82E+05	1,74	1,19	8,19E+05	3,63	8,59E-01
TS18C	3,10E+05	2,30	-1,52	1,38E+06	2,11	-1,35E-01
TS8N	7,39E+04	2,65	3,94E-01	4,60E+05	1,52	1,19E-01
TS14N	1,82E+05	1,44	1,23	8,16E+05	2,53	5,34E-01
TS18N	3,10E+05	2,27	-1,38	1,38E+06	2,17	-2,06E-01

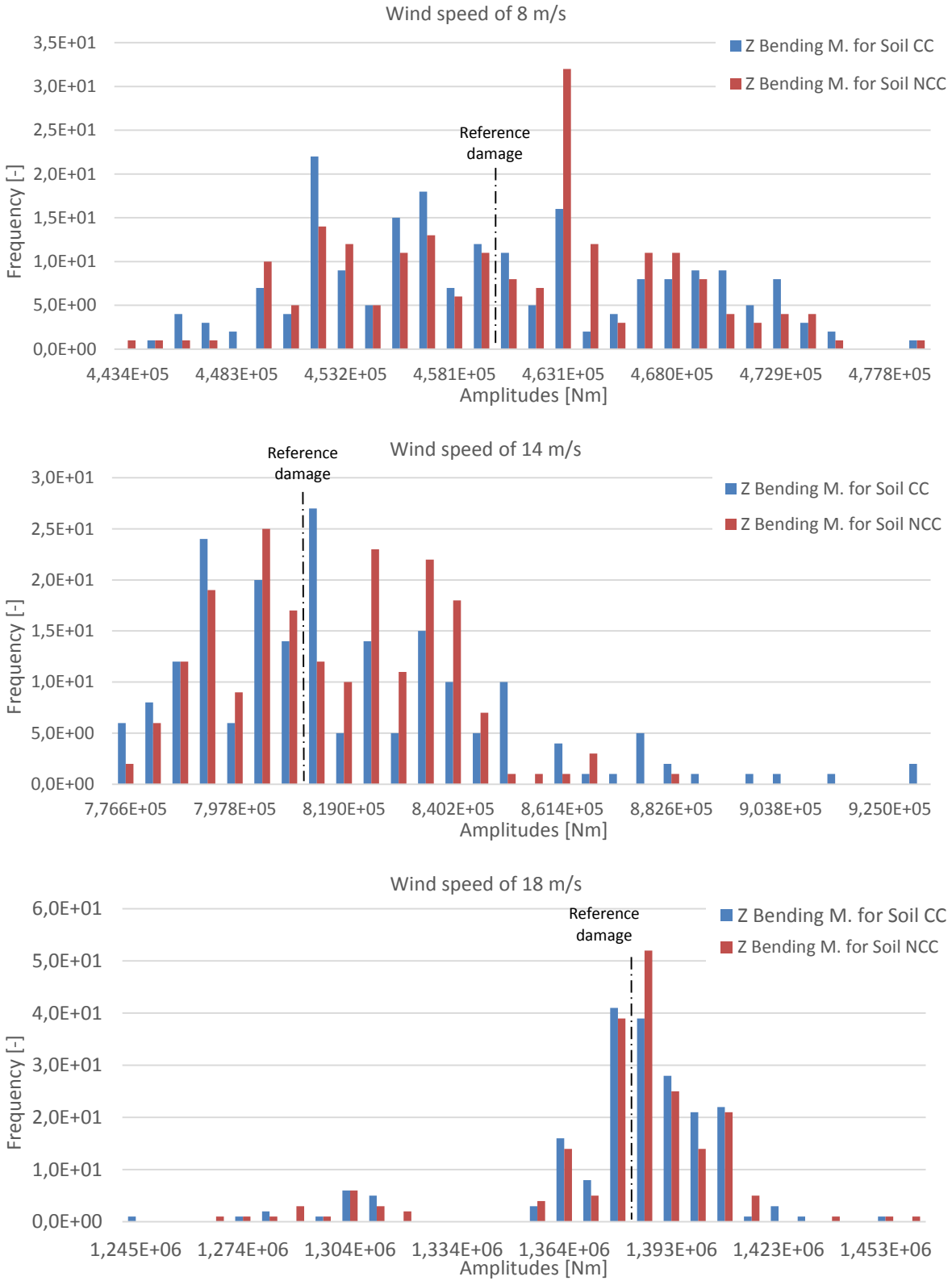

Figure 5.12: Distribution of amplitudes of the equivalent fatigue damage bending moment in the z axis for the study case of the soil stiffness. Each histogram correspond to a wind speed: 8 m/s (top), 14 m/s (centre) and 18 m/s (bottom).

5.3.3. Natural Frequencies

The variations introduced in this study case results in different value of the soil stiffness. This, in turn, is translated in different natural frequencies for each simulation due to the dependence of this parameter on the stiffness matrix of the structure.

As seen from Table 5.15 and Figure 5.13, the natural frequencies of the different cases analysed in this section have approximately the same average value. It is interesting to note that the mean values are very similar to those obtained in the reference case, with a maximum variation of the 0.0192%. Furthermore, these variations with the reference case do not seem to indicate a clear trend, since in some cases the average natural frequency is above the mean value of the reference case and in other cases the opposite is observed.

Table 5.15: Mean, standard deviation, variation coefficient and variation with respect to the reference case of the natural frequency of the structure for the study case of the soil stiffness.

Case	μ [Hz]	σ [Hz]	CV [%]	Diff. with ref. case [%]
TS8C	0,287102	7,32E-04	0,2548	-0,0162
TS14C	0,287097	8,03E-04	0,2799	-0,0180
TS18C	0,287203	6,81E-04	0,2370	0,0192
TS8N	0,287162	6,73E-04	0,2345	0,0048
TS14N	0,287125	6,08E-04	0,2116	-0,0082
TS18N	0,287159	6,76E-04	0,2353	0,0035

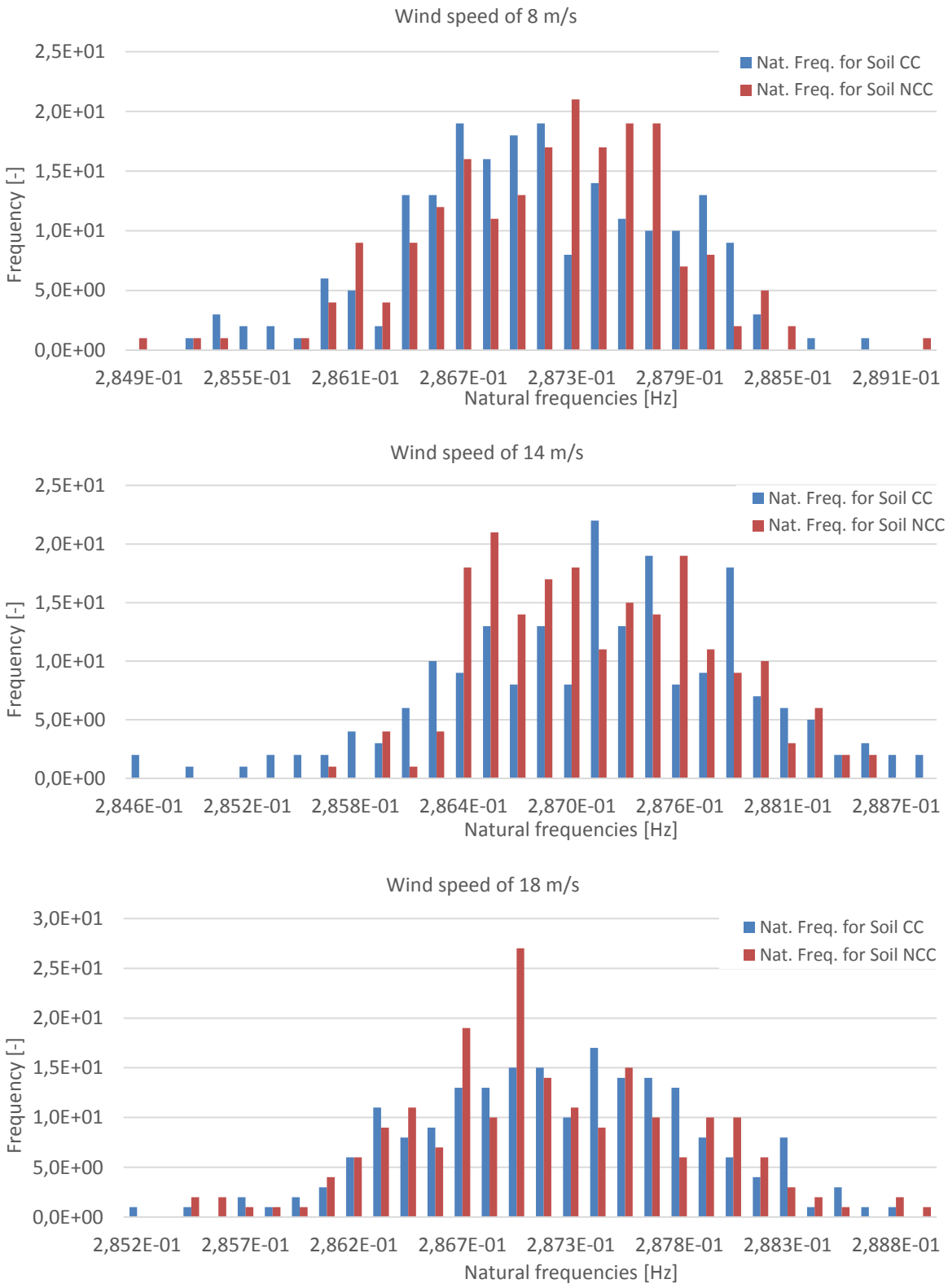

Figure 5.13: Distribution of natural frequencies for the study case of the soil stiffness. Each histogram correspond to a wind speed: 8 m/s (top), 14 m/s (centre) and 18 m/s (bottom).

5.3.4. Summary

The probability analysis of the soil stiffness has shown a weak influence on the results obtained from the simulations. The displacements and the bending moments are comparable to those obtained in the reference case and the differences between the correlated and non-correlated case are minimum. The results do not show an overall increase or decrease in displacements or bending moments relative to the reference case, but rather that in some cases the average values are above the mean values of the reference case and in other cases the opposite is observed.

The fatigue damage has a similar behaviour to which has been observed in displacements and the bending moments, in other words, the mean values of the fatigue damage obtained in this study case are equivalent to the ones obtained in the reference case. Additionally, the differences between the correlated and non-correlated case are difficult to analyse because there is not a clear trend that explains these differences. It is interesting to emphasize that the distribution of the amplitudes has a certain degree of symmetry around the average value of the samples, which, in turn, corresponds roughly to the mean value of the reference case.

To conclude, the natural frequencies of the structure seem to validate the results obtained in the analysis of the fatigue damage. The results obtained indicate that the differences with the reference case are small and do not seem to show a clear trend, having mean values higher and lower than those obtained in the reference case.

5.4. Case of Study: Structure Geometry

5.4.1. Displacements and Bending Moments

As can be seen in the results presented below, the mean value and the standard deviation of the displacements increase when the wind speed is higher, an overall trend also observed in the results of the two previous study cases. The standard deviation has different behaviour for each axis and for each damping approach. On the one hand, the standard deviation of the displacements of the *y* axis has an irregular trend and it is not possible to make assumptions about it. On the other hand, the variation coefficient of the displacements of the *x* axis for the DD case is reduced when the wind speed is higher, whereas for the TD case it is increased.

The results of the bending moments are similar to which has been observed in the displacements. The mean value of the bending moments in both axes increases when the wind speed is higher and the standard deviation has an irregular behaviour, making difficult to achieve a clear conclusion. The variation coefficients have an equivalent trend in most cases to which has been observed in the previous sections, where the maximum and the minimum values are reached for a wind speed of 14 m/s and 18 m/s, respectively.

Looking at the differences between the correlated and non-correlated case, one can see that there are significant variations between both cases in the results obtained from the simulations. The displacements and bending moments of the correlated case are generally lower than the ones obtained in the uncorrelated case, both on the mean values and the standard deviation of the results.

Comparing the results obtained here with the ones of the reference case, it can be seen that the results of the correlated case are slightly higher than those obtained in the reference case, including the mean value and the scattering of the results. In the uncorrelated case, these differences are larger and it can be observed that the results of the uncorrelated case are significantly higher than those obtained in the reference case. This difference is clearly observed in the mean values of the displacements of the *x* axis, since there is a constant variation around 45% between the correlated and uncorrelated cases with regard to the reference case.

Figure 5.14 and Figure 5.15 present the results obtained in the study case of the soil stiffness. These figures show the displacements and bending moments with boxplots. Additionally, the Table 5.16 and Table 5.17 present the mean values, variation coefficients and the percentage variances between the mean values of the different cases analysed in this section and the reference cases.

Table 5.16: Mean, variation coefficient and variation with respect to the reference case of the displacements in the y and x axes for the study case of the cross section of the structure.

Case	Top displacements Y			Top displacements X		
	μ [m]	CV [%]	Diff. with ref. case [%]	μ [m]	CV [%]	Diff. with ref. case [%]
DA8C	4,05E-02	94,22	1,555	1,31E-05	120,10	1,820
DA14C	7,46E-02	116,86	2,420	4,11E-05	98,07	2,216
DA18C	1,00E-01	91,87	5,125	5,94E-05	91,53	3,710
DA8N	3,95E-02	105,24	-0,796	1,86E-05	120,06	44,061
DA14N	9,54E-02	108,04	30,952	5,89E-05	99,50	46,543
DA18N	1,29E-01	86,43	35,351	8,50E-05	92,33	48,397
TA8C	7,57E-02	74,68	6,358	1,51E-05	111,55	6,448
TA14C	1,84E-01	78,90	33,470	3,81E-05	115,09	6,566
TA18C	2,75E-01	68,58	-11,223	4,86E-05	119,03	4,252
TA8N	7,34E-02	83,23	3,138	2,19E-05	109,26	54,494
TA14N	2,28E-01	71,01	65,984	5,40E-05	110,65	50,941
TA18N	3,42E-01	64,71	10,414	7,10E-05	113,39	52,428

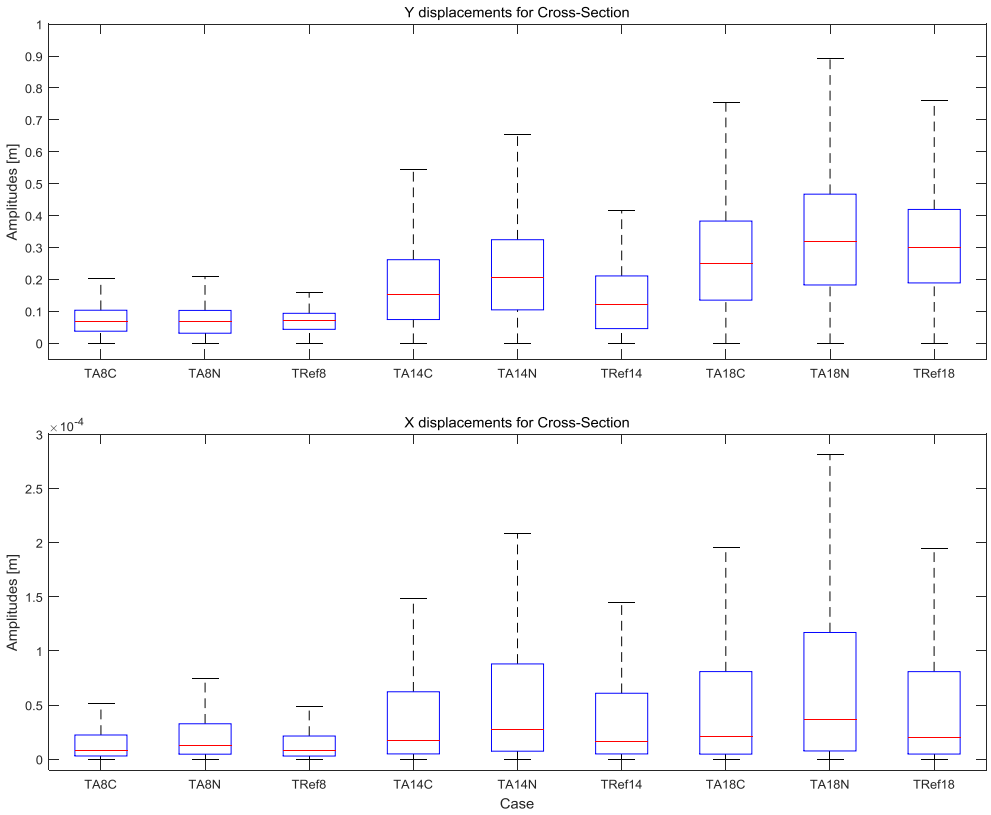

Figure 5.14: Boxplot of the amplitudes of the displacements obtained in the rainflow counting for the study case of the cross section of the structure. Each graph correspond to the displacements in the y axis (top) and in the x axis (bottom).

Table 5.17: Mean, variation coefficient and variation with respect to the reference case of the bending moments in the y and z axes for the study case of the cross section of the structure.

Case	Mud-line bending moment Y			Mud-line bending moment Z		
	μ [Nm]	CV [%]	Diff. with ref. case [%]	μ [Nm]	CV [%]	Diff. with ref. case [%]
DA8C	8,87E+05	101,43	4,283	4,06E+06	122,22	3,096
DA14C	1,38E+06	104,72	-0,351	7,01E+06	139,70	3,445
DA18C	2,25E+06	110,47	2,659	9,96E+06	108,23	-1,130
DA8N	7,06E+05	109,54	-17,013	3,05E+06	135,25	-22,608
DA14N	1,29E+06	108,01	-6,887	7,02E+06	141,35	3,599
DA18N	2,22E+06	115,21	1,327	9,84E+06	114,06	-2,287
TA8C	1,09E+06	126,00	13,114	4,89E+06	140,64	3,227
TA14C	2,25E+06	124,11	-2,272	1,06E+07	139,56	38,856
TA18C	4,44E+06	119,31	-2,662	1,94E+07	119,11	-25,573
TA8N	8,98E+05	137,64	-7,000	4,09E+06	141,89	-13,639
TA14N	2,04E+06	128,92	-11,526	1,09E+07	144,11	42,639
TA18N	4,78E+06	122,95	4,765	1,87E+07	130,19	-28,259

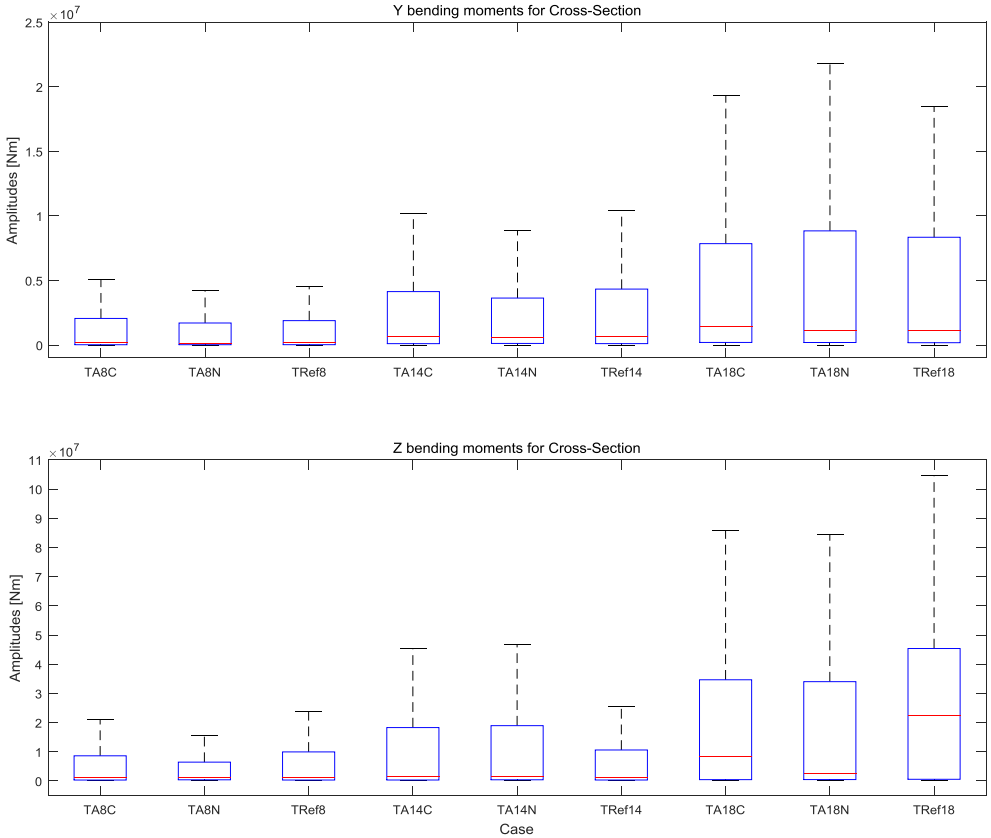

Figure 5.15: Boxplot of the amplitudes of the bending moments obtained in the rainflow counting for the study case of the cross section of the structure. Each graph correspond to the displacements in the y axis (top) and in the z axis (bottom).

5.4.2. Fatigue Damage

5.4.2.1. Displacements

From the fatigue damage results presented in Table 5.18 and Figure 5.16, one can see that in all cases the fatigue damage equivalent displacements increases when the wind speed is higher, as well as its standard deviation. The variation coefficient of the displacements of the *y* axis increase when the wind speed is higher, while the displacements of the *x* axis has different values for each case and it not possible to achieve a clear conclusion about their behaviour.

The correlated and uncorrelated cases show the most interesting results. The differences between this two alternatives indicate that the mean values of the equivalent fatigue damage of the uncorrelated case are higher than those obtained in the correlated case. This difference can be seen in the histograms presented below, where the distribution of amplitudes of the uncorrelated case is slightly shifted to the right in reference to the distribution of amplitudes of the correlated case, translating to greater fatigue damage in the structure.

Looking at the differences with the reference case, the mean values of the equivalent fatigue damage obtained here are higher to those obtained in the reference case. This difference is especially significant in relation to the uncorrelated case, where the variation reaches almost 50%. In both cases, the centre of the distributions of amplitudes, corresponding to the means of the distributions, are shifted to the right in reference to the mean values of the reference case, which means higher fatigue damage. It must be stressed that the distributions of amplitudes are quite irregular, making this analysis difficult.

Table 5.18: Mean, variation coefficient and variation with respect to the reference case of the fatigue damage equivalent displacement in the y and x axes for the study case of the cross section of the structure.

Case	Damage -Top displacements Y			Damage -Top displacements X		
	μ [m]	CV [%]	Diff. with ref. case [%]	μ [m]	CV [%]	Diff. with ref. case [%]
DA8C	2,76E-03	10,72	1,239	1,33E-06	18,92	1,672
DA14C	4,39E-03	17,34	-2,309	3,10E-06	19,51	2,200
DA18C	4,58E-03	21,50	5,863	4,14E-06	18,37	3,588
DA8N	3,04E-03	9,24	11,394	1,85E-06	23,79	40,869
DA14N	5,01E-03	13,93	11,559	4,40E-06	24,95	44,947
DA18N	5,56E-03	16,14	28,579	5,87E-06	22,54	46,743
TA8C	3,51E-03	11,11	6,536	1,62E-06	19,69	5,763
TA14C	6,97E-03	29,14	18,475	3,85E-06	21,63	6,213
TA18C	9,59E-03	30,02	-2,730	5,03E-06	20,29	3,685
TA8N	3,74E-03	9,42	13,536	2,23E-06	24,08	45,364
TA14N	8,25E-03	20,66	40,202	5,17E-06	21,84	42,676
TA18N	1,17E-02	24,78	18,793	6,86E-06	22,18	41,240

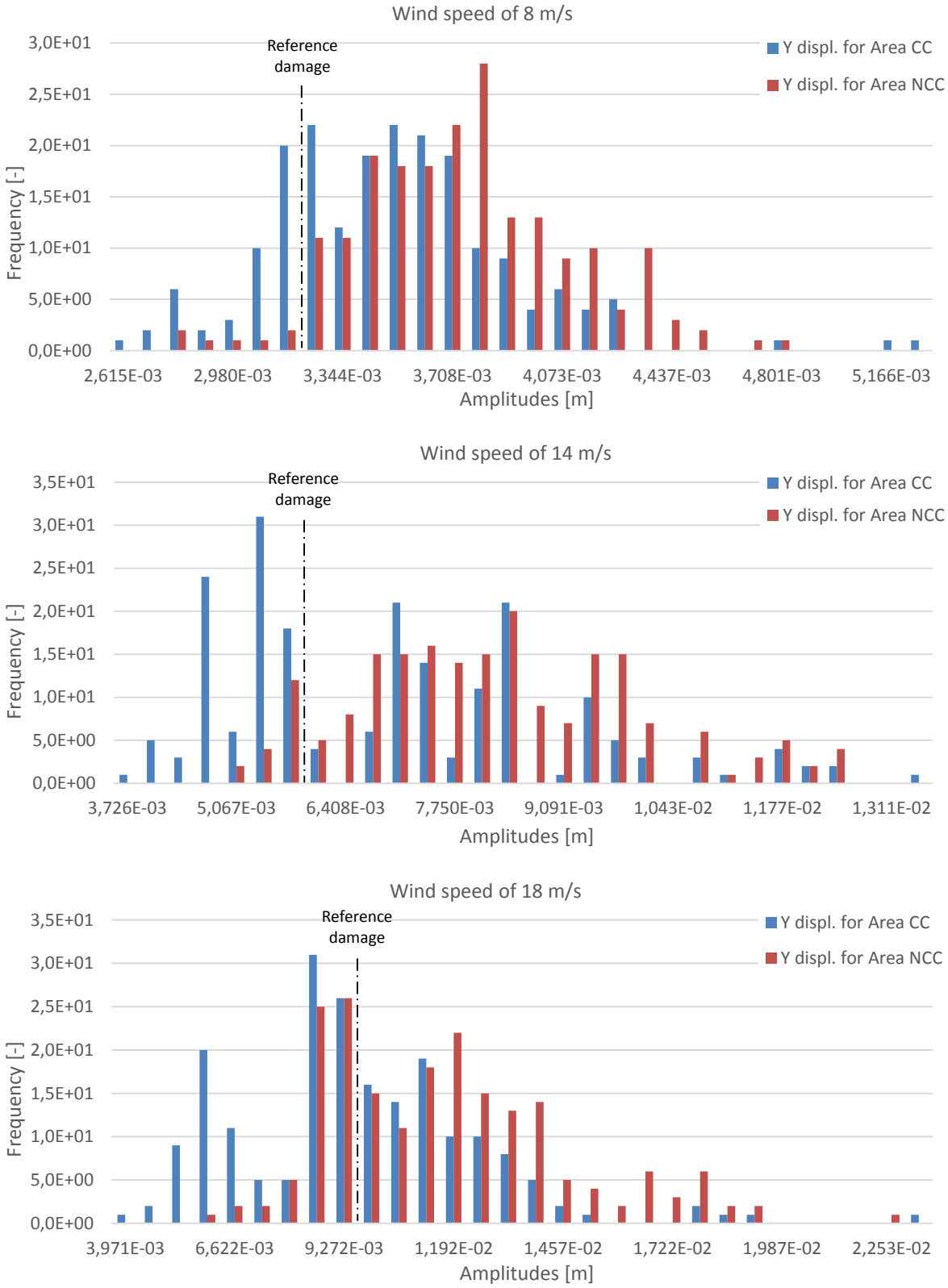

Figure 5.16: Distribution of amplitudes of the equivalent fatigue damage displacement in the y axis for the study case of the cross section of the structure. Each histogram correspond to a wind speed: 8 m/s (top), 14 m/s (centre) and 18 m/s (bottom).

5.4.2.2. Bending Moments

As seen from Table 5.19 and Figure 5.17, the fatigue damage equivalent bending moment increases when the wind speed is higher. The dispersion of these results is difficult to analyse due to the irregular trend observed in the values of the variation coefficient and, especially, standard deviation. The variation coefficient of the DD case decreases when the wind speed is higher in the different cases analysed of the two bending moments.

In contrast to the displacements, the differences between the correlated and uncorrelated cases are not so clear here. Overall, the results obtained in of both approaches are equivalent and it is difficult to determine in which case the fatigue damage is higher.

Looking at the differences with the reference case, the behaviour of the equivalent fatigue damage obtained here do not follow a regular pattern and in some cases the average values are above the mean values of the reference case and in other cases the opposite trend is observed. As has been noted in the displacements, the distributions of amplitudes are irregular and it is difficult to analyse the histograms.

Table 5.19: Mean, variation coefficient and variation with respect to the reference case of the fatigue damage equivalent bending moment in the y and z axes for the study case of the cross section of the structure.

Case	Damage - Mud-line bending moment Y			Damage - Mud-line bending moment Z		
	μ [Nm]	CV [%]	Diff. with ref. case [%]	μ [Nm]	CV [%]	Diff. with ref. case [%]
DA8C	5,55E+04	15,83	4,841	3,73E+05	9,53	1,382
DA14C	1,00E+05	4,16	-0,432	5,75E+05	6,21	-4,069
DA18C	1,61E+05	1,51	1,946	5,90E+05	4,02	0,797
DA8N	5,00E+04	6,87	-5,610	3,41E+05	8,36	-7,150
DA14N	9,97E+04	3,30	-1,220	5,67E+05	7,79	-5,378
DA18N	1,64E+05	1,71	3,805	6,10E+05	5,31	4,119
TA8C	8,23E+04	16,43	11,767	4,85E+05	12,75	5,386
TA14C	1,71E+05	12,37	-4,660	9,00E+05	9,57	10,809
TA18C	3,12E+05	13,94	-0,733	1,27E+06	15,08	-7,925
TA8N	7,75E+04	8,95	5,271	4,36E+05	11,40	-5,154
TA14N	1,67E+05	11,09	-6,898	9,65E+05	9,69	18,823
TA18N	3,42E+05	11,38	8,895	1,38E+06	15,84	-0,278

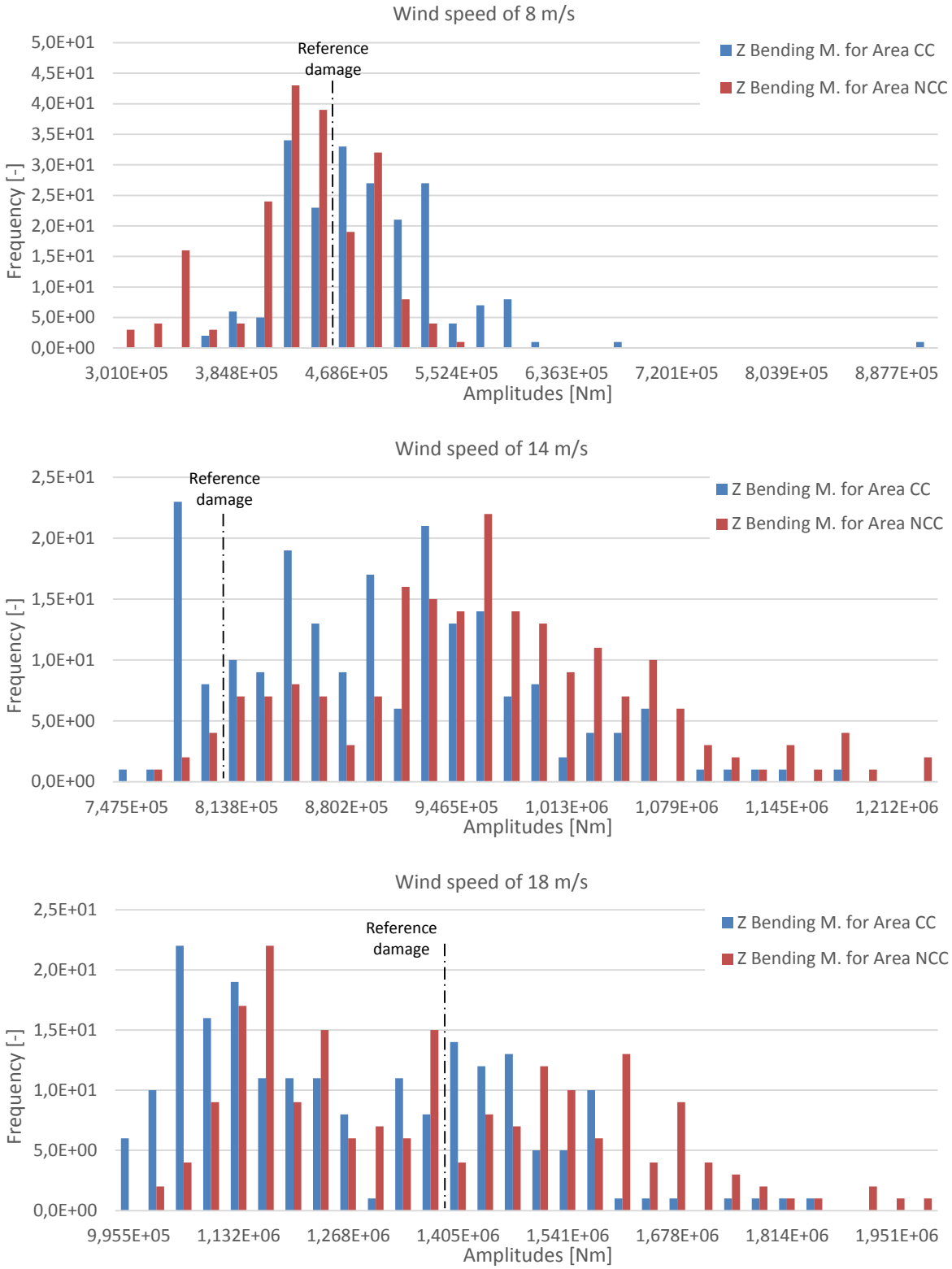

Figure 5.17: Distribution of amplitudes of the equivalent fatigue damage bending moment in the z axis for the study case of the cross section of the structure. Each histogram correspond to a wind speed: 8 m/s (top), 14 m/s (centre) and 18 m/s (bottom).

5.4.3. Additional Fatigue Damage Analysis

The magnitude of the effects observed in the equivalent fatigue damage of this study case and the irregular behaviour of the distributions of amplitudes observed in the histograms have motivated to repeat some simulations by increasing the number of samples. The reason behind is to validate the previous results and deepen into the analysis.

From the fatigue damage results presented in Table 5.20 and Table 5.21 and Figure 5.18 and Figure 5.19, one can see that the results obtained are similar to those obtained for 200 simulations. By increasing the number of simulation until 1000 samples, the histograms show a better distribution of amplitudes of displacements and bending moments. The distribution of amplitudes of the displacements shown in Figure 5.18 and Figure 5.19 indicates that the uncorrelated case has a more even distribution compared with the distribution observed in the correlated case.

Looking at other aspects, the comments made about the mean values, standard deviations and variation coefficients are analogous to which has been indicated previously, as well as the differences with the reference case.

Table 5.20: Mean, variation coefficient and variation with respect to the reference case of the fatigue damage equivalent displacement in the y and x axes for the additional study case of the cross section of the structure.

Case	Damage -Top displacements Y			Damage -Top displacements X		
	μ [m]	CV [%]	Diff. with ref. case [%]	μ [m]	CV [%]	Diff. with ref. case [%]
TA8C_2	3,51E-03	11,37	6,510	1,62E-06	21,27	5,362
TA14C_2	6,78E-03	28,75	15,165	3,77E-06	21,41	4,001
TA18C_2	9,64E-03	32,37	-2,266	5,06E-06	20,64	4,263
TA8N_2	3,70E-03	10,44	12,455	2,19E-06	22,85	43,158
TA14N_2	8,35E-03	18,83	41,832	5,18E-06	21,89	42,943
TA18N_2	1,18E-02	23,83	19,761	6,87E-06	22,68	41,590

Table 5.21: Mean, variation coefficient and variation with respect to the reference case of the fatigue damage equivalent bending moment in the y and z axes for the additional study case of the cross section of the structure.

Case	Damage - Mud-line bending moment Y			Damage - Mud-line bending moment Z		
	μ [Nm]	CV [%]	Diff. with ref. case [%]	μ [Nm]	CV [%]	Diff. with ref. case [%]
TA8C_2	8,40E+04	20,28	14,021	4,91E+05	18,10	6,687
TA14C_2	1,72E+05	12,36	-4,372	8,95E+05	9,39	10,271
TA18C_2	3,14E+05	12,98	-0,107	1,27E+06	15,60	-8,093
TA8N_2	7,71E+04	8,54	4,752	4,33E+05	12,21	-5,813
TA14N_2	1,65E+05	10,62	-8,127	9,73E+05	8,91	19,843
TA18N_2	3,44E+05	12,48	9,441	1,38E+06	15,33	0,147

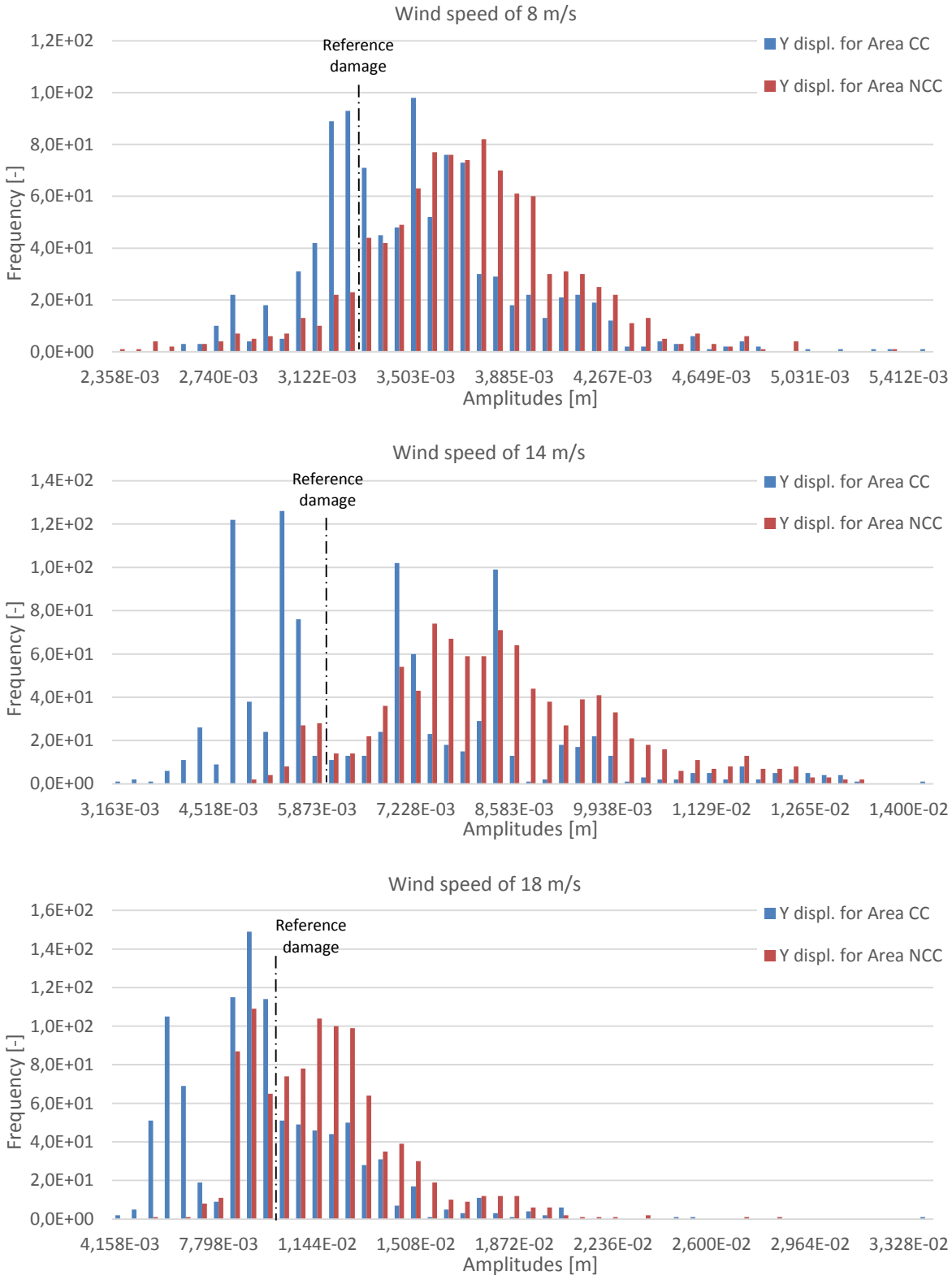

Figure 5.18: Distribution of amplitudes of the equivalent fatigue damage displacement in the y axis for the additional study case of the cross section of the structure. Each histogram correspond to a wind speed: 8 m/s (top), 14 m/s (centre) and 18 m/s (bottom).

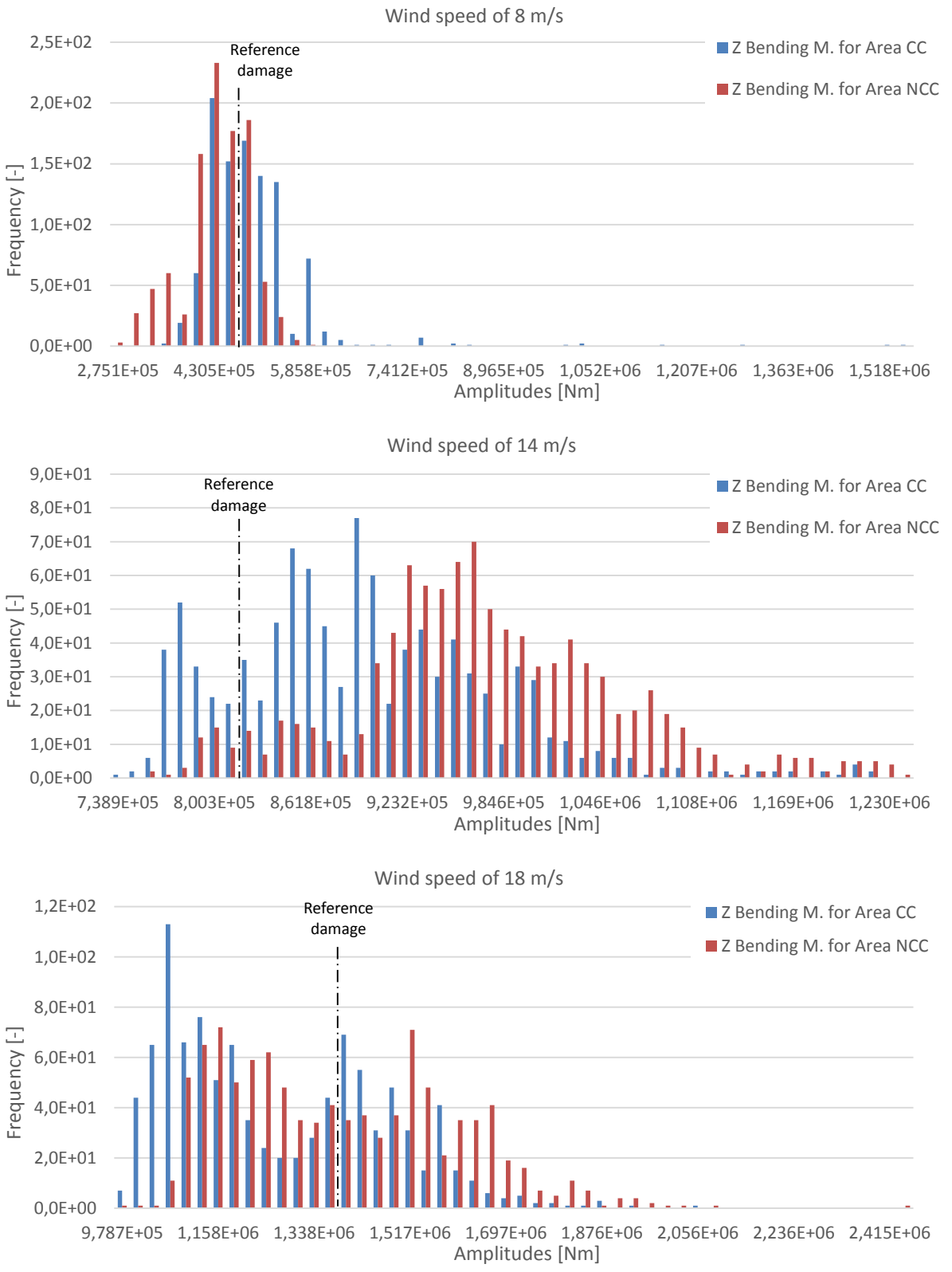

Figure 5.19: Distribution of amplitudes of the equivalent fatigue damage bending moment in the z axis for the additional study case of the cross section of the structure. Each histogram correspond to a wind speed: 8 m/s (top), 14 m/s (centre) and 18 m/s (bottom).

5.4.4. Natural Frequencies

The variations introduced in this study case results in different values of the cross section of the support structure. This, in turn, is translated in different natural frequencies for each simulation due to the dependence of this parameter on the stiffness matrix of the structure.

The results presented in Table 5.22 and Figure 5.20 correspond to the natural frequencies obtained for the analysis performed with 1000 samples. The variations in the cross section of the structure are not affected by a variation of the wind speed, which is why the mean values of the natural frequencies have a similar value for the correlated and uncorrelated case. The natural frequencies of the correlated case are on average a 0.6% lower than the natural frequency of the reference case. On the other hand, the natural frequencies of the uncorrelated case are on average a 7.5% lower than the natural frequency of the reference case.

It must be emphasized that the distribution of amplitudes of the histograms shown in Figure 5.20 has approximately the same shape for the correlated and uncorrelated cases. This behaviour is reasonable due to the fact that the natural frequencies are not affected by a variation of the wind speed. This can be clearly observed because of the large number of samples, in contrast to the results obtained in the case study of the soil stiffness.

Table 5.22: Mean, standard deviation, variation coefficient and variation with respect to the reference case of the natural frequency for the additional study case of the cross section of the structure.

Case	μ [Hz]	σ [Hz]	CV [%]	Diff. with ref. case [%]
TA8C_2	0,284662	2,36E-02	8,2791	-0,8661
TA14C_2	0,285966	2,41E-02	8,4357	-0,4118
TA18C_2	0,285406	2,36E-02	8,2748	-0,6068
TA8N_2	0,265242	1,52E-02	5,7365	-7,6291
TA14N_2	0,265898	1,49E-02	5,5979	-7,4006
TA18N_2	0,265887	1,51E-02	5,6721	-7,4044

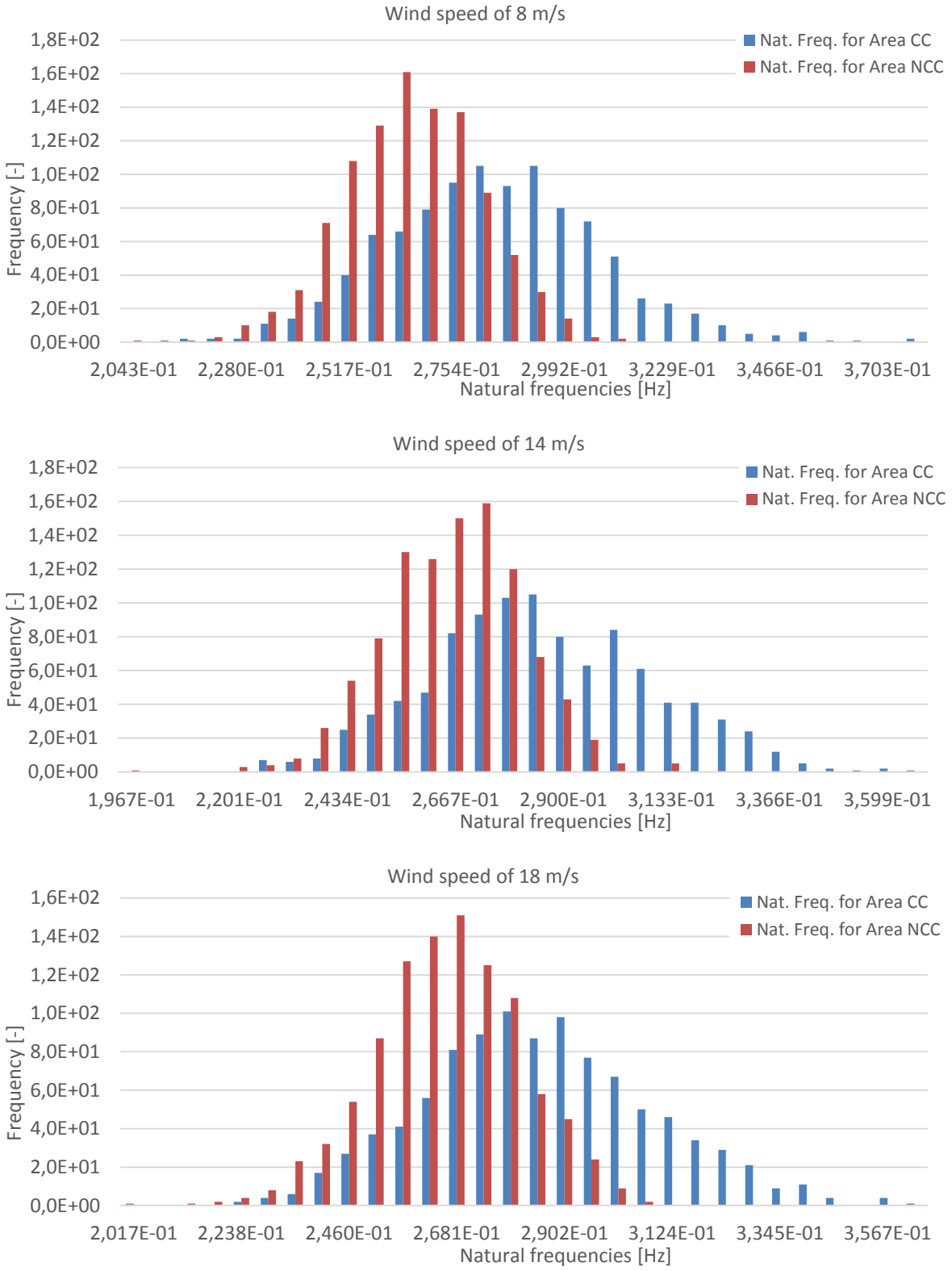

Figure 5.20: Distribution of natural frequencies for the study case of the cross section of the structure. Each histogram correspond to a wind speed: 8 m/s (top), 14 m/s (centre) and 18 m/s (bottom).

5.4.5. Summary

The study case of the geometry of the structure has a notable impact on the dynamic response of the structure as has been seen in the results obtained in this section. First, the displacements and the bending moments are higher than those obtained in the reference case, both on the mean values and the scattering of the results. This difference is particularly large in the uncorrelated case. Looking at the differences between the correlated and non-correlated case, the results of the correlated case are lower than the ones obtained in the uncorrelated case.

As regards fatigue damage, on average the mean values of the equivalent fatigue damage are higher than those obtained in the reference case. This is especially evident in the case of the displacements, where it is reached a maximum variation of 47%. Comparing the correlated with the uncorrelated case, the fatigue damage is higher in the uncorrelated case. It is worth stressing that, in both cases, the distribution of amplitudes is shifted to the right in reference to the mean value of the reference case, translating to higher fatigue damage. Furthermore, the irregular distributions observed in the histograms have suggested that the number of samples used in the analysis could be inadequate and, for this reason, some simulations have been repeated by increasing the number of samples to 1000. Overall, the results obtained are analogous to those have been obtained with 200 samples, but it can be observed a more regular and natural distribution of amplitudes.

The natural frequencies of the structure indicate a clear difference between the correlated and uncorrelated case. The results show that the natural frequencies of the uncorrelated case are a 7% lower than the ones obtained in the correlated case. In both cases, the natural frequencies are higher than those obtained in the reference case. Furthermore, the additional simulations with 1000 samples enable to indicate that the natural frequencies are not affected by a variation of the wind speed and it can clearly be observed the bell-shape of the histograms that are used to represent the distribution of natural frequencies.

5.5. Case of Study: Combined Analysis

The results obtained in this study case are a combination of the performances observed in the previous sections. This means that many of the behaviours noticed in the other cases are the same here and, therefore, they will not be mentioned.

5.5.1. Displacements and Bending Moments

In the study case of the combined analysis, one can clearly see which variables analysed probabilistically have a large effect on the dynamic response of the structure. Both displacements and bending moments have shown the geometry of the structure as the variable with the large effects on the results. The uncorrelated cases of this variable show the higher mean values of displacements and bending moments. The effects of the other two variables, degree of damping and soil stiffness, have analogous responses to which have been observed in the previous sections. Therefore, the effects observed are small and irregular, making difficult to achieve a clear conclusion of their trend.

Looking at the differences with the reference case, in general the cases analysed here have mean values of displacements and bending moments higher than those obtained in the reference case. Taking into account only the effect of the geometry of the structure, these differences are as expected. Additionally, it is reasonable to think that the superposition of the different effects of each variable results in higher differences with regard to the reference case. In this sense, it has been obtained the higher difference with respect to the reference case, with a variation around 73% in the displacements of the *y* axis.

Figure 5.21 and Figure 5.22 present the results obtained in the study case of the combined analysis. These figures show with boxplots the displacements and bending moments. Additionally, the Table 5.23 and Table 5.24 present the mean values, variation coefficients and the percentage variances between the mean values of the different cases analysed in this section and the reference cases.

Table 5.23: Mean, variation coefficient and variation with respect to the reference case of the displacements in the y and x axes for the combined study case.

Case	Top displacements Y			Top displacements X		
	μ [m]	CV [%]	Diff. with ref. case [%]	μ [m]	CV [%]	Diff. with ref. case [%]
DC8CC	4,69E-02	91,68	17,74	1,38E-05	119,09	6,75
DC14CC	8,13E-02	114,91	11,63	4,03E-05	101,98	0,17
DC18CC	1,10E-01	96,91	14,98	5,75E-05	97,85	0,42
DC8C	4,81E-02	92,43	20,72	1,38E-05	118,05	7,29
DC14C	8,04E-02	115,46	10,37	4,06E-05	101,18	1,01
DC18C	1,14E-01	92,53	19,21	5,67E-05	97,99	-0,88
DC8NC	4,63E-02	101,26	16,22	2,00E-05	116,63	55,37
DC14NC	1,02E-01	107,70	40,07	5,73E-05	101,51	42,64
DC18NC	1,46E-01	85,34	52,89	8,00E-05	98,72	39,78
DC8NN	4,52E-02	103,74	13,48	1,87E-05	115,45	44,99
DC14NN	1,05E-01	106,37	44,59	5,77E-05	104,09	43,46
DC18NN	1,43E-01	86,34	49,26	7,96E-05	97,18	38,99
TC8CC	7,74E-02	73,89	6,15	1,50E-05	112,62	6,78
TC14CC	1,77E-01	80,09	28,87	3,74E-05	115,63	4,40
TC18CC	2,73E-01	72,21	-6,65	4,89E-05	119,61	9,24
TC8CN	7,61E-02	73,73	6,14	1,49E-05	111,28	5,06
TC14CN	1,78E-01	77,73	29,25	3,72E-05	114,31	6,09
TC18CN	2,78E-01	67,70	-12,80	4,86E-05	118,45	3,79
TC8NC	7,31E-02	82,44	4,30	2,14E-05	107,32	54,09
TC14NC	2,29E-01	69,20	71,10	5,31E-05	110,20	52,89
TC18NC	3,44E-01	62,96	10,40	6,97E-05	113,29	60,53
TC8NN	7,44E-02	83,25	2,46	2,22E-05	107,24	52,35
TC14NN	2,38E-01	68,58	73,17	5,50E-05	109,94	53,80
TC18NN	3,46E-01	62,43	15,81	7,22E-05	112,83	54,97

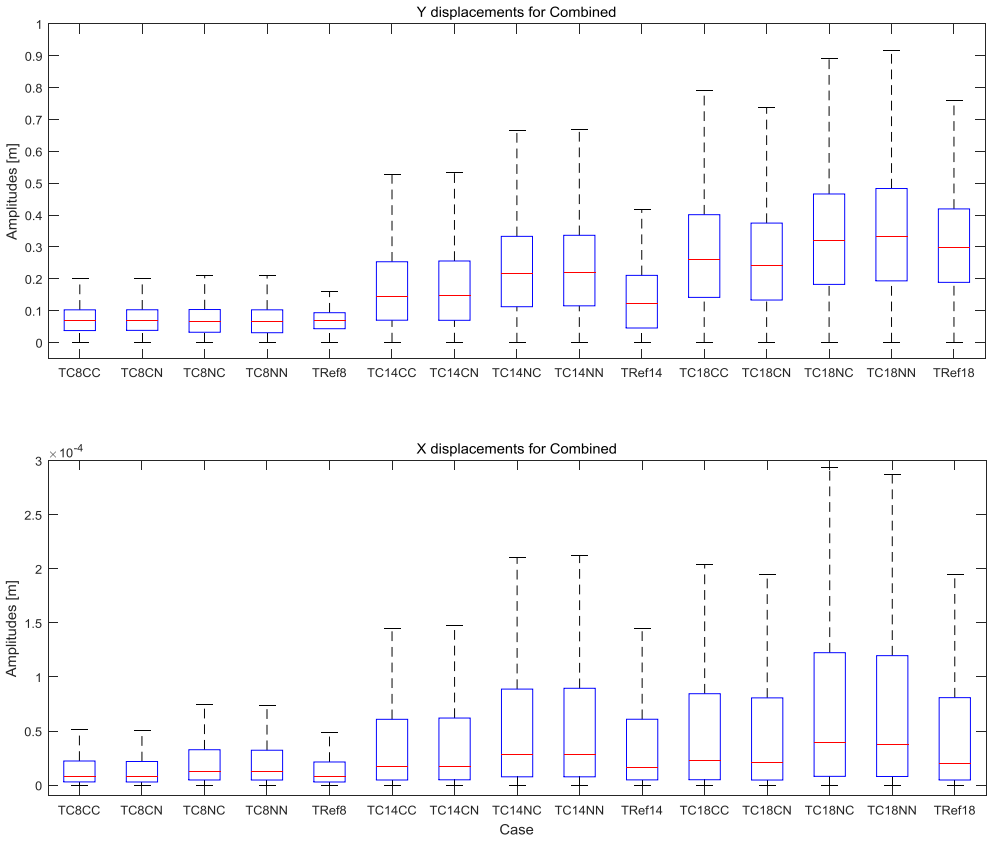

Figure 5.21: Boxplot of the amplitudes of the displacements obtained in the rainflow counting for the combined study case. Each graph correspond to the displacements in the y axis (top) and in the x axis (bottom).

Table 5.24: Mean, variation coefficient and variation with respect to the reference case of the bending moments in the y and z axes for the combined study case.

Case	Mud-line bending moment Y			Mud-line bending moment Z		
	μ [Nm]	CV [%]	Diff. with ref. case [%]	μ [Nm]	CV [%]	Diff. with ref. case [%]
DC8CC	9,11E+05	111,27	7,08	4,09E+06	131,16	3,70
DC14CC	1,45E+06	108,93	4,72	7,14E+06	142,48	5,39
DC18CC	2,35E+06	115,77	7,38	1,04E+07	113,88	3,70
DC8C	9,15E+05	115,21	7,56	4,12E+06	135,31	4,60
DC14C	1,42E+06	108,63	2,36	7,15E+06	141,26	5,57
DC18C	2,43E+06	115,88	10,89	1,08E+07	113,86	6,79
DC8NC	7,31E+05	122,75	-14,08	3,21E+06	140,60	-18,63
DC14NC	1,33E+06	111,14	-4,10	7,18E+06	144,21	5,98
DC18NC	2,47E+06	121,51	13,06	1,06E+07	120,53	5,15
DC8N	7,26E+05	122,15	-14,65	3,22E+06	140,00	-18,22
DC14N	1,34E+06	111,71	-2,99	7,24E+06	145,22	6,92
DC18N	2,45E+06	120,14	12,18	1,04E+07	120,46	2,95
TC8CC	1,16E+06	128,52	15,20	5,17E+06	145,05	4,67
TC14CC	2,29E+06	122,98	-0,92	1,05E+07	140,05	37,13
TC18CC	4,41E+06	119,68	-4,17	1,89E+07	120,98	-24,18
TC8CN	1,14E+06	125,41	19,14	5,03E+06	141,36	7,23
TC14CN	2,25E+06	123,29	-2,48	1,06E+07	139,29	33,59
TC18CN	4,44E+06	120,21	-3,06	1,95E+07	118,72	-26,99
TC8NC	9,00E+05	137,16	-7,65	4,10E+06	141,73	-12,82
TC14NC	2,04E+06	128,56	-13,12	1,11E+07	142,87	46,05
TC18NC	4,76E+06	123,56	5,02	1,90E+07	128,04	-30,31
TC8NN	8,74E+05	138,86	-7,31	4,05E+06	142,94	-13,24
TC14NN	1,99E+06	129,65	-13,79	1,12E+07	142,57	46,79
TC18NN	4,73E+06	124,61	3,84	1,85E+07	129,26	-26,81

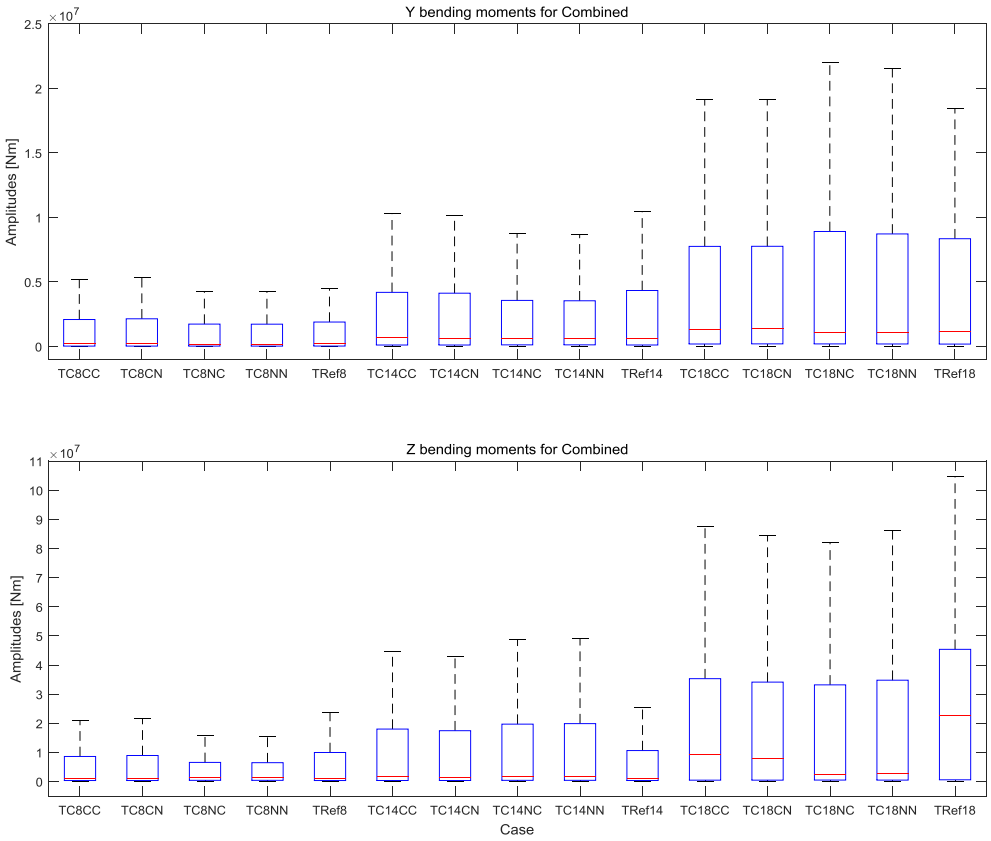

Figure 5.22: Boxplot of the amplitudes of the bending moments obtained in the rainflow counting for the combined study case. Each graph correspond to the displacements in the y axis (top) and in the z axis (bottom).

5.5.2. Fatigue Damage

From the fatigue damage results presented in Table 5.25 and Table 5.26, and Figure 5.23 and Figure 5.24, one can see that, here too, the main effects on the equivalent fatigue damage of displacements and bending moments are caused by the geometry of the structure, as a probabilistic variable. The histograms of the Figure 5.23 and Figure 5.24 show a clear trend for the cases in which the geometry of the structure is treated as correlated, and a different trend when it is treated as uncorrelated. As noted in the study case of the geometry of the structure, the higher equivalent fatigue damage is obtained for the uncorrelated case of the geometry of the structure. The effect of the soil stiffness can be appreciated in the histograms, but is small and irregular, making difficult to achieve a clear conclusion about in which cases the fatigue damage is higher.

Regarding the differences with respect to the reference case, the equivalent fatigue damage obtained for the different cases analysed here is in general higher than the one obtained in the reference case. This consideration is evident in the case of the displacements, where in all the cases the mean values are higher than those obtained in the reference case. Furthermore, the results of the displacements show the higher differences with respect to the reference case, with a maximum variation around 50% in the displacements of the *x* axis. This trend, however, is not observed in the bending moments, since the differences with respect to the reference case are lower and in some cases the average values are above the mean values of the reference case and in other cases the opposite trend is observed.

Table 5.25: Mean, variation coefficient and variation with respect to the reference case of the fatigue damage equivalent displacement in the y and x axes for the combined study case.

Case	Damage - Top displacements Y			Damage - Top displacements X		
	μ [m]	CV [%]	Diff. with ref. case [%]	μ [m]	CV [%]	Diff. with ref. case [%]
DC8CC	2,89E-03	15,38	6,11	1,41E-06	24,69	7,22
DC14CC	4,60E-03	21,52	2,42	3,16E-06	22,97	4,04
DC18CC	4,97E-03	30,83	14,76	4,16E-06	26,53	4,04
DC8C	2,98E-03	12,45	9,18	1,43E-06	21,11	9,12
DC14C	4,57E-03	21,43	1,79	3,15E-06	22,94	3,71
DC18C	5,03E-03	27,79	16,14	4,21E-06	23,10	5,25
DC8NC	3,17E-03	13,73	16,35	1,98E-06	26,05	51,40
DC14NC	5,24E-03	19,44	16,68	4,37E-06	26,73	44,03
DC18NC	6,05E-03	21,34	39,73	5,88E-06	26,84	47,14
DC8N	3,19E-03	12,26	17,00	1,84E-06	23,77	40,44
DC14N	5,35E-03	18,97	19,11	4,43E-06	30,58	46,20
DC18N	5,97E-03	22,02	37,86	5,81E-06	24,55	45,27
TC8CC	3,51E-03	11,50	6,11	1,61E-06	22,15	5,86
TC14CC	6,83E-03	29,28	16,07	3,78E-06	22,43	4,35
TC18CC	9,61E-03	32,61	2,13	5,06E-06	21,18	7,94
TC8CN	3,50E-03	12,41	4,68	1,60E-06	22,13	4,35
TC14CN	6,77E-03	28,02	16,56	3,76E-06	20,95	5,77
TC18CN	9,65E-03	30,98	-4,32	5,04E-06	19,72	3,33
TC8NC	3,69E-03	9,96	13,39	2,18E-06	23,06	44,32
TC14NC	8,23E-03	19,35	42,37	5,10E-06	22,44	43,98
TC18NC	1,16E-02	23,97	18,65	6,77E-06	24,12	47,81
TC8NN	3,75E-03	10,08	12,12	2,24E-06	21,74	43,06
TC14NN	8,47E-03	18,85	43,93	5,25E-06	21,37	44,77
TC18NN	1,17E-02	25,53	24,05	6,95E-06	20,16	43,24

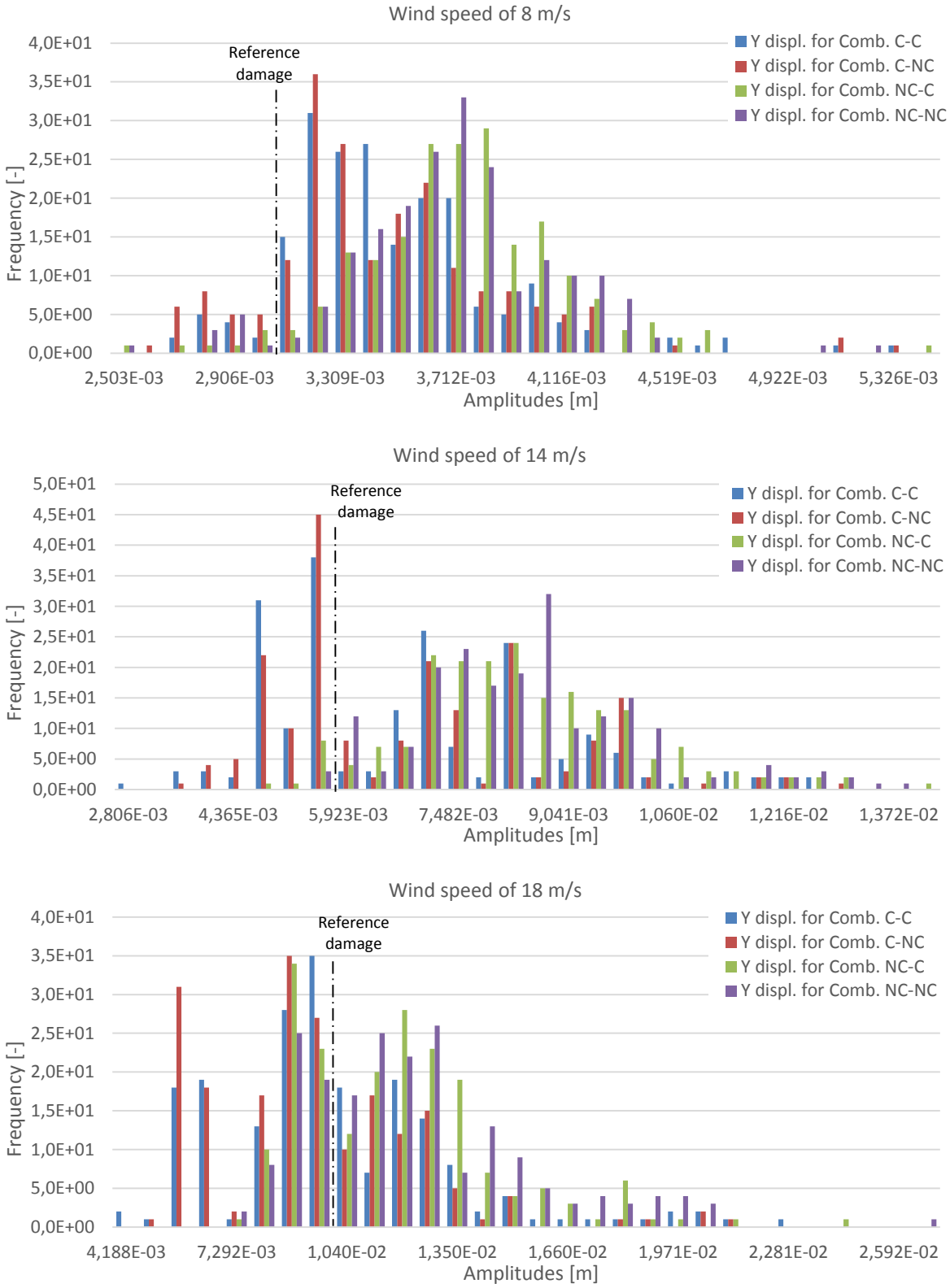

Figure 5.23: Distribution of amplitudes of the equivalent fatigue damage displacement in the y axis for the combined study case. Each histogram correspond to a wind speed: 8 m/s (top), 14 m/s (centre) and 18 m/s (bottom).

Table 5.26: Mean, variation coefficient and variation with respect to the reference case of the fatigue damage equivalent bending moment in the y and z axes for the combined study case.

Case	Damage - Mud-line bending moment Y			Damage - Mud-line bending moment Z		
	μ [Nm]	CV [%]	Diff. with ref. case [%]	μ [Nm]	CV [%]	Diff. with ref. case [%]
DC8CC	6,06E+04	20,29	14,45	3,91E+05	13,61	6,42
DC14CC	1,06E+05	12,73	5,02	6,04E+05	8,99	0,85
DC18CC	1,68E+05	17,19	6,59	6,32E+05	17,02	7,83
DC8C	6,15E+04	25,93	16,21	3,98E+05	17,61	8,21
DC14C	1,04E+05	11,92	2,80	5,95E+05	9,48	-0,78
DC18C	1,73E+05	17,97	9,81	6,50E+05	17,72	11,01
DC8NC	5,58E+04	17,20	5,30	3,55E+05	16,53	-3,33
DC14NC	1,02E+05	10,88	1,50	5,92E+05	13,07	-1,19
DC18NC	1,82E+05	19,62	15,23	6,79E+05	16,85	16,01
DC8N	5,48E+04	17,68	3,49	3,57E+05	13,05	-2,78
DC14N	1,03E+05	11,33	2,50	6,08E+05	12,15	1,51
DC18N	1,80E+05	18,07	14,00	6,68E+05	16,19	14,04
TC8CC	8,66E+04	20,43	13,56	5,02E+05	21,47	6,97
TC14CC	1,71E+05	13,28	-4,56	8,98E+05	9,51	10,67
TC18CC	3,12E+05	13,53	-1,00	1,26E+06	16,03	-6,95
TC8CN	8,43E+04	20,91	16,33	4,92E+05	21,42	7,89
TC14CN	1,70E+05	11,88	-4,58	8,97E+05	9,46	9,61
TC18CN	3,16E+05	14,59	0,62	1,28E+06	15,42	-8,71
TC8NC	7,74E+04	7,73	4,51	4,35E+05	10,89	-3,84
TC14NC	1,66E+05	11,10	-7,53	9,69E+05	9,70	19,59
TC18NC	3,44E+05	11,16	10,42	1,38E+06	16,17	-1,18
TC8NN	7,64E+04	9,19	4,93	4,33E+05	11,03	-3,97
TC14NN	1,64E+05	10,95	-8,38	9,74E+05	8,61	20,04
TC18NN	3,45E+05	13,31	9,95	1,36E+06	15,49	1,22

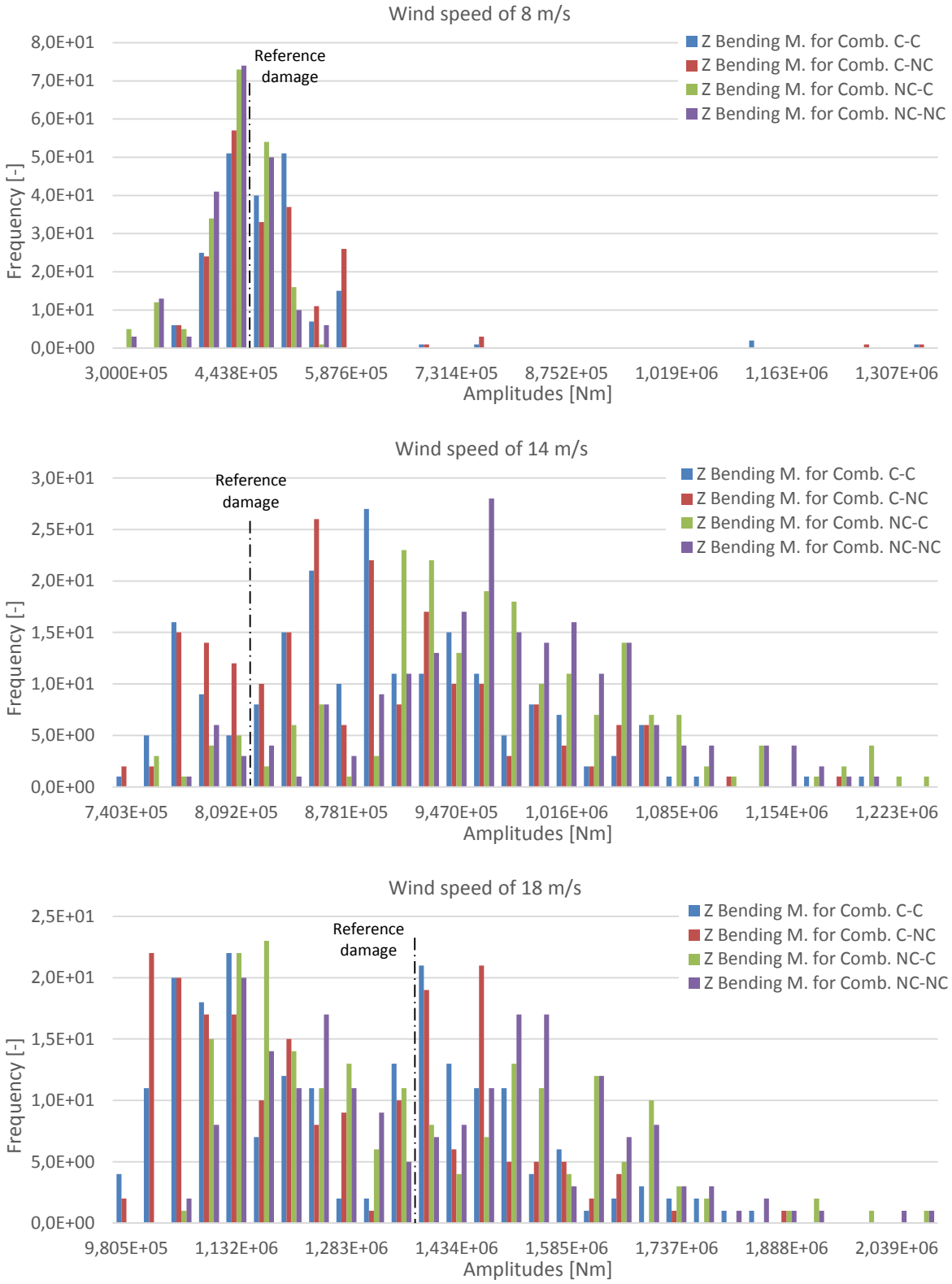

Figure 5.24: Distribution of amplitudes of the equivalent fatigue damage bending moment in the z axis for the combined study case. Each histogram correspond to a wind speed: 8 m/s (top), 14 m/s (centre) and 18 m/s (bottom).

5.5.3. Natural Frequencies

In this study case, the natural frequencies of the structure are modified due to the variable value of the soil stiffness and the cross section of the support structure.

From the natural frequencies presented in Table 5.27 and Figure 5.25, one can see the same tendency observed in the other results of this thesis, ergo, a high influence of the cross section when it is analysed in an uncorrelated manner. The natural frequencies of the correlated case of both variables are on average a 1% lower than the natural frequency of the reference case. On the other hand, the natural frequencies of the uncorrelated case are on average a 7.6% lower than the natural frequency of the reference case. By comparing these results with those obtained in the study case of the cross section of the structure, one can see a small increase of these two percentage probably related with the fact of adding the contribution of the soil stiffness.

In contrast with the study case of the cross section of the structure, the amplitudes of the histograms shown in Figure 5.25 have different distributions for each wind speed. However, as explained previously, the variations in the soil stiffness and the cross section of the structure are not affected by a variation of the wind speed and, therefore, it should be observed the same natural frequencies for each wind speed.

Table 5.27: Mean, standard deviation, variation coefficient and variation with respect to the reference case of the natural frequency of the structure for the combined study case.

Case	μ [Hz]	σ [Hz]	CV [%]	Diff. with ref. case [%]
TC8CC	0,284541	2,42E-02	8,4996	-0,9079
TC14CC	0,286051	2,59E-02	9,0529	-0,3822
TC18CC	0,282003	2,43E-02	8,6298	-1,7918
TC8CN	0,286448	2,49E-02	8,6823	-0,2441
TC14CN	0,283841	2,36E-02	8,3106	-1,1519
TC18CN	0,286556	2,26E-02	7,8792	-0,2062
TC8NC	0,267085	1,55E-02	5,8066	-6,9871
TC14NC	0,265752	1,51E-02	5,6962	-7,4515
TC18NC	0,265512	1,41E-02	5,3059	-7,5350
TC8NN	0,267120	1,53E-02	5,7104	-6,9748
TC14NN	0,264766	1,50E-02	5,6759	-7,7949
TC18NN	0,264049	1,59E-02	6,0172	-8,0444

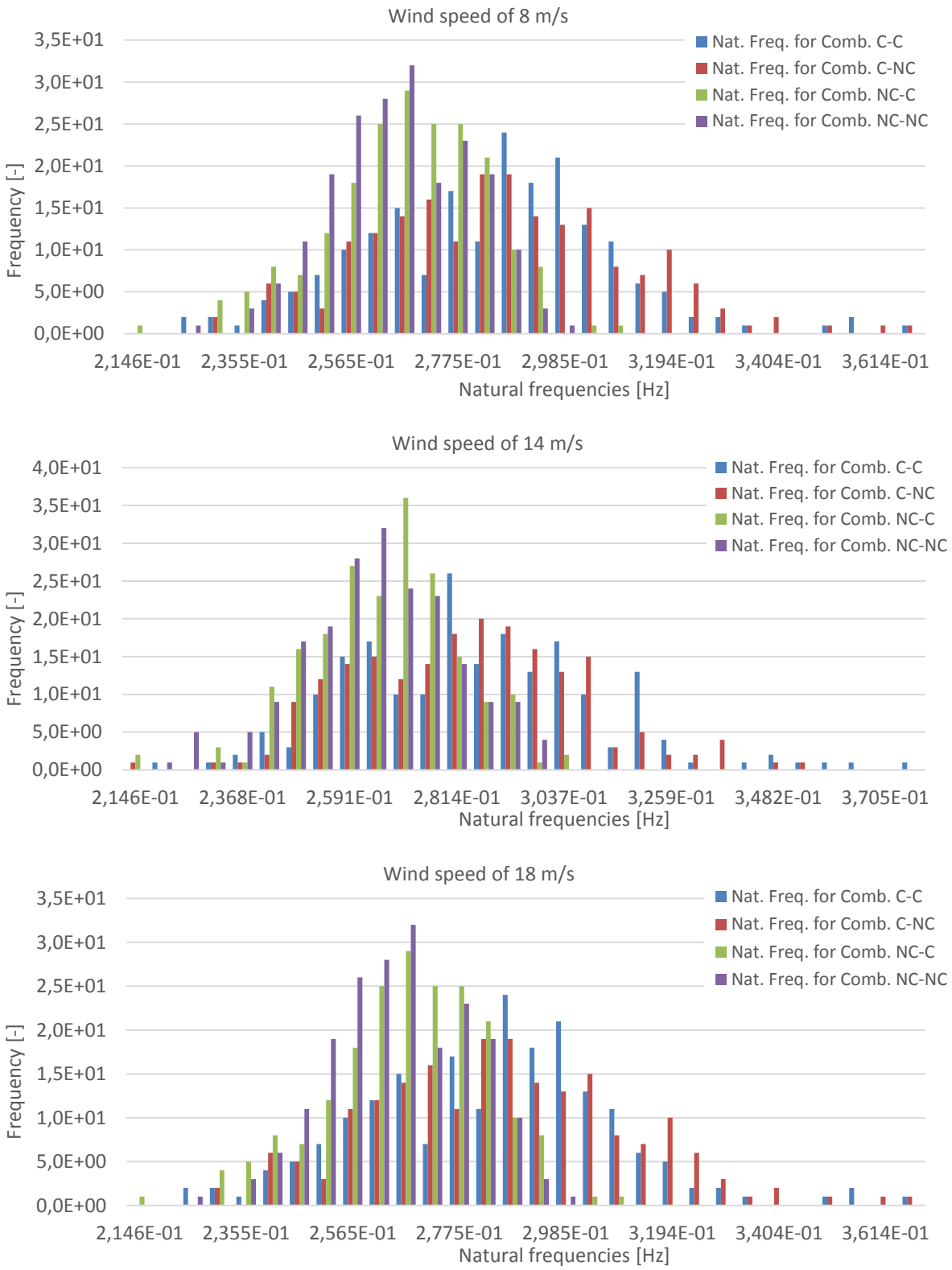

Figure 5.25: Distribution of natural frequencies for the combined study case. Each histogram correspond to a wind speed: 8 m/s (top), 14 m/s (centre) and 18 m/s (bottom).

5.5.4. Summary

In this section all the variables have been analysed probabilistically at the same time and, as has been indicated at the beginning, the results obtained have been a combination of the performances observed in the previous sections. That said, the displacements and bending moments obtained in the simulations have shown that the cross section of the structure is the variable with the large effect on the dynamic response of the structure. Looking at the differences between the correlated and uncorrelated cases, it is noted again that the uncorrelated cases show the higher mean values of displacements and bending moments.

The fatigue damage has a similar behaviour to which has been observed in the analysis of the displacements and bending moments, in other words, the cross section of the structure is the variable with the large fatigue damage, as well as the uncorrelated case is the situation where the larger fatigue damage occurs. The contribution of the soil stiffness and, especially, the aerodynamic damping are difficult to appreciate because it is not observed relevant effects on the results. As regards the differences with respect to the reference case, the equivalent fatigue damage of this study case is, on average, higher than the one obtained in the reference case. This is especially evident in the case of the displacements, where in all the cases the mean values are higher than those obtained in the reference case.

To conclude, the behaviour noticed in the displacements, bending moments and fatigue damage is also observed in the natural frequencies of the structure. The larger effects occur in the uncorrelated case of the geometry of the structure analysed probabilistically. On the other hand, the largest differences with respect to the reference case are mainly due to the sum of contributions that supposes analyse probabilistically all the variables jointly.

CHAPTER 6

Discussion

6.1. Damping of the Offshore Wind Turbine

The degree of damping has been divided in two contributions, structural and aerodynamic damping. One of the lines of research has been the study of the way used to add the aerodynamic damping in the FE model, by using two different approaches. On the one hand, the aerodynamic damping has been distributed in the entire structure, that is, it has been added at each element damping matrix of the structure. On the other hand, it has been considered that this type of damping could only affect one finite element, which represents the wind turbine and is located in the top of the support structure.

The results obtained have shown that the fact of locating the aerodynamic damping in the top of the structure has resulted in a considerable increase of the displacements, bending moments and, in turn, fatigue damage. In other words, the dynamic response of the structure has been more critical in the case of the aerodynamic damping located in the top of the structure than in the case of this damping distributed in the entire structure.

This behaviour is due to the overestimation of damping when the aerodynamic damping is distributed in the entire structure, which results in lower displacements and bending moments because the dynamic response of the structure is compensated by a high degree of damping.

Therefore, the fact of locating the aerodynamic damping in the top of the structure is an approach more realistic and conservative of the dynamic response of the structure.

6.2. Effect of the Aerodynamic Damping

The aerodynamic damping has been analysed probabilistically in order to study the effect of uncertainties associated to this system parameter. The study of Schafhirt (2014) has been used as a basis to obtaining the mean value of the aerodynamic damping corresponding to each wind speed and its standard deviation.

The simulations have shown that the aerodynamic damping has had a reduced impact on the response of the structure as it can be deduced from the small differences observed with respect to the reference case. This behaviour was not expected given that it is supposed a great importance of the aerodynamic damping in the dynamic response of the structure. The reason of this behaviour could be linked to the values of the standard deviation used in the analysis, which have a coefficient of variation between 2 and 7 per cent. These values are obtained from the variability of the results observed in the logarithmic decay tests in FEDEM Windpower and the degree of uncertainty taken into account in these tests can be insufficient for the purpose of this research.

It is worth pointing out that the highest dispersion of the fatigue damage has been observed in the case of the aerodynamic damping distributed in the entire structure. This behaviour means here a great fatigue damage of the structure. However, it is contrary to the considerations explained in the previous section. This is caused by the high scattering associated to the fact of analysing all the elements of the FE model probabilistically, instead of only one specific element.

6.3. Effect of the Soil Stiffness

The effect of uncertainties have also been studied by analysing probabilistically the stiffness of the soil. In this case, the analysis is based on the study of Carswell *et al.* (2014) and the value of the soil stiffness depends on the angle of internal friction, which varies with the depth.

The probability analysis of the soil stiffness has shown a weak impact on the results obtained from the simulations, as illustrated by the low differences with respect to the reference case have been obtained in the analysis of this system parameter. As in the case of the aerodynamic damping, this lesser influence was not expected because of the importance of the foundation on the dynamic response of an offshore wind turbine.

The degree of uncertainty associated to the soil stiffness can be the answer to these results, since it has been used the coefficient of variation described in Carswell *et al.* (2014), with a value of 5%. This value of variation coefficient is conservative because it does not include all the uncertainties connected to the real behaviour of the soil stiffness. A more appropriate value of the variation coefficient could be around 20%, which takes into account a larger number of uncertainties associated with this system parameter.

6.4. Effect of the Structure Geometry

The geometry of the structure has been studied by analysing probabilistically the cross section of the offshore wind turbine support structure described in this study. This analysis enable optimization and development of a cost effective design in the future and, to that end, it has been used a coefficient of variation of 5%.

The results obtained from the simulations have shown that the cross section of the support structure is the system parameter with the larger impact on the dynamic response of the structure. This effect is observed in the high differences with respect to the references case, where the variations concerning the mean values of the fatigue damage equivalent displacement reach 47%.

It is interesting to note that the mean values of the fatigue damage are generally higher than for the reference case, translating to greater damage in the structure. To correctly understand this behaviour it is advisable to observe how the natural frequencies of the structure vary with the probability analysis of the cross section of the support structure, because differences in eigenfrequencies are often correlated with, but not cause of, differences in fatigue damage. In this sense, it may be seen that the natural frequencies are lower than those obtained in the reference case, and this diminution coincides with an increase of the fatigue damage. Furthermore, the lower the natural frequency, the higher the fatigue damage. The increase of the fatigue damage with a reduction of the natural frequency of the structure can be caused by dynamic resonance. These types of problem occur when a structure is excited by external forces with a frequency close to the natural frequency of the structure. In this case, the reduction observed on the natural frequency implies that this frequency is nearer to the rotational frequency of the rotor, f_{1P}, which results in higher fatigue damage due to a dynamic amplification of the response of the structure.

6.5. Combined Analysis

The effect of uncertainties have also been studied by analysing probabilistically all the system parameters at the same time. To that end, the different system parameters have been analysed following the same criteria applied in their individual analyses.

The combined analysis has shown that the results are a combination of the effects observed in the individual analysis corresponding to each system parameter. This has enabled to compare the magnitude of the effects of each variable in the dynamic response of the structure. In this sense, the cross section of the structure has been the system parameter with the highest effects on the combined analysis. The effect of other system parameters may also be observed, but their magnitude is lower and, in some, cases is difficult to detect. The magnitude and the reason of these effects are analogous to which has been described in the different analyses of the system parameters.

It is interesting to highlight that the combined analysis of the system parameters is a simple superposition of the effects produced by each variable. In other words, this combined analysis does not produce an amplification or reduction of the response of the structure due to the fact that all the variables are analysed probabilistically at the same time.

6.6. Correlated and Uncorrelated Analysis

This approach raises that the system parameters with different values along the height of the support structure can be analysed probabilistically in correlation with a reference value or without correlation. Consequently, this alternative analysis has been applied to the soil stiffness and the cross section of the structure, since both system parameters have different values along the height of the support structure.

On the one hand, the results obtained from the simulations concerning the soil stiffness have shown that the differences between the correlated and uncorrelated cases are not significant and there is no clear trend that explains the results observed. This makes it impossible to find a comprehensive explanation of how the correlation analysis of this variable affects the dynamic response of the structure.

On the other hand, the results derived from the analysis of the cross section of the structure show large differences between the correlated and uncorrelated cases. In this case, it is observed a notable trend towards higher equivalent fatigue damage in the uncorrelated analysis. In order to understand these results, it is interesting to focus once again on the behaviour of the natural frequency of the structure. As has been seen previously, in the uncorrelated case the natural frequencies are, on average, 7.5% lower than in the reference case. There is a considerable difference by comparison with the variation observed in the correlated case, which is around 0.5%.

The large variation in the uncorrelated case is reasonable if one considers the following aspects. For the correlated case, the dimensions of the elements in the FE model come from just one sample, whose mean value is at the reference value and, therefore, it is expected that the natural frequencies are distributed around the reference frequency. However, in the uncorrelated case, each element is sampled individually. Taking into account how this affects the mass matrix of the structure, it is expected to obtained, on average, the same total mass of the structure, but not each individual mass of the FE model. This difference in the distribution or shape of the sampling may explain the variations observed between the correlated and uncorrelated cases.

6.7. Equivalent Fatigue Damage Analysis

The investigation of the fatigue damage has been done by obtaining the equivalent fatigue damage of the support structure as it is described in Blasques *et al.* (2013). This way to analyse the fatigue damage does not allow to calculate the actual probability of failure, which is the basis of a structural reliability analysis. Instead, it has been obtained general or qualitative statements about which parameters produce higher or lower fatigue damage based on the distribution of the results.

First, the probability analysis corresponding to each study case has shown that the differences with respect to the reference case depend highly on the system parameter analysed. Anyway, these differences are similar to the ones exposed in previous sections, so it is not necessary to go into detail. That said, the study case of the aerodynamic damping shows small variations with respect to the reference case, but large differences between the two damping approaches. The lowest differences are observed in the probability analysis of the soil

stiffness, where the maximum variation with respect to the reference case does not reach the 2%. In contrast, the greatest differences are observed in the probability analysis of the cross section of the structure, where the maximum variation with respect to the reference case reaches the 46%. Obviously, these greatest differences are obtained in the probability analysis of the cross section of the structure if it is not considered the combined case, where the superposition of the effects of each variable increases the equivalent fatigue damage and, therefore, the differences with respect to the reference case.

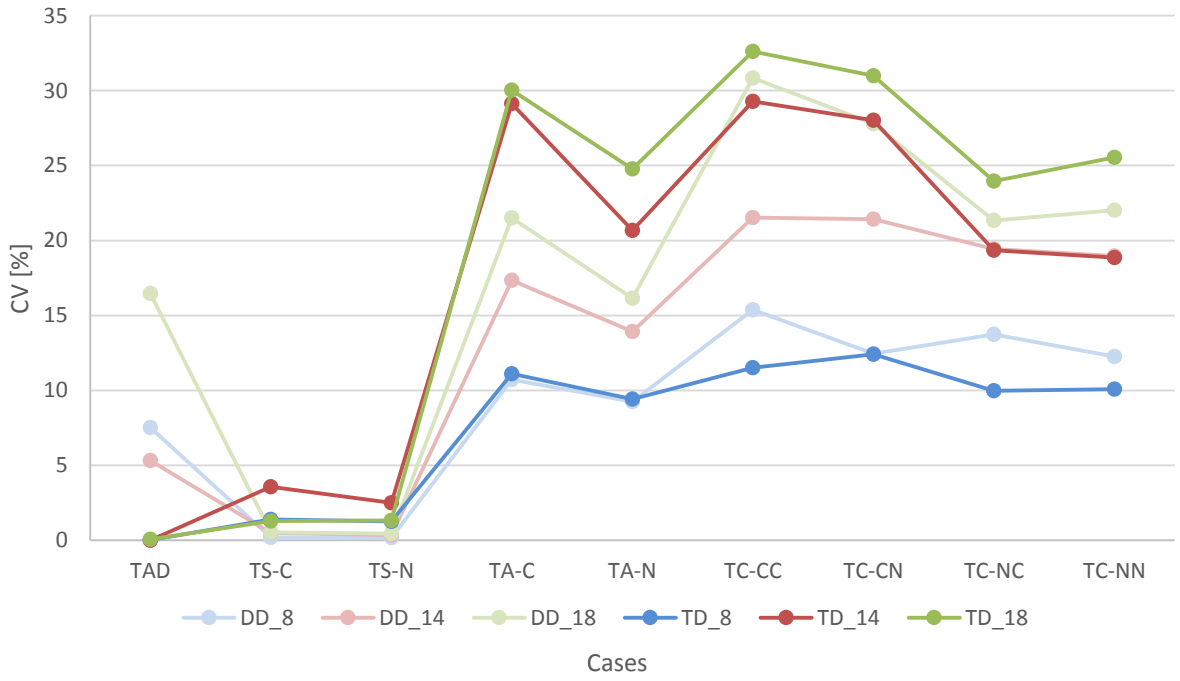

Figure 6.1: Coefficient of variation of each study case analysis. The curves relate to the different wind speeds and the damping approaches.

Regarding the scattering of the equivalent fatigue damage results, Figure 6.1 gives the variation coefficients obtained in the analysis corresponding to each study case in this research. This figure shows that the magnitude of the effects in the variation coefficient is similar to which has been observed in previous analyses. In other words, the study case of the cross section of the support structure has the greatest impact on the scattering of the equivalent fatigue damage.

As previously stated, for the study case of the aerodynamic damping, the highest variation coefficient is observed in the case of the aerodynamic damping distributed in the entire structure, which is contrary to the general trend of the other cases. The reason can be comparable to the one presented in order to explain the differences between the correlated and uncorrelated cases in the study case of the cross section of the structure. That is to say, distributing the aerodynamic damping in all the elements of simplified FE model instead of only one element results in considerable increase of the scattering of the equivalent fatigue damage.

On the other hand, the variation coefficients of the study case of the soil stiffness show a lower impact of this system parameter on the results in comparison to the other variables.

This behaviour, however, has been observed in all analyses and shows the general trend of the effects of this variable on the dynamic response of the structure.

To conclude, in the study case of the cross section of the structure the highest values of the variation coefficient are obtained in the correlated analysis. This observation is worth pointing out because the highest mean values of the equivalent fatigue damage have been obtained in the uncorrelated case. Nevertheless, the highest scattering has been obtained in the correlated case.

CHAPTER 7

Conclusions and Recommendations

In this thesis an investigation to develop and evaluate a novel approach for performing structural reliability analysis and robust design of offshore wind turbine support structures is performed. The effect of uncertainty associated to some system parameters is investigated by performing a probabilistic analysis in terms of the degree of uncertainty corresponding to each system parameter. The effect of these uncertainties is also investigated in terms of their contribution to the fatigue damage of the offshore wind turbine.

A simplified model of a support structure is developed in order to allow for doing the necessary calculations of the probability analysis efficiently. This model is implemented as a time-domain simulation in MATLAB by using the finite element method, and allows to solve the transient dynamics of a beam. The simplified FE model is based on the analysis of beam elements with 12 degrees of freedom, 3 translations and 3 rotations per node. The equation of motion is solved by using a direct numerical time integration method, the Newmark method, and the rotor loads are obtained from rotor simulations with an external software, FEDEM Windpower. The model represents the reference offshore wind turbine described in the OC3 project.

The degree of uncertainty associated to the aerodynamic damping and the soil stiffness is investigated on the basis of the studies performed in other researches. On the other hand, the geometry of the support structure is also investigated through a probability analysis. In this

case, the degree of variability of the cross section of the structure is selected in order to be equivalent to the degree of uncertainty used in two other system parameters.

The probability analysis is performed on the basis of several approaches. First, it is raised an individual analysis for each system parameter and for 3 different wind speeds. Secondly, the way used to add the aerodynamic damping in the simplified FE model has led to two different analysis. Furthermore, the effect of the soil stiffness and the cross section of the structure is investigated through a correlated and uncorrelated sampling of both variables. Finally, a combined analysis of the three system parameters is performed in order to observe the effect of analysing these parameters probabilistically at the same time. Additionally, the reference offshore wind turbine is also analysed in order to evaluate the effects of the other analyses.

The investigation of the aerodynamic damping of the offshore wind turbine has shown that the fact of locating the aerodynamic damping in the top of the structure has resulted in a considerable increase of the dynamic response of the structure. The reason of this behaviour could be that the response of the structure is compensated by a high degree of damping because of the overestimation of damping linked to this approach. On the other hand, the probability analysis of the aerodynamic damping has shown a reduced impact on the response of the structure, probably bound to the reduced standard deviation used to perform the simulations.

Regarding the investigation of the soil stiffness, the probability analysis has shown a weak effect of this variable on the response of the structure. The reason could be linked to the degree of uncertainty used to perform the simulations, since the research used as a basis proposed a degree of uncertainty that did not include all the possible uncertainties connected to the soil stiffness.

The investigation of the geometry of the offshore wind turbine support structure has shown that this system parameter has the large impact on the dynamic response of the structure. The results concerning the equivalent fatigue damage have been generally higher than those obtained in the reference case and have reached a maximum difference with respect to the mean value of the reference case around 47%. A hypothesis to explain this behaviour is related to the natural frequency of the structure. The increase observed in the results of equivalent fatigue damage coincide with a reduction of the natural frequency, and this reduction can result in dynamic resonance of the structure, given that the natural frequency is nearer to the rotational frequency of the rotor.

The investigation of the combined analysis has been useful to observe the contribution corresponding to each system parameter to the global dynamic response of the structure. In this sense, the cross section of the structure has been the variable with the larger impact on the results. The effects observed in this analysis seem a simple superposition of the individual effects produced by each system parameter.

Regarding the investigation of the correlated and uncorrelated cases, the mean values of the outputs analysed have shown that the greatest differences with respect to the reference case are obtained in the uncorrelated case. This greater difference could be connected to the differences in the distribution or shape of the sampling. The scattering of the uncorrelated sampling is greater since the sampling does not depend on a reference value and this implies that the shape of the support structure changes its pattern for each sample.

To conclude, the equivalent fatigue damage has shown that the effects of the different study cases on the scattering of the results, represented by the variation coefficient, have a similar trend to which has been observed in previous analyses, given that the study case of the cross section of the support structure has the greatest impact on the scattering of the equivalent fatigue damage. However, in this case the greater differences with respect to the reference case are found in the correlated case, in contrast to the pattern observed for the mean values of the equivalent fatigue damage.

7.1. Recommendation for Further Work

The objective of this thesis has been to look closer into the structural reliability analysis and robust design by developing and evaluating a novel approach, so several improvements can be carried out to further investigate on this issue.

First, the limitations of this study explained in Chapter 2 can be reduced if it poses a research with more resources, in other words, by developing the research with more time. This would allow to increase the number of elements of the simplified FE model up to the accuracy required in the results. Furthermore, the probability analysis would also be improved by increasing the number of samples in the simulations. This point is important given that it has been observed problems in the results due to an insufficient number of samples. Additionally, the number of wind speeds used in the analyses could also be increased, in greater concordance with the design standards of offshore wind turbines. These aspects are related with the computational cost of the simplified model, so a second possibility is to optimize the model to reduce the time needed to perform the simulations.

On the other hand, the simplified FE model implemented in this study in itself represents a limitation since it simplifies the complex behaviour of an offshore wind turbine in order to enable the calculations efficiently. That said, it would be interesting to investigate a model with a higher degree of complexity that would obtain a more realistic response of the structure.

Looking at the results obtained in the simulations, the probability analysis of the aerodynamic damping and the soil stiffness has shown some flaws in the approach. The degree of uncertainty of these two variables has resulted insufficient in order to observer interesting effects in the response of the structure. Therefore, it would be appropriate a thorough analysis of the uncertainties associated to the aerodynamic damping and the soil stiffness.

The novel approach raised here is just the first step towards a complete structural reliability analysis and robust design. The results obtained in this research should be the basis for investigating the design optimization of offshore wind turbine support structures. In order to do so, the probability of failure of the structure should be analysed in a probabilistic way and the design optimization could be investigated using an iterative approach, where each segment of the monopile is sized individually.

References

Almar-Næss, A. (1985). *Fatigue Handbook*. Tapir.

American Petroleum Institute (API) (2005). *Recommended Practice for Planning, Designing, and Constructing Fixed Offshore Platforms – Working Stress Design*. American Petroleum Institute: Washington, D. C.

Badii, M.H., Castillo, J. (2007). *Role of statistics in scientific research*. UANL, San Nicolás.

Berge, S. (2006). *Fatigue and fracture design (II): Fatigue design of welded structures*.

Blasques, J.P.A.A., Natarajan, A. (2013). *Mean load effect on the fatigue life of offshore wind turbine monopile foundations*. In B. Brinkmann, & P. Wriggers (Eds.), Computational Methods in Marine Engineering V - Proceedings of the 5th International Conference on Computational Methods in Marine Engineering, MARINE 2013. (pp. 818-829).

Böker, C. (2009*). Load Simulation and Local Dynamics of Support Structures for Offshore Wind Turbines*. PhD thesis, Leibniz Universität Hannover.

Canet, J.M., Barbat, A.H. (2013). *Introducción al cálculo dinámico de estructuras*, CIMNE.

Carswell, W., Arwade, S.R., DeGroot, D.J., Lackner, M.A. (2014). *Soil-Structure reliability of offshore wind turbine monopile foundations*, Wind Energy.

Cerda, D. J. and van der Tempel, J. (2005). Aerodynamic Damping in the Design of Support Structures for Offshore Wind Turbines.

Cook, R.D., et al. (2002). *Concepts and Applications of Finite Element Analysis*. John Wiley & Sons, Inc., 4th edition.

Devrient, C., Jordaens, P. J., Sitter, G. D., and Guillaume, P. (2013). *Damping Estimation of an Offshore Wind Turbine on a Monopile Foundation*. IET Renewable Power Generation.

DNV (2010a). *Offshore Standard DNV-OS-J101: Design of Offshore Wind Turbine Structures*. DNV.

DNV (2011). *Recommended Practice DNV-OS-J101: Design of Offshore Wind Turbine Structures*. DNV.

DNV (2012). *Recommended Practice DNV-RP-C203: Fatigue Design of Offshore Steel Structures*. DNV.

Doltsinis, I. (1999). *Stochastic Analysis of Multivariate Systems in Computational Mechanics and Engineering*. CIMNE, Barcelona, Spain, 1999.

Fischer, T., de Vries, W., and Schmidt, B. (2010). *Upwind Design Basis*, Upwind Deliverable (WP4: Offshore Foundations and Support Structures) 4-10-PU-0204, Endowed Chair of

Wind Energy (SWE) at the Institute of Aircraft Design Universität Stuttgart, Stuttgart, Germany.

Jonkman, J., Butterfield, S., Musial, W., and Scott, G. (2009). *Definition of a 5-MW Reference Wind Turbine for Offshore System Development*. Technical report, National Renewable Energy Laboratory, NREL.

Jonkman, J., Passon, P., Kühn, M., Butterfield, S., Camp, T., and Larsen, T. J. (2007). OC3 Benchmark Exercise of Aero-Elastic Offshore Wind Turbine Codes. In *Proceedings of the 2007 Science of Making Torque from Wind Conference. Journal of Physics: Conference Series 75*, volume 75, page 12 pp. IOP Publishing Ltd.

Kallehave, D., Byrne, B.W., Leblanc Thilsted, C., Mikkelsen, K.K. (2014). *Optimization of monopiles for offshore wind turbines*. Phil. Trans. R. Soc. A 373.

Kühn, M. (2001). *Dynamics and Design Optimization of Offshore Wind Energy Conversion Systems*. PhD thesis, DUWIND Delft University Wind Energy Research Institute.

Langen, I. and Sigbjörnsson, R. (1979). *Dynamisk analyse av konstruksjoner*. Tapir.

Melchers, R. E. (1999). *Structural Reliability Analysis and Prediction*, John Wiley & Sons, 2nd Edition.

Muskulus, M., Schafhirt, S. (2014). *Design Optimization of Wind Turbine Support Structures-A Review*. NTNU.

Oñate, E. (2009). *Structural Analysis with the Finite Element Method. Linear Statics. Volume 1. Basics and Solids*. CIMNE.

Rackwitz, R (2001). *Reliability analysis - a review and some perspectives*. Structural Safety, 23:365–395.

Schafhirt, S., Muskulus, M. (2014). *Aerodynamic damping of wind turbines under constant and turbulent wind*, EAWE.

Sieros, G., Chaviaropoulos, P., Sørensen, J. D., Bulder, B. H., and Jamieson, P. (2012). Upscaling wind turbines: theoretical and practical aspects and their impact on the cost of energy. *Wind Energy*, 15:3–17.

Taguchi, G. (1993). *Taguchi on Robust Technology Development: Bringing Quality Engineering Upstream*. ASME Press, New York.

Tarp-Johansen, N. J., Christensen, E. D., Mørch, C., and ans Sten Frandsen, B. K. (2009). Comparing Sources of Damping of Cross-Wind Motion. In *Conference Proceedings EOW 2009*, Stockholm.

The Carbon Trust (2008). *Offshore Wind Power: Big Challenge, Big Opportunity – Maximizing the Environmental, Economic and Security Benefits*, The Carbon Trust, Rept CTC743 112pp.

The Crown Estate (2012). *Offshore Wind Cost – Pathways Study*, the Crown Estate, Rept, 88pp.

Van der Tempel, J. (2006). *Design of Support Structures for Offshore Wind Turbines*. PhD thesis, TU Delft.

Zaaijer, M.B. (2000). Sensibility analysis for foundations of offshore wind turbines, Section Wind Energy, WE 02181, Delft.

Appendix A

In this appendix are defined the parameters that comprise the local stiffness and mass matrices of the element defined in Chapter 4.

A.1. Stiffness Matrix

In this appendix, the different parameters that compose the local stiffness matrix are defined. In order to facilitate the understanding, the local stiffness matrix is again defined and then the different parameters are defined.

$$K^{(e)} = \begin{bmatrix} \frac{EA}{L} & & & & & & & & & & & \\ 0 & \frac{12EI_z}{L^3\beta_y} & & & & & & & & & & \\ 0 & 0 & \frac{12EI_y}{L^3\beta_z} & & & & & & & & & \\ 0 & 0 & 0 & \frac{GJ}{L} & & & & & & & & \\ 0 & 0 & -\frac{6EI_y}{L^2\beta_z} & 0 & \gamma_z\frac{EI_y}{L} & & & & & & & \\ 0 & \frac{6EI_z}{L^2\beta_y} & 0 & 0 & 0 & \gamma_y\frac{EI_z}{L} & & & & & & \\ -\frac{EA}{L} & 0 & 0 & 0 & 0 & 0 & \frac{EA}{L} & & & & & \\ 0 & \frac{12EI_z}{L^3\beta_y} & 0 & 0 & 0 & \frac{-6EI_z}{L^2\beta_y} & 0 & \frac{12EI_z}{L^3\beta_y} & & & & \\ 0 & 0 & -\frac{12EI_y}{L^3\beta_z} & 0 & \frac{6EI_y}{L^2\beta_z} & 0 & 0 & 0 & \frac{12EI_y}{L^3\beta_z} & & & \\ 0 & 0 & 0 & -\frac{GJ}{L} & 0 & 0 & 0 & 0 & 0 & \frac{GJ}{L} & & \\ 0 & 0 & -\frac{6EI_y}{L^2\beta_z} & 0 & \eta_z\frac{EI_y}{L} & 0 & 0 & 0 & \frac{6EI_y}{L^2\beta_z} & 0 & \gamma_z\frac{EI_y}{L} & \\ 0 & \frac{6EI_z}{L^2\beta_y} & 0 & 0 & 0 & \eta_y\frac{EI_z}{L} & 0 & -\frac{6EI_z}{L^2\beta_y} & 0 & 0 & 0 & \gamma_y\frac{EI_z}{L} \end{bmatrix} \quad (A.1)$$

Where,

$$\beta_y = \left(1 + \Phi_y\right) \quad (A.2)$$

$$\beta_z = (1 + \Phi_z) \quad (A.3)$$

$$\gamma_y = \frac{(4 + \Phi_y)}{(1 + \Phi_y)} \quad (A.4)$$

$$\gamma_z = \frac{(4 + \Phi_z)}{(1 + \Phi_z)} \quad (A.5)$$

$$\eta_y = \frac{(2 - \Phi_y)}{(1 + \Phi_y)} \quad (A.6)$$

$$\eta_z = \frac{(2 - \Phi_z)}{(1 + \Phi_z)} \quad (A.7)$$

A.2. Mass Matrix

In this appendix, the different parameters that compose the local mass matrix are defined. In order to facilitate the understanding, the local mass matrix is again defined and then the different parameters are defined.

$$M_{el} = \begin{bmatrix} 1/3 & & & & & & & & & & & \\ 0 & a_z & & & & & & & & & & \\ 0 & 0 & a_y & & & & & & & SYM & & \\ 0 & 0 & 0 & \frac{J}{3A} & & & & & & & & \\ 0 & 0 & -c_y & 0 & e_y & & & & & & & \\ 0 & c_z & 0 & 0 & 0 & e_z & & & & & & \\ 1/6 & 0 & 0 & 0 & 0 & 0 & 1/3 & & & & & \\ 0 & b_z & 0 & 0 & 0 & d_z & 0 & a_z & & & & \\ 0 & 0 & b_y & 0 & -d_y & 0 & 0 & 0 & a_y & & & \\ 0 & 0 & 0 & \frac{J}{6A} & 0 & 0 & 0 & 0 & 0 & \frac{J}{3A} & & \\ 0 & 0 & d_y & 0 & f_y & 0 & 0 & 0 & c_y & 0 & e_y & \\ 0 & -d_z & 0 & 0 & 0 & f_z & 0 & -c_z & 0 & 0 & 0 & e_z \end{bmatrix} \quad (A.8)$$

Where,

$$a_y = \frac{\frac{13}{35} + \frac{7}{10}\Phi_z + \frac{1}{3}{\Phi_z}^2 + \frac{6}{5}\left(\frac{r_y}{L}\right)^2}{(1+\Phi_z)^2} \quad (A.9)$$

$$a_z = \frac{\frac{13}{35} + \frac{7}{10}\Phi_y + \frac{1}{3}{\Phi_y}^2 + \frac{6}{5}\left(\frac{r_z}{L}\right)^2}{(1+\Phi_y)^2} \quad (A.10)$$

$$b_y = \frac{\frac{9}{70} + \frac{3}{10}\Phi_z + \frac{1}{6}{\Phi_z}^2 + \frac{6}{5}\left(\frac{r_y}{L}\right)^2}{(1+\Phi_z)^2} \quad (A.11)$$

$$b_z = \frac{\frac{9}{70} + \frac{3}{10}\Phi_y + \frac{1}{6}{\Phi_y}^2 + \frac{6}{5}\left(\frac{r_z}{L}\right)^2}{(1+\Phi_y)^2} \quad (A.12)$$

$$c_y = \frac{\frac{11}{210} + \frac{11}{120}\Phi_z + \frac{1}{24}{\Phi_z}^2 + \left(\frac{1}{10} + \frac{\Phi_z}{2}\right)\left(\frac{r_y}{L}\right)^2}{(1+\Phi_z)^2} L \quad (A.13)$$

$$c_z = \frac{\frac{11}{210} + \frac{11}{120}\Phi_y + \frac{1}{24}{\Phi_y}^2 + \left(\frac{1}{10} + \frac{\Phi_y}{2}\right)\left(\frac{r_z}{L}\right)^2}{(1+\Phi_y)^2} L \quad (A.14)$$

$$d_y = \frac{\frac{13}{420} + \frac{3}{40}\Phi_z + \frac{1}{24}{\Phi_z}^2 + \left(\frac{1}{10} + \frac{\Phi_z}{2}\right)\left(\frac{r_y}{L}\right)^2}{(1+\Phi_z)^2} L \qquad \text{(A.15)}$$

$$d_z = \frac{\frac{13}{420} + \frac{3}{40}\Phi_y + \frac{1}{24}{\Phi_y}^2 + \left(\frac{1}{10} + \frac{\Phi_y}{2}\right)\left(\frac{r_z}{L}\right)^2}{(1+\Phi_y)^2} L \qquad \text{(A.16)}$$

$$e_y = \frac{\frac{1}{105} + \frac{1}{60}\Phi_z + \frac{1}{120}{\Phi_z}^2 + \left(\frac{2}{15} + \frac{\Phi_z}{6} + \frac{{\Phi_z}^2}{3}\right)\left(\frac{r_y}{L}\right)^2}{(1+\Phi_z)^2} L^2 \qquad \text{(A.17)}$$

$$e_z = \frac{\frac{1}{105} + \frac{1}{60}\Phi_y + \frac{1}{120}{\Phi_y}^2 + \left(\frac{2}{15} + \frac{\Phi_y}{6} + \frac{{\Phi_y}^2}{3}\right)\left(\frac{r_z}{L}\right)^2}{(1+\Phi_y)^2} L^2 \qquad \text{(A.18)}$$

$$f_y = -\frac{\frac{1}{140} + \frac{1}{60}\Phi_z + \frac{1}{120}{\Phi_z}^2 + \left(\frac{1}{30} + \frac{\Phi_z}{6} + \frac{{\Phi_z}^2}{6}\right)\left(\frac{r_y}{L}\right)^2}{(1+\Phi_z)^2} L^2 \qquad \text{(A.19)}$$

$$f_z = -\frac{\frac{1}{140} + \frac{1}{60}\Phi_y + \frac{1}{120}{\Phi_y}^2 + \left(\frac{1}{30} + \frac{\Phi_y}{6} + \frac{{\Phi_y}^2}{6}\right)\left(\frac{r_z}{L}\right)^2}{(1+\Phi_y)^2} L^2 \qquad \text{(A.20)}$$

Appendix B

In this appendix are presented the main MATLAB scripts used to build the simplified model of an offshore wind turbine support structure. The simplified model is composed of five parts: the main script that connects the different scripts and perform the probability analysis, the script used to obtain the geometry of the structure, the script used to obtain the soil stiffness, the script used to perform the FE analysis and, finally, the script used to obtain the fatigue damage of the support structure.

B.1. Main MATLAB script

```
%% PROBABILISTIC ANALYSIS

clear all; close all; clc
disp(' PROBABILISTIC ANALYSIS ')

%% Input Data:

global Damping WindSpeed ProbAnalysis numberSamples

% Damping: DStr (Structure), DTop (Top support structure)
Damping = 'DTop';
fprintf('\n- Damping: %s.\n',Damping)

% Wind Speeds: 8 m/s, 14 m/s, 18 m/s
WindSpeed = '18 m/s';
fprintf('- Wind Speed: %s.\n',WindSpeed)

% Prob. Analysis: Area, Soil, Aerodynamic Damping, Combined
ProbAnalysis = 'Combined';
fprintf('- Variable Analysis: %s.\n',ProbAnalysis)

% Study case: Correlated case, Non-Correlated case
Case = 'Correlated';
fprintf('- Case: %s.\n',Case)

    % Study case: Correlated case, Non-Correlated case
    CombinedAreaCase = 'Non-Correlated';
    fprintf('- Combined Area Case: %s.\n',CombinedAreaCase)

    % Study case: Correlated case, Non-Correlated case
    CombinedSoilCase = 'Non-Correlated';
    fprintf('- Combined Soil Case: %s.\n\n',CombinedSoilCase)

% Number of samples
numberSamples = 200;

tic;                            % Start clock
ttim = 0;                       % Initialize time counter

% Units: m; N; kg; Pa
global E G poisson rho Ls

E = 210e9;                      % E: modulus of elasticity
G = 80.8e9;                     % Shear modulus (G = E/2/(1+poisson)
poisson = 0.30;                 % poisson: Poisson's ratio
rho = 8500;                     % rho: specific weight of steel

Ltp = 77.6;                     % Ltp: Tower-Top Height Above Ltb
Ltb = 10;                       % Ltb: Tower-Base Height Above MSL
Lw = 20;                        % Lw: Water Depth (From MSL)
Ls = 40;                        % Ls: length of the foundation
L = Ltp+Ltb+Lw+Ls;              % L: length total

%% Generation of coordinates and connectivities
```

```
global numberElementsTowerTop numberElementsTowerBase ...
    numberElementsFoundation

numberElementsTowerTop=11;
numberElementsTowerBase=3;
numberElementsFoundation=40;
numberElements=numberElementsTowerTop+numberElementsTowerBase+...
    numberElementsFoundation;

nodeCoordinatesBeam=[linspace(0,Ls,numberElementsFoundation+1)';Ls+...
    (linspace((Ltb+Lw)/numberElementsTowerBase,(Ltb+Lw),...
    numberElementsTowerBase))';
    Ls+Ltb+Lw+(linspace(Ltp/numberElementsTowerTop,Ltp,...
    numberElementsTowerTop))'];
nodeCoordinates=[nodeCoordinatesBeam zeros(numberElements+1,1) ...
    zeros(numberElements+1,1)];
numberNodes=size(nodeCoordinates,1);

elementNodes=zeros(numberElements,2);
bendingCoord=zeros(numberElements,1);

for i=1:numberElements;
    elementNodes(i,1)=i;
    elementNodes(i,2)=i+1;

    bendingCoord(i) =(nodeCoordinates(elementNodes(i,1)) + ...
        nodeCoordinates(elementNodes(i,2)))/2;

end

global NElement GDofPN GDof GDofPE

NElement=2;                 % NElement: number of nodes per element
GDofPN=6;                   % GDofPN: degrees of freedom per node
GDof=GDofPN*numberNodes;    % GDof: global number of degrees of freedom
GDofPE=GDofPN*NElement;     % GDofPE: degrees of freedom per element

ttim = Timing('Time needed to set initial values',ttim); %Reporting time

%% Boundary conditions

% prescribed DOF
prescribed_Dof=(1:1)';

% active DOF
active_Dof=setdiff((1:GDof)',prescribed_Dof);

%% Loads

addpath('Loads');

switch WindSpeed

    case '8 m/s'
        data1 = dlmread('FxWs8.txt');
        data2 = dlmread('FyWs8.txt');
        data3 = dlmread('FzWs8.txt');
```

```
    case '14 m/s'
        data1 = dlmread('FxWs14.txt');
        data2 = dlmread('FyWs14.txt');
        data3 = dlmread('FzWs14.txt');

    case '18 m/s'
        data1 = dlmread('FxWs18.txt');
        data2 = dlmread('FyWs18.txt');
        data3 = dlmread('FzWs18.txt');

end

global t dt load1 load2 load3

t=data1(:,1);
dt=data1(2,1)-data1(1,1);
load1=data3(:,2);           % Load in the x-axis
load2=data1(:,2);           % Load in the y-axis
load3=data2(:,2);           % Load in the z-axis

ttim = Timing('Time needed to read the input file',ttim); %Reporting time

%% Probability distribution

% Area analysis
PDArea = zeros(numberElements,numberSamples);
Di = zeros(numberElements,1);
Ai = zeros(numberElements,1);

% Soil analysis
phi = [38;35;38;38;42;42.5];
PDSoil = zeros(length(phi),numberSamples);

% Aerodynamic analysis
PDAeroDy = zeros(numberElements,numberSamples);

switch Damping

case 'DStr'

switch ProbAnalysis

% PDF Area

case 'Area'

    switch Case

        case 'Non-Correlated'
                for i=1:numberElements

                    [A,~,~,~,Dint] = Beam_Geometry (elementNodes(i,1),...
                        numberElements);

                    mean1=A;
                    sd1=0.05;
```

```
                    mu = log((mean1^2)/sqrt(sd1+mean1^2));
                    sigma = sqrt(log(sd1/(mean1^2)+1));
                    X = lognrnd(mu,sigma,1,numberSamples);

                    PDArea(i,:) = X;
                    Di(i)=Dint;

                end

        case 'Correlated'
                for i=1:numberElements

                    [A,~,~,~,Dint] = Beam_Geometry (elementNodes(i,1),...
                        numberElements);

                    Ai(i)=A;
                    Di(i)=Dint;

                end

                mean1=Ai(1);
                sd1=0.05;
                mu = log((mean1^2)/sqrt(sd1+mean1^2));
                sigma = sqrt(log(sd1/(mean1^2)+1));
                X = lognrnd(mu,sigma,1,numberSamples);

                PDArea(1,:) = X;

                for i=2:numberElements

                        mean2 = Ai(i);
                        sd2 = 0.05;
                        X=mean2*(((PDArea(1,:)-mean1)/mean1)*(sd2/sd1)+1);

                    PDArea(i,:) = X;

                end

    end

% PDF Soil

case 'Soil'

    switch Case

        case 'Non-Correlated'

            for i=1:length(phi)

                mean1 = phi(i);
                sd1 = phi(i)*0.05;
                mu = log((mean1^2)/sqrt(sd1+mean1^2));
                sigma = sqrt(log(sd1/(mean1^2)+1));
                X = lognrnd(mu,sigma,1,numberSamples);

                PDSoil(i,:) = X;
```

```
            end

        case 'Correlated'

            mean1=phi(1);
            sd1=mean1*0.05;
            mu = log((mean1^2)/sqrt(sd1+mean1^2));
            sigma = sqrt(log(sd1/(mean1^2)+1));
            X = lognrnd(mu,sigma,1,numberSamples);

            PDSoil(1,:) = X;

            for i=2:length(phi)

                mean2=phi(i);
                sd2=mean2*0.05;
                X = mean2*(((PDSoil(1,:)-mean1)/mean1)*(sd2/sd1)+1);

                PDSoil(i,:) = X;

            end

    end

% PDF Aerodynamic Damping

case 'Aerodynamic Damping'

    switch WindSpeed

        case '8 m/s'

                mean1 = 0.0349;
                sd1 = 0.0025;
                mu = log((mean1^2)/sqrt(sd1+mean1^2));
                sigma = sqrt(log(sd1/(mean1^2)+1));
                X = lognrnd(mu,sigma,1,numberSamples);

                PDAeroDy(1,:) = X;

                for i=2:numberElements

                        mean2=mean1;
                        sd2 = 0.0025;
                        X=mean2*(((PDAeroDy(1,:)-mean1)/mean1)*(sd2/sd1)...
                            +1);

                    PDAeroDy(i,:) = X;

                end

            case '14 m/s'

                mean1 = 0.0573;
                sd1 = 0.0015;
                mu = log((mean1^2)/sqrt(sd1+mean1^2));
```

```
                sigma = sqrt(log(sd1/(mean1^2)+1));
                X = lognrnd(mu,sigma,1,numberSamples);

                PDAeroDy(1,:) = X;

                for i=2:numberElements

                        mean2=mean1;
                        sd2 = 0.0015;
                        X=mean2*(((PDAeroDy(1,:)-mean1)/mean1)*(sd2/sd1)...
                            +1);

                    PDAeroDy(i,:) = X;

                end

            case '18 m/s'

                mean1 = 0.0641;
                sd1 = 0.0031;
                mu = log((mean1^2)/sqrt(sd1+mean1^2));
                sigma = sqrt(log(sd1/(mean1^2)+1));
                X = lognrnd(mu,sigma,1,numberSamples);

                PDAeroDy(1,:) = X;

                for i=2:numberElements

                        mean2=mean1;
                        sd2=0.0031;
                        X=mean2*(((PDAeroDy(1,:)-mean1)/mean1)*(sd2/sd1)...
                            +1);

                    PDAeroDy(i,:) = X;
                end

    end

case 'Combined'

% Area

    switch CombinedAreaCase

        case 'Non-Correlated'
                for i=1:numberElements

                    [A,~,~,~,Dint] = Beam_Geometry (elementNodes(i,1),...
                        numberElements);

                    mean1=A;
                    sd1=0.05;
                    mu = log((mean1^2)/sqrt(sd1+mean1^2));
                    sigma = sqrt(log(sd1/(mean1^2)+1));
                    X = lognrnd(mu,sigma,1,numberSamples);

                    PDArea(i,:) = X;
```

```
                    Di(i)=Dint;

                end

        case 'Correlated'
                for i=1:numberElements

                    [A,~,~,~,Dint] = Beam_Geometry (elementNodes(i,1),...
                        numberElements);

                    Ai(i)=A;
                    Di(i)=Dint;

                end

                mean1=Ai(1);
                sd1=0.05;
                mu = log((mean1^2)/sqrt(sd1+mean1^2));
                sigma = sqrt(log(sd1/(mean1^2)+1));
                X = lognrnd(mu,sigma,1,numberSamples);

                PDArea(1,:) = X;

                for i=2:numberElements

                        mean2=Ai(i);
                        sd2=0.05;
                        X=mean2*(((PDArea(1,:)-mean1)/mean1)*(sd2/sd1)+1);

                    PDArea(i,:) = X;

                end

    end

% PDF Soil

    switch CombinedSoilCase

        case 'Non-Correlated'

            for i=1:length(phi)

                mean1 = phi(i);
                sd1 = phi(i)*0.05;
                mu = log((mean1^2)/sqrt(sd1+mean1^2));
                sigma = sqrt(log(sd1/(mean1^2)+1));
                X = lognrnd(mu,sigma,1,numberSamples);

                PDSoil(i,:) = X;

             end

        case 'Correlated'

            mean1=phi(1);
            sd1=mean1*0.05;
```

```
            mu = log((mean1^2)/sqrt(sd1+mean1^2));
            sigma = sqrt(log(sd1/(mean1^2)+1));
            X = lognrnd(mu,sigma,1,numberSamples);

            PDSoil(1,:) = X;

            for i=2:length(phi)

                mean2=phi(i);
                sd2=mean2*0.05;
                X = mean2*(((PDSoil(1,:)-mean1)/mean1)*(sd2/sd1)+1);

                PDSoil(i,:) = X;

            end

    end

% PDF Aerodynamic Damping

    switch WindSpeed

        case '8 m/s'

                mean1 = 0.0349;
                sd1 = 0.0025;
                mu = log((mean1^2)/sqrt(sd1+mean1^2));
                sigma = sqrt(log(sd1/(mean1^2)+1));
                X = lognrnd(mu,sigma,1,numberSamples);

                PDAeroDy(1,:) = X;

                for i=2:numberElements

                        mean2=mean1;
                        sd2 = 0.0025;
                        X=mean2*(((PDAeroDy(1,:)-mean1)/mean1)*(sd2/sd1)...
                            +1);

                    PDAeroDy(i,:) = X;

                end

            case '14 m/s'

                mean1 = 0.0573;
                sd1 = 0.0015;
                mu = log((mean1^2)/sqrt(sd1+mean1^2));
                sigma = sqrt(log(sd1/(mean1^2)+1));
                X = lognrnd(mu,sigma,1,numberSamples);

                PDAeroDy(1,:) = X;

                for i=2:numberElements

                        mean2=mean1;
                        sd2 = 0.0015;
```

```
                        X=mean2*(((PDAeroDy(1,:)-mean1)/mean1)*(sd2/sd1)...
                            +1);

                    PDAeroDy(i,:) = X;

                end

            case '18 m/s'

                mean1 = 0.0641;
                sd1 = 0.0031;
                mu = log((mean1^2)/sqrt(sd1+mean1^2));
                sigma = sqrt(log(sd1/(mean1^2)+1));
                X = lognrnd(mu,sigma,1,numberSamples);

                PDAeroDy(1,:) = X;

                for i=2:numberElements

                        mean2=mean1;
                        sd2 = 0.0031;
                        X=mean2*(((PDAeroDy(1,:)-mean1)/mean1)*(sd2/sd1)...
                            +1);

                    PDAeroDy(i,:) = X;
                end

    end

end

case 'DTop'

switch ProbAnalysis

% PDF Area

case 'Area'

    switch Case

        case 'Non-Correlated'
                for i=1:numberElements

                    [A,~,~,~,Dint] = Beam_Geometry (elementNodes(i,1),...
                        numberElements);

                    mean1=A;
                    sd1=0.05;
                    mu = log((mean1^2)/sqrt(sd1+mean1^2));
                    sigma = sqrt(log(sd1/(mean1^2)+1));
                    X = lognrnd(mu,sigma,1,numberSamples);

                    PDArea(i,:) = X;
                    Di(i)=Dint;

                end
```

```
        case 'Correlated'
                for i=1:numberElements

                    [A,~,~,~,Dint] = Beam_Geometry (elementNodes(i,1),...
                        numberElements);

                    Ai(i)=A;
                    Di(i)=Dint;

                end

                mean1=Ai(1);
                sd1=0.05;
                mu = log((mean1^2)/sqrt(sd1+mean1^2));
                sigma = sqrt(log(sd1/(mean1^2)+1));
                X = lognrnd(mu,sigma,1,numberSamples);

                PDArea(1,:) = X;

                for i=2:numberElements

                        mean2=Ai(i);
                        sd2=0.05;
                        X=mean2*(((PDArea(1,:)-mean1)/mean1)*(sd2/sd1)+1);

                    PDArea(i,:) = X;

                end

    end

% PDF Soil

case 'Soil'

    switch Case

        case 'Non-Correlated'

            for i=1:length(phi)

                mean1 = phi(i);
                sd1 = phi(i)*0.05;
                mu = log((mean1^2)/sqrt(sd1+mean1^2));
                sigma = sqrt(log(sd1/(mean1^2)+1));
                X = lognrnd(mu,sigma,1,numberSamples);

                PDSoil(i,:) = X;

             end

        case 'Correlated'

            mean1=phi(1);
            sd1=mean1*0.05;
            mu = log((mean1^2)/sqrt(sd1+mean1^2));
```

```
            sigma = sqrt(log(sd1/(mean1^2)+1));
            X = lognrnd(mu,sigma,1,numberSamples);

            PDSoil(1,:) = X;

            for i=2:length(phi)

                mean2=phi(i);
                sd2=mean2*0.05;
                X = mean2*(((PDSoil(1,:)-mean1)/mean1)*(sd2/sd1)+1);

                PDSoil(i,:) = X;

            end

    end

% PDF Aerodynamic Damping

case 'Aerodynamic Damping'

    switch WindSpeed

        case '8 m/s'

                mean1 = 0.0349;
                sd1 = 0.0025;
                mu = log((mean1^2)/sqrt(sd1+mean1^2));
                sigma = sqrt(log(sd1/(mean1^2)+1));
                X = lognrnd(mu,sigma,1,numberSamples);

                PDAeroDy(1,:) = X;

            case '14 m/s'

                mean1 = 0.0573;
                sd1 = 0.0015;
                mu = log((mean1^2)/sqrt(sd1+mean1^2));
                sigma = sqrt(log(sd1/(mean1^2)+1));
                X = lognrnd(mu,sigma,1,numberSamples);

                PDAeroDy(1,:) = X;

            case '18 m/s'

                mean1 = 0.0641;
                sd1 = 0.0031;
                mu = log((mean1^2)/sqrt(sd1+mean1^2));
                sigma = sqrt(log(sd1/(mean1^2)+1));
                X = lognrnd(mu,sigma,1,numberSamples);

                PDAeroDy(1,:) = X;

    end

case 'Combined'
```

```
% PDF Area

    switch CombinedAreaCase

        case 'Non-Correlated'
                for i=1:numberElements

                    [A,~,~,~,Dint] = Beam_Geometry (elementNodes(i,1),...
                        numberElements);

                    mean1=A;
                    sd1=0.05;
                    mu = log((mean1^2)/sqrt(sd1+mean1^2));
                    sigma = sqrt(log(sd1/(mean1^2)+1));
                    X = lognrnd(mu,sigma,1,numberSamples);

                    PDArea(i,:) = X;
                    Di(i)=Dint;

                end

        case 'Correlated'
                for i=1:numberElements

                    [A,~,~,~,Dint] = Beam_Geometry (elementNodes(i,1),...
                        numberElements);

                    Ai(i)=A;
                    Di(i)=Dint;

                end

                mean1=Ai(1);
                sd1=0.05;
                mu = log((mean1^2)/sqrt(sd1+mean1^2));
                sigma = sqrt(log(sd1/(mean1^2)+1));
                X = lognrnd(mu,sigma,1,numberSamples);

                PDArea(1,:) = X;

                for i=2:numberElements

                        mean2=Ai(i);
                        sd2=0.05;
                        X=mean2*(((PDArea(1,:)-mean1)/mean1)*(sd2/sd1)+1);

                    PDArea(i,:) = X;

                end

    end

% PDF Soil

    switch CombinedSoilCase

        case 'Non-Correlated'
```

```
            for i=1:length(phi)

                mean1 = phi(i);
                sd1 = phi(i)*0.05;
                mu = log((mean1^2)/sqrt(sd1+mean1^2));
                sigma = sqrt(log(sd1/(mean1^2)+1));
                X = lognrnd(mu,sigma,1,numberSamples);

                PDSoil(i,:) = X;

             end

        case 'Correlated'

            mean1=phi(1);
            sd1=mean1*0.05;
            mu = log((mean1^2)/sqrt(sd1+mean1^2));
            sigma = sqrt(log(sd1/(mean1^2)+1));
            X = lognrnd(mu,sigma,1,numberSamples);

            PDSoil(1,:) = X;

            for i=2:length(phi)

                mean2=phi(i);
                sd2=mean2*0.05;
                X = mean2*(((PDSoil(1,:)-mean1)/mean1)*(sd2/sd1)+1);

                PDSoil(i,:) = X;

            end

    end

% PDF Aerodynamic Damping

    switch WindSpeed

        case '8 m/s'

                mean1 = 0.0349;
                sd1 = 0.0025;
                mu = log((mean1^2)/sqrt(sd1+mean1^2));
                sigma = sqrt(log(sd1/(mean1^2)+1));
                X = lognrnd(mu,sigma,1,numberSamples);

                PDAeroDy(1,:) = X;

            case '14 m/s'

                mean1 = 0.0573;
                sd1 = 0.0015;
                mu = log((mean1^2)/sqrt(sd1+mean1^2));
                sigma = sqrt(log(sd1/(mean1^2)+1));
                X = lognrnd(mu,sigma,1,numberSamples);
```

```
                PDAeroDy(1,:) = X;

            case '18 m/s'

                mean1 = 0.0641;
                sd1 = 0.0031;
                mu = log((mean1^2)/sqrt(sd1+mean1^2));
                sigma = sqrt(log(sd1/(mean1^2)+1));
                X = lognrnd(mu,sigma,1,numberSamples);

                PDAeroDy(1,:) = X;

    end

end

end

%% Finite element analysis

DeleteTime = 120/dt+1;
tf = t(DeleteTime:end);

Freq=zeros(25,numberSamples);

DisplTopXT = zeros(numberSamples,length(tf));
DisplTopYT = zeros(numberSamples,length(tf));
DisplTopZT = zeros(numberSamples,length(tf));

BMMudlineYT = zeros(numberSamples,length(tf));
BMMudlineZT = zeros(numberSamples,length(tf));

dmg_DisplTopXT = zeros(numberSamples,1);
dmg_DisplTopYT = zeros(numberSamples,1);
dmg_DisplTopZT = zeros(numberSamples,1);

dmg_BMMudlineYT = zeros(numberSamples,1);
dmg_BMMudlineZT = zeros(numberSamples,1);

for i=1:numberSamples

    [depli,veli,accli,Myi,Mzi,f] = FEM_Beam (numberElements,...
        nodeCoordinates,elementNodes,active_Dof,PDArea(:,i),Di,...
        PDSoil(:,i),PDAeroDy(:,i));

    Freq(:,i)=f;

    [DisplTopX,DisplTopY,DisplTopZ,BMMudlineY,BMMudlineZ] = Save_Data ...
        (depli,Myi,Mzi,DeleteTime);

    DisplTopXT(i,:) = DisplTopX;
    DisplTopYT(i,:) = DisplTopY;
    DisplTopZT(i,:) = DisplTopZ;

    BMMudlineYT(i,:) = BMMudlineY;
    BMMudlineZT(i,:) = BMMudlineZ;
```

```
    [RF_DisplTopX_dmg,RF_DisplTopY_dmg,RF_DisplTopZ_dmg,...
        RF_BMMudlineY_dmg,RF_BMMudlineZ_dmg] = RF_Results_Damage ...
        (DisplTopX,DisplTopY,DisplTopZ,BMMudlineY,BMMudlineZ);

    dmg_DisplTopXT(i)=RF_DisplTopX_dmg;
    dmg_DisplTopYT(i)=RF_DisplTopY_dmg;
    dmg_DisplTopZT(i)=RF_DisplTopZ_dmg;

    dmg_BMMudlineYT(i)=RF_BMMudlineY_dmg;
    dmg_BMMudlineZT(i)=RF_BMMudlineZ_dmg;

ttim = Timing('Time needed to solve the FE model',ttim); %Reporting time

end

%% Rainflow counting computation

[RF_DisplTopX,RF_DisplTopY,RF_DisplTopZ,RF_BMMudlineY,RF_BMMudlineZ] ...
    = RF_Results(DisplTopXT,DisplTopYT,DisplTopZT,BMMudlineYT,BMMudlineZT);

%% Graphs

NSamples = 1;

Graphs (NSamples,DisplTopX,DisplTopY,DisplTopZ,BMMudlineY,...
    BMMudlineZ,tf);

fprintf(1,'\nTotal running time %12.6f \n\n',ttim); %Reporting final time
```

B.2. MATLAB script used to obtain the geometry of the structure

The some geometric parameters of the structure has been obtained in two different ways depending on the study case. The following MATLAB script corresponds to the general script used to obtain the main geometric parameters of the structure.

```
function [A,Iy,Iz,J,Di] = Beam_Geometry (elementNodes,numberElements)

global numberElementsTowerBase numberElementsFoundation

    if (elementNodes<=(numberElementsFoundation+numberElementsTowerBase))

        D = 6;                      % D: external diameter
        thic = 0.06;                % thic: thickness
        Di = D-2*thic;              % Di: internal diameter
        ro = D/2;                   % ro: external radius
        ri = D/2-thic;              % ri: intenal radius

        A = pi*(ro^2-ri^2);         % A: area of the section
        Iy = (pi/4)*(ro^4-ri^4);    % Second moment of area about the axis y
        Iz = (pi/4)*(ro^4-ri^4);    % Second moment of area about the axis z
        J = Iy+Iz;                  % Polar moment of inertia

    else

        Dt = 3.87;
        Db = 6;
        a1 = (Dt-Db)/(numberElements-(numberElementsFoundation+...
            numberElementsTowerBase+1));
        b1 = Db-(numberElementsFoundation+numberElementsTowerBase+1)*a1;
        D = a1*elementNodes+b1;       % D: external diameter

        thict = 0.019;
        thicb = 0.027;
        a2 = (thict-thicb)/(numberElements-(numberElementsFoundation+...
            numberElementsTowerBase+1));
        b2 = thicb-(numberElementsFoundation+numberElementsTowerBase+1)*a2;
        thic = a2*elementNodes+b2; % thic: thickness

        Di = D-2*thic;              % Di: internal diameter
        ro = D/2;                   % ro: external radius
        ri = D/2-thic;              % ri: intenal radius
        A  = pi*(ro^2-ri^2);        % A: area of the section
        Iy = (pi/4)*(ro^4-ri^4);    % Second moment of area about the axis y
        Iz = (pi/4)*(ro^4-ri^4);    % Second moment of area about the axis z
        J = Iy+Iz;                  % Polar moment of inertia

    end

end
```

On the other hand, the second MATLAB script linked to the geometry of the structure has been used in the study case of the geometry of the structure to obtain only some of the parameters of the structure.

```
function [Iy,Iz,J] = Beam_Geometry_PDFArea (PDArea,Di)

        D = 2*sqrt((PDArea/pi)+(Di/2)^2);          % D: external diameter
        thic = (D-Di)/2;                           % thic: thickness
        ro = D/2;                                  % ro: external radius
        ri = D/2-thic;                             % ri: intenal radius

        Iy = (pi/4)*(ro^4-ri^4);    % Second moment of area about the axis y
        Iz = (pi/4)*(ro^4-ri^4);    % Second moment of area about the axis z
        J = Iy+Iz;                  % Polar moment of inertia

end
```

B.3. MATLAB script used to obtain the soil stiffness

The soil stiffness has been obtained using two different codes. As has been explained in the methodology of the thesis, this parameter depends on the angle of internal friction of the soil, which in turn depends on the depth. The following MATLAB script corresponds to the script used to obtain the soil stiffness of the soil.

```
function f = Stiffness_Soil_Funct(x)

    if (x<=30)
        f = 8.9274e+00*x.^2 -5.0240e+02*x+7.0707e+03;

    elseif (x<=36)
        f = 4.0123e-01*x.^2 -1.6581e+01*x+1.6987e+02;

    else
        f = 1.1408e+00*x.^2 -7.1021e+01*x+1.1718e+03;

    end

    f = f*271447; % convert to SI units [lbf/in^3] to [N/m^3]

end
```

The second MATLAB script presented below has been used to obtain the angles of internal friction of the soil.

```
function phi = Friction_Angle_Funct(x,PDSoil)

global ProbAnalysis

switch ProbAnalysis
    case {'Area','Aerodynamic Damping'}

        if (x<=3)
            phi = 38;
        elseif (x<=5)
            phi = 35;
        elseif (x<=7)
            phi = 38;
        elseif (x<=10)
            phi = 38;
        elseif (x<=15)
            phi = 42;
        else
            phi = 42.5;
        end

    case {'Soil','Combined'}
```

```
        if (x<=3)
            phi = PDSoil(1);
        elseif (x<=5)
            phi = PDSoil(2);
        elseif (x<=7)
            phi = PDSoil(3);
        elseif (x<=10)
            phi = PDSoil(4);
        elseif (x<=15)
            phi = PDSoil(5);
        else
            phi = PDSoil(6);
        end

end

end
```

B.4. MATLAB script used to perform the FE analysis

The FE analysis has been performed using four MATLAB scripts, which jointly provide the dynamic response of the structure. The main script of FE analysis is presented below.

```
%% 3D Beam Elements FEM

function [depl,vel,accl,My,Mz,f] = FEM_Beam(numberElements,...
    nodeCoordinates,elementNodes,active_Dof,PDFArea,Di,PDSoil,PDAeroDy)
%% Stiffness and Mass Matrix

global Damping WindSpeed ProbAnalysis
global Ls
global numberElementsFoundation
global NElement GDofPN GDof GDofPE
global t

EDof=zeros(elementNodes(end,1),NElement*GDofPN);

% Topology Matrix
for i=1:numberElements
    for j=1:GDofPE
        EDof(i,j)=(i-1)*6+j;
    end
end

K = sparse(GDof,GDof);
M = sparse(GDof,GDof);
C = sparse(GDof,GDof);
Iy = zeros(numberElements,1);
Iz = zeros(numberElements,1);

for i=1:numberElements

% Ki element stiffness matrix
% Mi element mass matrix
% Ci element damping matrix
% Kis element stiffness matrix for soil
% Mi element mass matrix for the rotor

    switch ProbAnalysis

        case {'Area','Combined'}

    [Iyi,Izi,Ji] = Beam_Geometry_PDFArea (PDFArea(i),Di(i));
    Lel = sqrt((nodeCoordinates(i+1,1)-nodeCoordinates(i,1))^2);

    Iy(i) = Iyi;
    Iz(i) = Izi;

    [Mi,Ki,Ci,Kis,Mirot] = Stiffness_Mass_Damping_Matrix (PDFArea(i),...
        Iyi, Izi, Ji, Lel, PDAeroDy(i));

        case {'Soil','Aerodynamic Damping'}
```

```
    [A,Iyi,Izi,Ji] = Beam_Geometry (elementNodes(i,1), numberElements);
    Lel = sqrt((nodeCoordinates(i+1,1)-nodeCoordinates(i,1))^2);

    Iy(i) = Iyi;
    Iz(i) = Izi;

    [Mi,Ki,Ci,Kis,Mirot] = Stiffness_Mass_Damping_Matrix (A, Iyi, Izi,...
        Ji, Lel, PDAeroDy(i));

    end

% Global Structure stiffness, mass and damping (referred to O in general
% axis)
    K(EDof(i,:), EDof(i,:))=K(EDof(i,:), EDof(i,:))+Ki;
    M(EDof(i,:), EDof(i,:))=M(EDof(i,:), EDof(i,:))+Mi;
    C(EDof(i,:), EDof(i,:))=C(EDof(i,:), EDof(i,:))+Ci;
end

% Add soil stiffness
for i=1:numberElementsFoundation/2
    Dsoil = 6;
    xsoil = linspace(Ls,0,numberElementsFoundation+1)';
    Ksoil = Dsoil*xsoil(i*2)*Stiffness_Soil_Funct(Friction_Angle_Funct...
        (xsoil(i*2),PDSoil));

    K(EDof(i*2,:), EDof(i*2,:))=K(EDof(i*2,:), EDof(i*2,:))+Ksoil*Kis;

end

% Add rotor mass
for i=numberElements
    M(EDof(i,:), EDof(i,:))=M(EDof(i,:), EDof(i,:))+Mirot;
end

% Add aerodynamic damping D2
switch Damping

case 'DTop'

switch ProbAnalysis

    case {'Area','Soil'}

        switch WindSpeed
            case '8 m/s'
                aerodynamicDamping = 0.0349;
            case '14 m/s'
                aerodynamicDamping = 0.0573;
            case '18 m/s'
                aerodynamicDamping = 0.0641;
        end

        for i=numberElements
            C(EDof(i,:), EDof(i,:))=C(EDof(i,:), EDof(i,:))+Ki*...
                aerodynamicDamping;
        end

    case {'Aerodynamic Damping','Combined'}
```

```
        for i=numberElements
            C(EDof(i,:), EDof(i,:))=C(EDof(i,:), EDof(i,:))+Ki*PDAeroDy(1);
        end

end

end

%% Eigenfrequencies

Keig=full(K);
Meig=full(M);
Kref=Keig(7:end,7:end);
Mref=Meig(7:end,7:end);
[V,W]=eig(Kref,Mref);
wn=sort(diag(sqrt(W)));
f=wn(1:25)/2/pi;

%% System solving - Dynamic problem

[depl,vel,accl] = Dynamic_Solution_Newmark(M,K,C,active_Dof);

%% Bending moment

My=zeros(numberElements,length(t));
Mz=zeros(numberElements,length(t));

for i=1:length(t)
    [Myi, Mzi] = Bending_Moment (numberElements,nodeCoordinates,...
        depl(:,i),EDof,Iy,Iz);

    My(:,i) = Myi;
    Mz(:,i) = Mzi;
end

end
```

The second MATLAB script of the FE analysis is used to obtain the stiffness, mass and damping matrices of the structure.

```
function [M,K,C,Ks,Mrot] = Stiffness_Mass_Damping_Matrix (A, Iy, Iz, J,...
    L, PDAeroDy)

global Damping WindSpeed ProbAnalysis
global E G poisson rho

kc = 10*(1+poisson)/(12+11*poisson);
Ay = A/kc;
Az = A/kc;

% Shear deformation effects
```

```
phiy = 1*12*E*Iz/(G*Az*L^2);
phiz = 1*12*E*Iy/(G*Ay*L^2);

az =  12*E*Iz/(L^3*(1+phiy));
ay =  12*E*Iy/(L^3*(1+phiz));
bz = -12*E*Iz/(L^3*(1+phiy));
by = -12*E*Iy/(L^3*(1+phiz));
cz =   6*E*Iz/(L^2*(1+phiy));
cy =   6*E*Iy/(L^2*(1+phiz));
dz =  -6*E*Iz/(L^2*(1+phiy));
dy =  -6*E*Iy/(L^2*(1+phiz));

ez = (4+phiy)*E*Iz/(L*(1+phiy));
ey = (4+phiz)*E*Iy/(L*(1+phiz));
fz = (2-phiy)*E*Iz/(L*(1+phiy));
fy = (2-phiz)*E*Iy/(L*(1+phiz));

% Rotational inertia
ry = sqrt(Iy/A);
rz = sqrt(Iz/A);

A_z = (13/35+7/10*phiy+1/3*phiy^2+6/5*(rz/L)^2)/(1+phiy)^2;
A_y = (13/35+7/10*phiz+1/3*phiz^2+6/5*(ry/L)^2)/(1+phiz)^2;
B_z = (9/70+3/10*phiy+1/6*phiy^2-6/5*(rz/L)^2)/(1+phiy)^2;
B_y = (9/70+3/10*phiz+1/6*phiz^2-6/5*(ry/L)^2)/(1+phiz)^2;
C_z = (11/210+11/120*phiy+1/24*phiy^2+(1/10-1/2*phiy)*(rz/L)^2)*L/...
    (1+phiy)^2;
C_y = (11/210+11/120*phiz+1/24*phiz^2+(1/10-1/2*phiz)*(ry/L)^2)*L/...
    (1+phiz)^2;
D_z = (13/420+3/40*phiy+1/24*phiy^2-(1/10-1/2*phiy)*(rz/L)^2)*L/(1+phiy)^2;
D_y = (13/420+3/40*phiz+1/24*phiz^2-(1/10-1/2*phiz)*(ry/L)^2)*L/(1+phiz)^2;
E_z = (1/105+1/60*phiy+1/120*phiy^2+(2/15+1/6*phiy+1/3*phiy^2)*(rz/L)^2)...
    *L^2/(1+phiy)^2;
E_y = (1/105+1/60*phiz+1/120*phiz^2+(2/15+1/6*phiz+1/3*phiz^2)*(ry/L)^2)...
    *L^2/(1+phiz)^2;
F_z = -1*(1/140+1/60*phiy+1/120*phiy^2+(1/30+1/6*phiy-1/6*phiy^2)*...
    (rz/L)^2)*L^2/(1+phiy)^2;
F_y = -1*(1/140+1/60*phiz+1/120*phiz^2+(1/30+1/6*phiz-1/6*phiz^2)*...
    (ry/L)^2)*L^2/(1+phiz)^2;

Ko= [...
  A*E/L  0     0     0     0     0  -A*E/L   0      0     0     0     0;
    0     az    0     0     0     cz    0     bz     0     0     0     cz;
    0     0     ay    0     dy    0     0     0      by    0     dy    0;
    0     0     0   G*J/L   0     0     0     0      0  -G*J/L   0     0;
    0     0     dy    0     ey    0     0     0      cy    0     fy    0;
    0     cz    0     0     0     ez    0     dz     0     0     0     fz;
 -A*E/L   0     0     0     0     0   A*E/L   0      0     0     0     0;
    0     bz    0     0     0     dz    0     az     0     0     0     -cz;
    0     0     by    0     cy    0     0     0      ay    0    -dy    0;
    0     0     0  -G*J/L   0     0     0     0      0   G*J/L   0     0;
    0     0     dy    0     fy    0     0     0     -dy    0     ey    0;
    0     cz    0     0     0     fz    0    -cz     0     0     0     ez];

Me=rho*A*L*[...
    1/3   0     0     0     0     0    1/6    0      0     0     0     0;
    0    A_z    0     0     0    C_z    0    B_z     0     0     0     -D_z;
    0     0    A_y    0   -C_y    0     0     0     B_y    0    D_y    0;
    0     0     0  J/(3*A)  0     0     0     0      0  J/(6*A)  0     0;
    0     0   -C_y    0    E_y    0     0     0    -D_y    0    F_y    0;
```

```
    0     C_z     0      0      0     E_z     0     D_z      0      0      0      F_z;
    1/6   0       0      0      0      0      1/3    0       0      0      0      0;
    0     B_z     0      0      0     D_z     0     A_z      0      0      0      -C_z;
    0      0     B_y     0    -D_y     0      0      0      A_y     0     C_y     0;
    0      0      0   J/(6*A)  0      0      0      0       0   J/(3*A)  0      0;
    0      0     D_y     0     F_y     0      0      0      C_y     0     E_y     0;
    0    -D_z     0      0      0     F_z     0    -C_z      0      0      0      E_z];

% Soil stiffness
kx=0;
ky=1;
kz=1;

kox=0;
koy=0;
koz=0;

Kos =[...
    kx     0      0      0      0      0      kx     0       0      0      0      0;
    0      ky     0      0      0      koz    0      ky      0      0      0      koz;
    0      0      kz     0      koy    0      0      0       kz     0      koy    0;
    0      0      0      kox    0      0      0      0       0      kox    0      0;
    0      0      koy    0      koy    0      0      0       kz     0      koy    0;
    0      koz    0      0      0      koz    0      ky      0      0      0      koz;
    kx     0      0      0      0      0      kx     0       0      0      0      0;
    0      ky     0      0      0      ky     0      ky      0      0      0      koz;
    0      0      kz     0      kz     0      0      0       kz     0      koy    0;
    0      0      0      kox    0      0      0      0       0      kox    0      0;
    0      0      koy    0      koy    0      0      0       koy    0      koy    0;
    0      koz    0      0      0      koz    0      koz     0      0      0      koz];

% Rotor mass
Mass_Rotor=110000+240000;
Mrot=Mass_Rotor*[...
    1/3    0      0      0      0      0      1/6    0       0      0      0      0;
    0     A_z     0      0      0     C_z     0     B_z      0      0      0      -D_z;
    0      0     A_y     0    -C_y     0      0      0      B_y     0     D_y     0;
    0      0      0   J/(3*A)  0      0      0      0       0   J/(6*A)  0      0;
    0      0    -C_y     0     E_y     0      0      0     -D_y     0     F_y     0;
    0     C_z     0      0      0     E_z     0     D_z      0      0      0      F_z;
    1/6    0      0      0      0      0      1/3    0       0      0      0      0;
    0     B_z     0      0      0     D_z     0     A_z      0      0      0      -C_z;
    0      0     B_y     0    -D_y     0      0      0      A_y     0     C_y     0;
    0      0      0   J/(6*A)  0      0      0      0       0   J/(3*A)  0      0;
    0      0     D_y     0     F_y     0      0      0      C_y     0     E_y     0;
    0    -D_z     0      0      0     F_z     0    -C_z      0      0      0      E_z];

% Stiffness and Mass matrix
K = Ko;
M = Me;
Ks= Kos;

% Damping Matrix

switch Damping

case 'DStr'

switch ProbAnalysis
```

```
    case {'Area','Soil'}

        switch WindSpeed
            case '8 m/s'
                aerodynamicDamping = 0.0349;
            case '14 m/s'
                aerodynamicDamping = 0.0573;
            case '18 m/s'
                aerodynamicDamping = 0.0641;
        end

        structuralDamping = 0.01;
        alp = 0;
        bet = structuralDamping+aerodynamicDamping;
        C = alp*M+bet*K;

    case {'Aerodynamic Damping','Combined'}

        structuralDamping = 0.01;
        aerodynamicDamping = PDAeroDy;
        alp = 0;
        bet = structuralDamping+aerodynamicDamping;
        C = alp*M+bet*K;

end

case 'DTop'

        structuralDamping = 0.01;
        alp = 0;
        bet = structuralDamping;
        C = alp*M+bet*K;

end
```

The third MATLAB script of the FE analysis is used to obtain the displacements, velocities and accelerations of the structure by using the Newmark method.

```
function [depl,vel,accl] = Dynamic_Solution_Newmark(M,K,C,active_Dof)

global t dt load1 load2 load3
global GDof

% Average
gaama = 1/2;
beta = 1/4;

% Time step
nt = length(t);

% Constants used in Newmark's integration
```

```
a1 = gaama/(beta*dt);
a2 = 1/(beta*dt^2);
a3 = 1/(beta*dt);
a4 = gaama/beta;
a5 = 1/(2*beta);
a6 = (gaama/(2*beta)-1)*dt;

depl = zeros(GDof,nt);
vel = zeros(GDof,nt);
accl = zeros(GDof,nt);

force = sparse(GDof,1);
force1 = sparse(GDof,1);
force2 = sparse(GDof,1);

% Initial Conditions
depl(:,1) = zeros;
vel(:,1) = zeros;
accl(:,1) = zeros;

% Acceleration t=0
force(end-5) = load1(1);
force(end-4) = load2(1);
force(end-3) = load3(1);
accl(active_Dof,1) = M(active_Dof,active_Dof)\(force(active_Dof)-...
    C(active_Dof,active_Dof)*vel(active_Dof,1)-K(active_Dof,active_Dof)...
    *depl(active_Dof,1)) ;

Kcap = K(active_Dof,active_Dof)+a1*C(active_Dof,active_Dof)+...
    a2*M(active_Dof,active_Dof);
L = chol(Kcap,'lower');

a = a3*M(active_Dof,active_Dof)+a4*C(active_Dof,active_Dof);
b = a5*M(active_Dof,active_Dof)+a6*C(active_Dof,active_Dof);

% Time step starts
for i = 1:nt-1

    force1(end-5) = load1(i);
    force1(end-4) = load2(i);
    force1(end-3) = load3(i);

    force2(end-5) = load1(i+1);
    force2(end-4) = load2(i+1);
    force2(end-3) = load3(i+1);

    delP = (force2(active_Dof)-force1(active_Dof))+a*vel(active_Dof,i)+...
        b*accl(active_Dof,i);
    temp = L\delP;
    delu = L'\temp ;
    delv = a1*delu-a4*vel(active_Dof,i)-a6*accl(active_Dof,i);
    dela = a2*delu-a3*vel(active_Dof,i)-a5*accl(active_Dof,i);
    depl(active_Dof,i+1) = depl(active_Dof,i)+delu;
    vel(active_Dof,i+1) = vel(active_Dof,i)+delv;
    accl(active_Dof,i+1) = accl(active_Dof,i)+dela;

end
```

Finally, the fourth MATLAB script of the FE analysis is used to obtain the bending moments in the mud-line of the structure.

```
function [Myi, Mzi] = Bending_Moment (numberElements,nodeCoordinates,...
    depl,EDof,Iy,Iz)

global E
global numberElementsFoundation

Myi=zeros(numberElements,1);
Mzi=zeros(numberElements,1);

    for i=numberElementsFoundation

        Lel = sqrt((nodeCoordinates(i+1)-nodeCoordinates(i))^2);

        deplTopFinal=depl;
        rot=deplTopFinal(EDof(i,:));
        Bf=[0,0,0,-1,-1,-1,0,0,0,1,1,1]/Lel;
        chiMy=Bf([5 11])*rot([5 11]);
        chiMz=Bf([6 12])*rot([6 12]);

        Myi(i)=E*Iz(i)*chiMy;
        Mzi(i)=E*Iy(i)*chiMz;

    end

end
```

B.4. MATLAB script used to obtain the fatigue damage

The fatigue damage is obtained using several MATLAB scripts. The rainflow counting is necessary to obtain the fatigue damage of the structure, but it has been used an external code to perform the rainflow counting, and therefore it will not be included in this appendix. The following MATLAB script is used to obtain the fatigue damage of the different outputs.

```
function [RF_DisplTopX,RF_DisplTopY,RF_DisplTopZ,RF_BMMudlineY, ...
    RF_BMMudlineZ] = RF_Results_Damage (DisplTopX,DisplTopY,DisplTopZ, ...
    BMMudlineY,BMMudlineZ)

m = 4;
N_eq = 1./(6.3*10^8)^(1/m);

[rfi_DisplTopX] = inrain_main(DisplTopX(:));
[nL,L] = hist(rfi_DisplTopX,50);
dmg = Damage_Equiv_Load(L,nL,m,N_eq);
RF_DisplTopX=dmg;
[rfi_DisplTopY] = inrain_main(DisplTopY(:));
[nL,L] = hist(rfi_DisplTopY,50);
dmg = Damage_Equiv_Load(L,nL,m,N_eq);
RF_DisplTopY=dmg;
[rfi_DisplTopZ] = inrain_main(DisplTopZ(:));
[nL,L] = hist(rfi_DisplTopZ,50);
dmg = Damage_Equiv_Load(L,nL,m,N_eq);
RF_DisplTopZ=dmg;

[rfi_BMBottomY] = inrain_main(BMMudlineY(:));
[nL,L] = hist(rfi_BMBottomY,50);
dmg = Damage_Equiv_Load(L,nL,m,N_eq);
RF_BMMudlineY=dmg;
[rfi_BMBottomZ] = inrain_main(BMMudlineZ(:));
[nL,L] = hist(rfi_BMBottomZ,50);
dmg = Damage_Equiv_Load(L,nL,m,N_eq);
RF_BMMudlineZ=dmg;

end
```

The second MATLAB script is used to calculate the equivalent fatigue damage of the support structure.

```
function dmg = Damage_Equiv_Load(L,nL,m,N_eq)

    dmg = 0;
    dmg = sum(L.^m .*nL);
    dmg = N_eq*(dmg)^(1/m);

end
```